

GIANT PULSE EVOLUTION IN A Nd<sup>3+</sup>-GLASS

Q-SWITCHED LASER

GIANT PULSE EVOLUTION IN A Nd<sup>3+</sup>-GLASS

Q-SWITCHED LASER

By

KENNETH OWEN HILL, B.ENG., M.ENG.

A Thesis

Submitted to the Faculty of Graduate Studies

in Partial Fulfilment of the Requirements

for the Degree

Doctor of Philosophy

McMaster University

March 1968

DOCTOR OF PHILOSOPHY (1968)  
(Electrical Engineering)

McMASTER UNIVERSITY  
Hamilton, Ontario

TITLE: Giant Pulse Evolution in a  $\text{Nd}^{3+}$ -Glass Q-Switched Laser

AUTHOR: Kenneth Owen Hill, B.Eng. (McMaster University)  
M.Eng. (McMaster University)

SUPERVISOR: Professor C. K. Campbell

NUMBER OF PAGES: xi, 180

SCOPE AND CONTENTS:

A rate equation model of a mechanically Q-switched  $\text{Nd}^{3+}$ -in-glass giant pulse laser is presented. The predictions of the model are compared with the experimentally observed behaviour of the device. Good quantitative agreement is obtained. To account for some of the observed features of the Q-switched laser, a non-radiative lifetime for the  ${}^4I_{11/2} \rightarrow {}^4I_{9/2}$  transition of  $\text{Nd}^{3+}$ -in-glass of 400 nsec. is introduced into the model. This lifetime is found to be in essential agreement with a quantum mechanical estimate of that quantity.

A plane-parallel cavity having either rectangular or circular geometry with an angular limiting device introduced within it is described analytically. The results of some calculations on the rectangular cavity are presented. This problem is of interest in considerations involving transverse mode selection in laser resonator design

## ABSTRACT

Of all the Q-switching methods employed to operate a laser in the giant pulse mode one of the simplest and most regularly used methods involves a rotating Porro prism. In this Thesis, experimental results are reported which show good agreement with predictions based on a rate equation model. The results indicate that it is possible to design a rotating prism Q-switched laser on the basis of those rate equations, and that the design when realized, should perform close to expectations.

## ACKNOWLEDGEMENTS

The author is especially grateful to Professor C. K. Campbell for his helpful advice and criticism during the course of this work and in the preparation of this Thesis.

An additional expression of gratitude is due to Professor R. G. Summers-Gill for his many helpful suggestions.

Dr. D. C. Johnson, during the course of his graduate work at McMaster, was a friend and a selfless helper.

To Dr. T. Timusk and Miss M. Buchanan, who helped the author to perform low temperature observations of the fluorescence of  $\text{Nd}^{+3}$  on their equipment, I extend my thanks.

I am indebted to the National Research Council of Canada for its support in the form of fellowships.

The continuous support of the Defence Research Board in the form of grants is gratefully acknowledged.

TABLE OF CONTENTS

	<u>PAGE</u>
CHAPTER 1: INTRODUCTION-----	1
1.1 Survey of Q-Switching Techniques-----	1
1.2 The Giant Pulse Laser--Some Preliminary Remarks-----	3
1.3 Scope of This Thesis-----	4
 CHAPTER 2: ANALYTICAL DESCRIPTION OF A ROTATING REFLECTOR Q-SWITCHED LASER-----	 6
2.1 Introduction-----	6
2.2 State Transitions In Nd <sup>+3</sup> -----	6
2.3 Formulation of the Rate Equations Governing Laser Action-----	 11
2.3-1 Some Introductory Notions-----	11
2.3-2 Threshold for Laser Action-----	14
2.3-3 The Rate Equations--The Case of Equal Laser Level Degeneracies-----	 18
2.3-4 Introduction of A Time Dependent Loss Factor Into the Rate Equations-----	 23
2.3-5 The Rate Equations for Nd <sup>+3</sup> in Glass-----	24
2.4 Some Properties of the Q-Switched Laser Rate Equations-----	 29
2.4-1 Normalization of the Rate Equations-----	29
2.4-2 Behaviour of the Rate Equations Under Limiting Terminal Level Lifetime Conditions---	 31

	<u>PAGE</u>
2.4-3 Some Properties of the Rate Equations of Wagner and Lengyel-----	33
2.4-4 Qualitative Behaviour of the Solutions of the Nd <sup>+3</sup> in Glass Laser Rate Equations-----	35
2.5 Determination of the Population Inversion Necessary to Maintain Laser Action-----	37
CHAPTER 3: MODES IN ANGULAR LIMITED RESONATORS-----	42
3.1 Introduction-----	42
3.2 Rectangular and Circular Plane Parallel Symmetric Resonators with Angular Limiting Devices - Formulation of the Problem-----	43
3.2-1 Rectangular Plane Parallel Resonators-----	43
3.3-2 Circular Plane Parallel Resonators-----	52
3.3 Solution of the Integral Equation Governing the Steady State Field Distribution in a Cavity Formed by Two Infinite Strip Reflectors and an Angular Limiting Device-----	55
CHAPTER 4: EXPERIMENTAL APPARATUS AND PROCEDURE-----	72
4.1 Introduction-----	72
4.2 Experimental Apparatus-----	73
4.2-1 The Q-Switched Laser System-----	73
4.2-2 Rotating Prism Laser Q-Spoiler-----	78
4.2-3 Nd <sup>+3</sup> in Glass Laser Rods-----	79

	<u>PAGE</u>
4.2-4 Optical Mounts-----	81
4.2-5 Laser Head and Power Supply-----	83
4.2-6 Detectors-----	86
4.2-7 The Synchronization Unit-----	88
4.2-8 The Lummer Gehrcke Plate-----	91
4.2-9 Reflectors-----	95
4.3 Procedure-----	97
4.3-1 Alignment Techniques-----	97
4.3-2 Q-Spoiled Pulse Output Energy Measurements and Complementary Measurements-----	99
4.3-3 Determination of the Loss Function $\gamma(T)$ -----	102
4.3-4 Measurement of the Q-Spoiled Output Energy Characteristics of a Mechanically Switched Laser-----	104
4.3-5 Fluorescence Measurements and the Energy Utilization Factor-----	106
CHAPTER 5: EXPERIMENTAL RESULTS-----	108
5.1 The Fluorescent Output Strength of the ${}^4F_{3/2} \rightarrow {}^4I_{11/2}$ Transition of $Nd^{+3}$ as a Function of the Pump Input Energy-----	108
5.2 The Experimental Determination of the Switching Function $\gamma(\theta)$ -----	112
5.3 The Switching Function $\gamma(\theta)$ with the Lummer Gehrcke Angular Limiting Device Present in the Cavity-----	115

	<u>PAGE</u>
5.4 The Output Energy Characteristics-----	119
5.5 Relation of the Time Evolution of the Giant Pulse to the Output Energy Characteristics-----	124
5.6 Output Energy Characteristics - Lummer Gehrcke Device Within the Cavity-----	128
5.7 Energy Utilization Factor Measurements-----	133
CHAPTER 6: DISCUSSION OF RESULTS-----	138
6.1 Determination of the Initial Flux in the Cavity and its Relation to the Positions of the Energy Maxima in the Switching Speed vs Energy Output Characteristics-----	138
6.2 Estimation of the Output Energy of the Nd <sup>+3</sup> Doped Glass Q-Switched Laser-----	141
6.3 Theoretical Switching Speed vs Output Energy Characteristics-----	144
6.4 De-excitation of the <sup>4</sup> I <sub>11/2</sub> level of Nd <sup>+3</sup> by Multiphonon Emission-----	155
6.5 Temporal Development of the Giant Pulse-----	161
CHAPTER 7: CONCLUSIONS -----	167
APPENDIX -----	170
REFERENCES -----	176

FIGURE CAPTIONS

<u>FIGURE</u>		<u>PAGE</u>
(2-1)	Nd <sup>+3</sup> Energy Level Scheme-----	7
(2-2)	The Four Energy Level System Described by the Rate Equations-----	26
(3-1)	Power Loss Per Transit of the Lowest Order Mode of an Infinite Strip Resonator as a Function of the Fresnel Number for Three Values of the Angular Number-----	61
(3-2)	The Phase Shift per Transit of the Lowest-Order Mode of an Infinite Strip Resonator as a Function of the Fresnel Number for Three Values of the Angular Number----	62
(3-3)	The Amplitude and Phase of the Lowest Order Even Mode of an Infinite Strip Cavity for Angular Numbers of 0.141 and 2.26-----	65
(3-4)	The Number of Transits Required for an Aperture Limited Plane Wave to Converge to the Lowest Order Even Mode for an Infinite Strip Cavity as a Function of the Fresnel Number for Angular Numbers of 2.26, 0.565 and 0.141-----	68
(3-5)	Power Ratio as a Function of the Number of Passes-----	70
(4-1)	Schematic of the Giant Pulse Laser System-----	74
(4-2)	Photograph of the System-----	75
(4-3)	Schematic of the Synchronization Unit-----	89
(4-4)	Schematic of Daly-Sims Accessory	

<u>FIGURE</u>	<u>PAGE</u>
(5-1) Intensity of the ${}^4F_{3/2} \rightarrow {}^4I_{11/2}$ Transition of Nd <sup>+3</sup> -in-Glass as a Function of Wavelength for various Values of the Pulsed Input Energy into the Flashlamp-----	109
(5-2) Peak Fluorescent Intensity of the ${}^4F_{3/2} \rightarrow {}^4I_{11/2}$ Transition of Nd <sup>+3</sup> -in-Glass as a Function of Pulsed Excitation Energy-----	111
(5-3) Threshold as a Function of Output Reflection Tilt-----	113
(5-4) Threshold as a Function of Output Reflector Tilt with the Lummer Gehrcke Plate in the Cavity-----	116
(5-5) Experimental Output Energy Characteristics-----	120
(5-6) Experimental Output Energy Characteristics-----	123
(5-7) Experimental Output Power Characteristics of the Leading Pulse-----	125
(5-8) Experimental Time Evolution of the Giant Pulse-----	127
(5-10) Experimental Output Energy Characteristics with the Lummer Gehrcke Plate in the Cavity-----	131
(5-11) Experimentally Observed Fluorescent Strength of the ${}^4F_{3/2} \rightarrow {}^4I_{11/2}$ Transition of Nd <sup>+3</sup> During the Pumping Interval -----	135
(6-1) The Calculated Output Energy Characteristics Together with the Observed Experimental Data-----	146
(6-2) The 450 Joule Excitation Characteristic for Long Terminal Level Lifetimes -----	148

FIGURE

PAGE

(6-3)	The 450 Joule Excitation Characteristic for Short Terminal Level Lifetimes-----	149
(6-4)	Calculated Time Development of the Giant Pulse-----	163
(6-5)	Calculated Time Development of the Giant Pulse in the Double Pulse Region -----	164

CHAPTER I  
INTRODUCTION

1.1 Survey of Q-Switching Techniques:

McClung and Hellwarth<sup>(1)</sup>, followed by others<sup>(2)</sup>, developed what is today known as a Q-spoiled laser. Their experiments were performed using a ruby laser rod as the active medium and a Kerr cell to control the regenerative action of resonant fluorescence within the cavity. They achieved a peak power of 0.6 Megawatts in their early work. Since the initial break-through in 1962, the field of giant pulse lasers has grown at a fast pace. This growth has been marked by an increasing quantity of available Q-switching techniques as well as new wave lengths.

During the oscillation period of a laser the induced emission effectively reduces the lifetime of the metastable upper laser level, thereby limiting the possible population inversion for a given pump power. This limitation of the inversion population in turn limits the peak output power of the device. Hellwarth<sup>(3)</sup> pointed out that if one constructs a laser with external reflectors and inserts a closed shutter in the optical feedback path, the device will not oscillate and a large overpopulation of the upper metastable laser level will result. If the shutter is opened when the overpopulation is maximized, positive feedback will be initiated and an extremely large output spike generated due to the presence of the large overpopulation.

Q-switching techniques must therefore concern themselves with methods of controlling the losses of a laser cavity. Ideally the control should be fast in order that the losses be a minimum when the giant pulse evolves. Just how fast depends, among other parameters, on the gain of the active material when the overpopulation has been maximized as well as on the separation between the cavity reflectors. Quantitatively, present solid state Q-switched lasers need to be switched in about 100 nsec.

Ultrasonic shutters<sup>(4)</sup>, Faraday effect shutters<sup>(5)</sup>, electro optic shutters such as Kerr cells and Pockel cells<sup>(6)</sup>, bleachable absorbers<sup>(7,8)</sup> and exploding filters<sup>(9)</sup> have been used to advantage as Q-switching elements. Among the more novel of the Q-switching techniques is that involving specially prepared laser rods which, upon being pumped, Q-switch themselves<sup>(10,10a)</sup>.

Among the mechanical methods of Q-switching a laser, perhaps the one which enjoys the most popularity makes use of a rotating Porro prism<sup>(11,12)</sup>. This thesis is concerned with the operating characteristics of a  $\text{Nd}^{+3}$  doped glass laser, Q-switched by means of a rotating Porro prism.

We have referred to some of the techniques employed to Q-switch a laser but the list we have given is by no means exhaustive. Future developments will most likely continue to enlarge the number of available switching techniques.

Finally we should point out that recently a technique has been developed whereby the multimode nature of a laser is used to advantage to obtain high power and very short duration pulses<sup>(13)</sup>. This technique, if used in conjunction with normal Q-switching methods, can result in the

availability of a light source of very high power and short duration pulses. The high power and short duration pulses result if several longitudinal modes are phase-locked so that the amplitudes of each mode are added in phase at particular periodic times whilst tending to interfere destructively at all other times.

### 1.2 The Giant Pulse Laser--Some Preliminary Remarks:

A giant pulse laser is a complex device. The factor which gives it that characteristic is its inherently non-linear and multimode nature. Coherence effects can influence the performance characteristics of the device; for example mode locking techniques depend on mode coherence. Also the non-uniform gain profiles of laser fluorescence lines introduce an added degree of complication to any analysis of the operation of giant pulse lasers. The dynamics of solid state fluorescent lines are not really well understood. For instance, what processes are involved in restoring the equilibrium line shape of an inhomogeneously broadened line originating from a transition between inverted levels after a hole has been burnt in its profile by an intense monochromatic beam? Evidence of such processes has been found<sup>(14)</sup> for the  $1.06\mu$  transition of  $\text{Nd}^{+3}$  in glass, but they have been treated only on a phenomenological basis. The non-uniform excitation and heating of the laser medium along the rod radius during the pumping pulse can only complicate attempts to describe the device performance analytically<sup>(15)</sup>. There has, however, been a recent effort to take into account the effects of a standing wave resonator, and the initial conditions of radial variation in gain on giant pulse laser energy release<sup>(16)</sup>.

To attempt to take into account all the factors that can influence the operating characteristics of a giant pulse laser would be a truly

difficult task. All one can hope for is to arrive at some simplifying assumptions which leave the essential influences of the various factors governing giant pulse evolution within the framework of the model. This is what the rate equation model<sup>(17,18,19)</sup> for Q-spoiled laser action attempts to do. In this thesis such a theory is applied to describe the observed operating characteristics of a Nd<sup>+3</sup> doped glass giant pulse laser.

### 1.3 Scope of This Thesis:

This thesis concerns itself with two quite separable topics. The major portion of it deals with an analytical model for a Porro prism Q-switched laser. Emphasis is placed on the ability of that model to successfully predict the operating characteristics of the particular Nd<sup>+3</sup> glass giant pulse laser which was used to extract the relevant experimental data. The second topic to be considered is of a theoretical nature. To be specific, the problem of transverse mode selection in a plane parallel passive interferometer will be treated. The use of an angular limiting device within the interferometer will be shown to result in mode selection.

The work on the behaviour of the giant pulse laser was undertaken because of the existence of a gap between theory and experiment. The properties of many experimental giant pulse lasers have been reported in the literature. Theories of giant pulse laser operation have also been abundant, however, there has been very little visible effort to bring out theoretical calculations and experimental results simultaneously. It is hoped that this thesis will serve to partially fill that gap. A somewhat unique method of approach to the problem is used--an approach that makes the operation of the mechanically Q-switched giant pulse laser

understandable in simple terms.

5

The method used to solve the problem of transverse mode selection in a plane parallel interferometer is presented as an original contribution. It is hoped that the results of the calculations, which were undertaken in this context, will be useful in laser cavity design considerations.

A method of increasing the apparent switching speed of the Porro prism switch will also be considered<sup>(20)</sup>. Other methods are also available<sup>(21)</sup>.

## CHAPTER 2

### ANALYTICAL DESCRIPTION OF A ROTATING REFLECTOR

#### Q-SWITCHED LASER

##### 2.1 Introduction:

This Chapter deals with the analytical description of a simplified model of a rotating mirror Q-switched laser. Certain concepts pertinent to an understanding of the operation of the physical device will be introduced. The equations forming the basis for the description of the device will be shown to be coupled non-linear differential equations. Since it has not been possible to obtain a closed form solution of these equations, numerical methods are invoked to deal with them. In particular, such solutions as will be presented, are based on parameters and initial conditions which describe the particular laser system used in this thesis. These solutions will be useful at a later stage when the feasibility of describing a physical Q-switched laser system is considered, in terms of the equations obtained from the simplified model of the system.

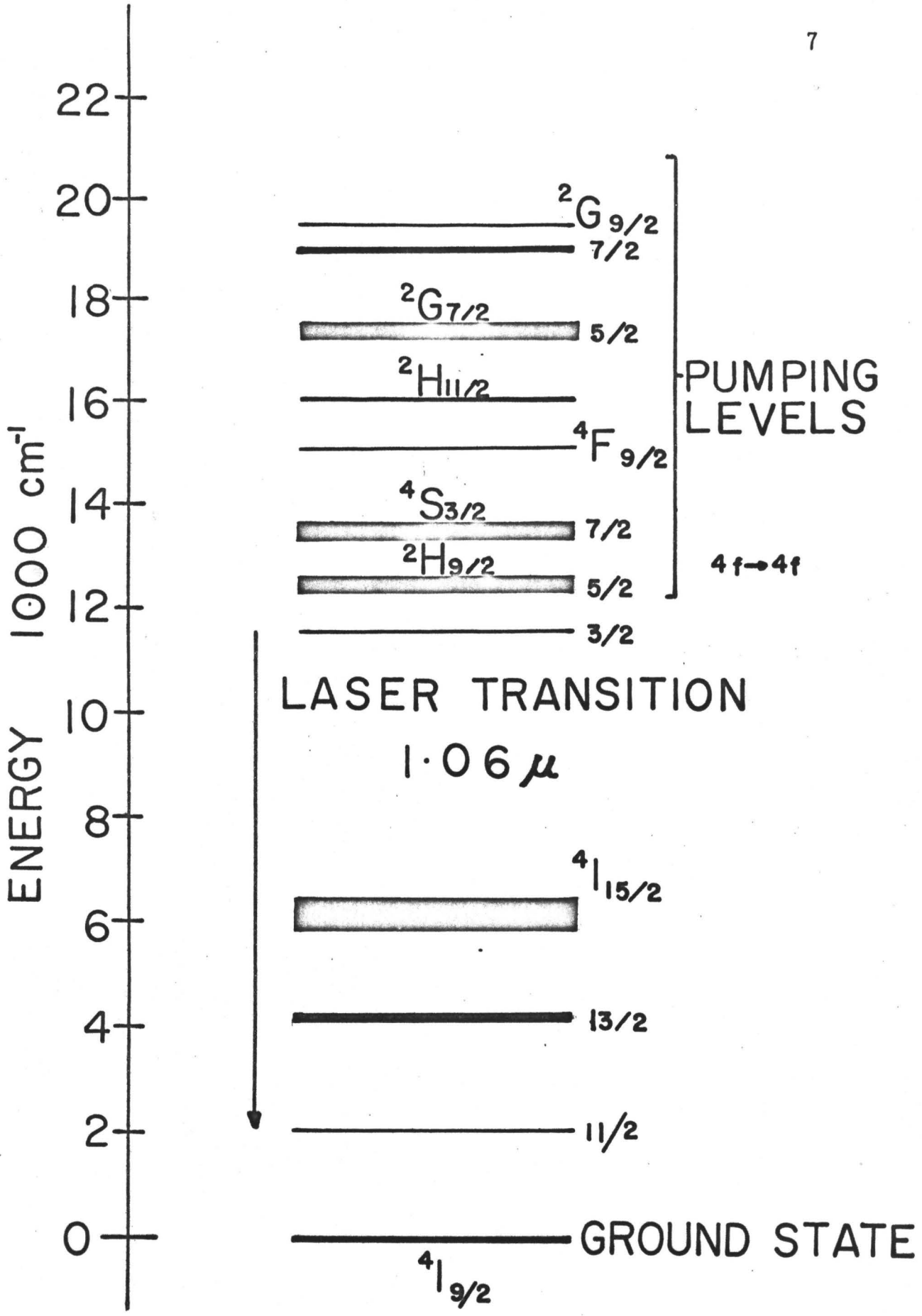
##### 2.2 State Transitions In $Nd^{+3}$ :

The energy level scheme of  $Nd^{+3}$  is shown in Figure (2-1) for reference<sup>(22)</sup>. It is well known that divalent and trivalent rare-earth ions contain only 4f electrons in their ground state in addition to the basic common xenon shell<sup>(23)</sup>. In particular, the  $Nd^{+3}$  ground state is obtained by removing two 6s electrons and one 4f electron from the Nd ground state, leaving the basic xenon core and three shielded 4f electrons

Figure (2-1)

Nd<sup>+3</sup> Energy Level Scheme

Width of the levels indicate the total separation of the Stark components in the Anhydrous Trichlorides (after G. H. Dieke: in "Advances in Quantum Electronics", edited by J. R. Singer, Columbia University Press, New York, 1961)



as the  $\text{Nd}^{+3}$  ground state configuration. In the case of the trivalent ions of the rare earths, with the exception of  $\text{Tb}^{+3}$ , all levels below  $50,000 \text{ cm}^{-1}$  belong to  $4f^n$  configurations<sup>(22)</sup>.

Thus, in considering the  $1.06\mu$  transition ( ${}^4F_{3/2} \rightarrow {}^4I_{11/2}$ ) generally used for obtaining laser action in  $\text{Nd}^{+3}$ , we are concerned with a  $4f \rightarrow 4f$  transition, which in the case of the free  $\text{Nd}^{+3}$  ion, is strictly parity forbidden.  $\text{Nd}^{+3}$  in a crystal matrix can be treated approximately in terms of the Russell-Saunders coupling scheme. In the LS approximation, we note the following violations by the  ${}^4F_{3/2} \rightarrow {}^4I_{11/2}$  transition of  $\text{Nd}^{+3}$  of the strong selection rules applicable to electric dipole transitions in the scheme, namely,

$$\Delta l \neq \pm 1$$

$$\Delta J \neq 0 \pm 1$$

Consideration of the magnetic dipole selection rules shows that the transition  ${}^4F_{3/2} \rightarrow {}^4I_{11/2}$ , although not strictly forbidden in this instance, nevertheless disobeys the selection rule  $\Delta J = 0 \pm 1$  applicable to those transitions. If it were not for this fact, the spontaneous transition probabilities calculated on the basis of electric dipole and magnetic dipole approximations could very easily turn out to be of the same order of magnitude. The calculation of the inherently weaker magnetic dipole transition probability in the case of the  ${}^4F_{3/2} \rightarrow {}^4I_{11/2}$  transition does not require a mixing of states of opposite parity, as does the same calculation undertaken in the electric dipole approximation. This might well be a compensating mechanism which could make the two transition probabilities roughly equal.

The explanation of the observed transition  ${}^4F_{3/2} \rightarrow {}^4I_{11/2}$  of  $\text{Nd}^{+3}$

in glass must concern itself with non-centro-symmetric interactions that lead to a mixing of states of opposite parity<sup>(24)</sup>. In general, the non-centro-symmetric interaction may have as its origin the non-centro symmetric portion of the microfields due to surrounding ions acting on the ion of interest. Thus, two states of a configuration  $n\ell^N$  which become slightly admixed by a non-symmetric field with states of the configuration  $n\ell^{N-1}n'\ell'$  and  $n'\ell', 4\ell+1_{n\ell}^{N+1}$  yield two mixed parity states which will become connected by the electric dipole operator. For f electrons the following selection rules apply: In the case of  $f^N$  configurations, the perturbing states may differ only by the single substitution of n'd or n'g electrons. (That is to say, the configurations obtained by removing a 3d or 4d electron from the xenon core and placing it in the 4f subshell, or exciting a 4f electron into any of the empty n'g or n'd subshells, in the case of  $Nd^{+3}$ ). Furthermore, the initial and final states of the transition must be such that:

$$\Delta S = 0 \quad \Delta L \leq 6 \quad \Delta J \leq 6$$

Under these selection rules, the observed transition  ${}^4F_{3/2} \rightarrow {}^4I_{11/2}$  of  $Nd^{+3}$  in glass becomes allowed. However, if the admixture of states of opposite parity with the states of  $4f^3$  configuration is small, the transition probability for spontaneous emission will also be small. This factor could qualitatively explain the observed lifetime of the  ${}^4F_{3/2}$  level of  $Nd^{+3}$  in glass, which is in the order of hundreds of microseconds at room temperature.

It is not difficult to see why the admixture of states of opposite parity by the crystal field will be small, in the case of rare earth ions. For ions of the rare earth series the inequality  $H_1 \gg H_2 \gg H_3$  holds.  $H_1$  is defined here as the residual electrostatic interaction Hamiltonian given by:

$$H_1 = \sum_{i>j=1}^N \frac{e^2}{r_{ij}} + \sum_{i=1}^N \left( -\frac{Ze^2}{r_i} - U(r_i) \right)$$

while  $H_2$  is the spin-orbit interaction Hamiltonian given by:

$$H_2 = \sum_i \xi(r_i) \bar{S}_i \cdot \bar{l}_i$$

with

$$\xi(r) = \frac{\hbar^2}{2m^2 c^2 r} \frac{dU}{dr},$$

where  $-\frac{U(r_i)}{e}$  is the effective potential seen by the  $i^{\text{th}}$  electron.

$H_3$  is the electrostatic Hamiltonian due to the influence of the electric field of surrounding atoms at the ion position<sup>(25)</sup>. Shielding of the 4f electrons by the averaged electrostatic field of the 5s and 5p electrons of the basic xenon configuration tends to minimize the effect of an external electrostatic field on the 4f electrons of the rare earth ions  $R^{+3}$ . It is this shielding that is responsible for the relative magnitude of  $H_3$  and the sharpness of the energy levels of rare earth ions located in a crystalline field. Since  $H_3$  is small relative to  $H_1$  and  $H_2$ , and since the admixture of states of opposite parity is assumed to be due only to the non-centro-symmetric portion of  $H_3$ , the admixture will be small and the LS coupling scheme will be approximately applicable.

We note that the  ${}^4F_{3/2} \rightarrow {}^4I_{11/2}$  transition being considered takes place between two deep lying states. Furthermore, the states with which slight admixture takes place lie at least  $50,000 \text{ cm}^{-1}$  above the  ${}^4F_{3/2}$  and  ${}^4I_{11/2}$  states. Since the admixture of a given state with another depends inversely on the energy difference between those states,

we again arrive at the conclusion that, in the case being treated, the admixture of states of opposite parity will be small.

A non-centro-symmetric field will act on an ion that is located in a site that lacks a centre of inversion symmetry. Thus, considering a  $\text{Nd}^{+3}$  ion to be located in a glass matrix and treating the glass matrix- $\text{Nd}^{+3}$  system as a solution, there is no a priori reason to believe that a centre of inversion will exist at the ion position. Hence, it is not unreasonable to suppose that the mechanism responsible for the  ${}^4\text{F}_{3/2} \rightarrow {}^4\text{I}_{11/2}$  transition of  $\text{Nd}^{+3}$  in glass is the odd portion of the crystal field Hamiltonian.

It is interesting to note that the selection rules for mixed parity states also explain the appearance of some of the absorption bands of  $\text{Nd}^{+3}$  in glass which are used in practice for optically pumping the material. However, a few absorption bands are observed which violate the  $\Delta S=0$  selection rule. These observed bands can be tentatively explained if it is recalled that spin-orbit interaction usually leads to a breakdown of selection rules on S and L<sup>(24)</sup>.

It is perhaps worthwhile to indicate at this stage that the theory of intensities of rare earth crystal and solution spectra in the visible region of the spectrum is still in a stage of development.

### 2.3 Formulation of the Rate Equations Governing

#### Laser Action:

##### 2.3-1 Some Introductory Notions-

We begin by establishing a simple relationship between intensity and photon density. Consider a stream of photons traveling in an arbitrary direction in a non-absorbing medium of index of refraction  $n$ . Let us neglect the effects of diffraction, and consider that the photon

beam may be characterized spatially by a cross sectional area  $A$ . Let the number of photons per unit volume within the beam with angular frequency between  $\omega$  and  $\omega + \Delta\omega$  be  $\eta\phi(\omega)\Delta\omega$ , where  $\phi(\omega)$  is the photon density per unit angular frequency range of the beam referred to vacuum. Each photon within the range  $\omega$  and  $\omega + \Delta\omega$  carries energy  $\hbar\omega$ . Therefore, since group velocity of the photons is  $\frac{c}{\eta}$ , the power per unit area flowing through the surface normal to the direction of propagation of the beam, and with perimeter defined by the boundary of the beam, is:

$$\eta\hbar\omega \frac{c}{\eta} \phi(\omega)\Delta\omega$$

The quantity obtained above is the intensity of the beam due to photons within the angular frequency range  $\omega$  and  $\omega + \Delta\omega$ . If we define a quantity,  $I(\omega)$ , as the intensity per unit angular frequency range, we have the relation:

$$I(\omega)\Delta\omega = \eta\hbar\omega \frac{c}{\eta} \phi(\omega)\Delta\omega \quad \dots(2-1)$$

In crossing a boundary, formed by two media whose indices of refraction differ, which is normal to the direction of propagation of the beam, it is seen that  $I(\omega)$  is constant as a consequence of continuity. Reflection at the interface has been neglected since one is concerned with boundaries formed by laser rod end faces and atmospheric air. The laser rod end faces are generally dielectric coated to minimize reflections at an appropriate wave length. It also follows from (2-1) that if  $\phi_1(\omega)$  is the photon density per unit angular frequency range in medium 1 and  $\phi_2(\omega)$  that in medium 2 then:

$$\frac{\phi_1(\omega)}{\eta_1} = \frac{\phi_2(\omega)}{\eta_2}$$

We have argued that in the case of  $\text{Nd}^{+3}$ -glass lasers we are probably concerned with predominantly dipole transitions. It, therefore, becomes advantageous at this stage to introduce some quantum mechanical results pertinent to such dipole transitions<sup>(26)</sup>.

In general it can be shown that the probabilities of reverse transitions between any pair of states under the influence of the same radiation field are equal. In particular, the transition probability for absorption or stimulated emission of a photon between two stationary states  $K$  and  $\ell$  of energies  $E_K$  and  $E_\ell$  ( $E_K > E_\ell$ ) such that  $|\omega_{K\ell}| = \frac{|E_K - E_\ell|}{\hbar}$  is proportional to  $I(\omega_{K\ell})$  and hence to  $\phi(\omega_{K\ell})$ . In the case of electric dipole absorption and induced emission of light quanta, both transition probabilities are also proportional to the square of the matrix element of the electric dipole moment  $e\bar{r}$  of the particle involved.

The spontaneous transition probability is proportional to the square of the matrix element of the dipole moment of the particle involved and does not depend on the intensity of the radiation field. The spontaneous emission probability can be thought of as arising from the influence of the zero-point energy of the electromagnetic field on the particle under consideration.

In the case of spontaneous emission, the radiation is distributed isotropically in angular space--in contrast to induced emission which maintains to a good approximation the angular distribution of the perturbing photon beam within the material.

A measurement of the decay time constant of a dipole transition, by observing the fluorescence from the transition, yields a measure of the dipole spontaneous transition probability if the lifetime of the

relevant level is not shortened significantly by processes which compete with dipole de-excitation.

### 2.3-2 Threshold for Laser Action-

A useful relationship, involving laser material properties and cavity reflector reflectivity, determining the conditions that must be met before laser action can commence will now be developed. To do this, let us consider a material of index of refraction  $\eta$  within which are located active ions possessing two non-degenerate stationary states labelled K and  $\ell$ , having energies  $E_K$  and  $E_\ell$  ( $E_K > E_\ell$ ) respectively. Let level K and level  $\ell$  have populations  $N_K$  per unit volume and  $N_\ell$  per unit volume of host material respectively. Let the two levels be connected by the electric dipole operator  $\bar{p} = e\bar{r}$ . We assume that the material hosting the ions is shaped in the form of a circular platelet of area A and thickness  $\Delta x$ . Further consider a beam of polychromatic photons of this area, normally incident on the platelet, which has an intensity  $I(\omega_{K\ell})$  per unit angular frequency range at  $\omega = \omega_{K\ell}$ . The transition probability<sup>PER UNIT TIME</sup> for absorption and induced emission in the dipole approximation is<sup>(26)</sup>:

$$\frac{4\pi^2 e^2 \eta}{3\hbar^2 c} I(\omega_{K\ell}) |(\bar{r})_{K\ell}|^2$$

where  $(\bar{r})_{K\ell}$  is the vector whose cartesian components are the K- $\ell$  matrix elements of x, y, and z. The net number of transitions per unit time per unit volume that will take place in the platelet, under the influence of the photon beam, can be written as  $\frac{d(N_K - N_\ell)}{dt}$  where:

$$\frac{d(N_K - N_\ell)}{dt} = - \frac{8\pi^2 e^2 \eta}{3\hbar^2 c} I(\omega_{K\ell}) |(\bar{r})_{K\ell}|^2 (N_K - N_\ell)$$

Now let

$$\alpha_o = \frac{4\pi^2 e^2}{3\hbar^2 c} |(\bar{r})_{K\ell}|^2$$

Then,

$$\frac{d(N_K - N_\ell)}{dt} = -2\alpha_o \eta I(\omega_{K\ell}) (N_K - N_\ell)$$

We can now substitute for  $I(\omega_{K\ell})$  from (2-1) giving

$$\frac{d(N_K - N_\ell)}{dt} = -2\alpha_o \hbar \omega_{K\ell} \phi(\omega)_{K\ell} (N_K - N_\ell)$$

Each net transition adds or subtracts one photon to or from the beam.

The change in  $\phi$  experienced by the beam on going through the platelet is then given by  $\Delta\phi$  where:

$$\Delta\phi = \alpha_o \eta \hbar \omega_{K\ell} \phi(\omega_{K\ell}) \frac{(N_K - N_\ell)}{\Delta\omega} \Delta x$$

The photons added to or subtracted from the beam will have angular frequencies in the approximate range  $\omega_{K\ell} \pm \frac{\Delta\omega}{2}$ , where  $\Delta\omega$  is the width at half maximum of the emitted or absorbed photon angular frequency distribution. Therefore by allowing  $\Delta x \rightarrow 0$  we arrive at the result,

$$\frac{d\phi(\omega_{K\ell})}{dx} = \alpha_o \hbar \omega_{K\ell} \phi(\omega_{K\ell}) \frac{(N_K - N_\ell)}{\Delta\omega} \dots (2-2)$$

~~Given now a host platelet of thickness  $\ell$  and assuming, as has been implicit in the above argument, that the intensity of the incident beam is low enough not to change the population of the two levels significantly, we arrive at the following result by integrating (2-2):~~

$$\phi(\omega_{K\ell}) = \phi_0(\omega_{K\ell}) e^{\alpha_0 \eta \hbar \omega_{K\ell} \frac{(N_K - N_\ell)}{\Delta\omega} \ell} \dots (2-3)$$

where  $\phi_0(\omega_{K\ell})$  is the incident photon density per unit frequency range, evaluated at  $\omega = \omega_{K\ell}$ , while  $\phi(\omega_{K\ell})$  is the resultant quantity after one traverse through the platelet.

To further our argument, let us consider a system consisting of two circular plane parallel mirrors of the same radius facing one another and of reflectivity  $r_1$  and  $r_2$ . In addition, let the mirrors be separated by a distance  $L^\dagger$  and imagine that the cylindrical rod of length  $\ell$  considered above is placed between, and coaxially with, those mirrors.

From equation (2-3) we know that a beam normal to the mirrors, (and of radius equal to the radius of the mirrors) characterized by a photon density per unit angular frequency,  $\phi(\omega_{K\ell})$ , in free space, incident on one end of the rod will emerge from the other end characterized by the following photon density per unit angular frequency range:

$$\phi(\omega_{K\ell}) e^{\alpha_0 \eta \hbar \omega_{K\ell} \frac{(N_K - N_\ell)}{\Delta\omega} \ell}$$

Upon striking the first mirror of reflectivity  $r_1$ , the region of the beam being considered will in part be transmitted and in part be reflected. The reflected portion of the beam will then be characterized by the photon density:

$$\phi(\omega_{K\ell}) r_1 e^{\alpha_0 \eta \hbar \omega_{K\ell} \frac{(N_K - N_\ell)}{\Delta\omega} \ell}$$

---

<sup>†</sup> The role of  $L$  will become clear as the development proceeds.

After a complete pass in the cavity, the photon beam will be characterized by a photon density per unit angular frequency given by:

$$\phi(\omega_{K\ell}) r_1 r_2 e^{\alpha_0 \eta \hbar \omega_{K\ell} \frac{(N_K - N_\ell)}{\Delta \omega} 2\ell} \dots (2-4)$$

The complete pass will take a time  $T_2$  where

$$T_2 = 2 \left( \frac{L + (\eta - 1)\ell}{c} \right)$$

For the photon beam to sustain itself undiminished the condition

$$r_1 r_2 e^{\alpha_0 \eta \hbar \omega_{K\ell} \frac{(N_K - N_\ell)}{\Delta \omega} 2\ell} = 1$$

must hold.

This yields, upon taking natural logarithms on both sides of the equality, the following result:

$$-\frac{1}{2} \ln r_1 r_2 = \alpha_0 \eta \hbar \omega_{K\ell} \frac{(N_K - N_\ell)}{\Delta \omega} \ell \dots (2-5)$$

which is independent of the photon density in the cavity.

The above condition is required to be met by the system in order to just maintain oscillation. It is consequently the condition at threshold energy for laser action. Since  $-\frac{1}{2} \ln r_1 r_2 \geq 0$ , we must therefore have  $N_K - N_\ell \geq 0$ . Condition (2-5) on the population inversion,  $N_K - N_\ell$ , is essentially one of unstable equilibrium, hence energy must be absorbed by the system from an external source in order that condition (2-5) can be met. In practice the required energy is provided by an excitation source (commonly a pulsed xenon flash lamp in the case of

optically pumped solid state lasers). Threshold is then the energy required to drive the excitation source, which results in condition (2-5) being satisfied in the system.

### 2.3-3 The Rate Equations--The Case of Equal Laser Level Degeneracies-

The coherent photon build up in a cavity of length  $L$  containing a laser rod of index  $\eta$  and length  $\ell$ , bounded by two mirrors of reflectivity  $r_1 = r_2 = R$ , obeys the following relation, based on equation (2-4), written in terms of the photon density per unit angular frequency range:

$$\phi(\omega_{K\ell}, T_1) = \phi(\omega_{K\ell}, 0) e^{\left[ \alpha_0 \eta \ell \omega_{K\ell} \frac{(N_K - N_\ell)}{\Delta\omega} \ell - \gamma \right]}$$

where  $T_1 = \frac{L + (\eta-1)\ell}{c}$  and  $\gamma = -\ln R$

This relationship results directly from integrating from 0 to  $T_1$  the following differential equation,

$$\frac{d\phi(\omega_{K\ell}, t)}{dt} = \phi(\omega_{K\ell}, t) \left[ \alpha_0 \eta \ell \omega_{K\ell} \frac{(N_K - N_\ell)}{\Delta\omega} \ell - \gamma \right] \frac{c}{L + (\eta-1)\ell} \dots (2-6)$$

after assuming that the level population is not significantly disturbed during the portion of the build up that is of interest, namely in one pass of the photon beam.

It is also inherently assumed that, in the time interval required for the photon beam to complete one pass, the photon density does not change appreciably. Thus, we are able, within the limits of the approximations involved, to attribute to the cavity at a particular instant of

time a uniform flux density. In actual fact, the photon density will vary from point to point in the cavity leading, in a more precise formulation of the problem, to relationships between quantities of interest involving partial differential equations. The more precise formulation would, in the end, involve the solution of coupled non-linear partial differential equations. Numerical methods for their solution would become extremely cumbersome and time consuming even if undertaken with the aid of high speed computers. In order to avoid this problem, we concentrate our attention on the simplified rate equations which are far more manageable numerically and likely to illustrate, for the parameters applicable to the Q-switched laser studied for this work, all the important features of the more general formulation. The number of photons in the cavity per unit angular frequency range is:

$$\phi(\omega_{K\ell}, t) [L + (\eta-1) \ell] A$$

where A is the photon beam area. This quantity changes through stimulated emission at a rate given by:

$$\frac{d}{dt} [\phi(\omega_{K\ell}, t) (L + (\eta-1) \ell) A] = \phi(\omega_{K\ell}, t) \left[ \alpha_0 \eta \hbar \omega_{K\ell} \frac{(N_K - N_\ell)}{\Delta\omega} \ell \right] AC$$

This rate must be balanced by corresponding transitions between levels K and  $\ell$ . Therefore, we arrive at the following equality:

$$\frac{d}{dt} \left[ \frac{N_K - N_\ell}{\Delta\omega} A \ell \right] = -2\phi(\omega_{K\ell}, t) \left[ \alpha_0 \eta \hbar \omega_{K\ell} \frac{(N_K - N_\ell)}{\Delta\omega} \ell \right] AC$$

The factor of 2 is necessary to take account of the fact that if  $\left( \frac{N_K - N_\ell}{\Delta\omega} \right) A \ell$  changes at a certain rate, the photon flux changes at half that rate.

We neglect the effects of upper level depopulation by spontaneous emission. In giant pulse experiments the pump serves to establish a condition of gain in the laser rod. During the times involved in giant pulse transients, of the order of tenths of a microsecond or less, the gain just before or immediately after the giant pulse has evolved will not be disturbed significantly by spontaneous emission, which in useful practical cases has lifetimes in the order of hundreds of microseconds.

We now consider the effect of incorporating into the above equation a lifetime for a terminal laser level,  $\ell$ , which we imagine being able to relax to a lower lying level by some undetermined mechanism. This latter transition may be radiative or non-radiative but is capable of being described by a relaxation time constant  $\tau$ . It follows immediately that the appropriate relationship is:

$$\frac{d}{dt} \left[ \frac{(N_K - N_\ell)}{\Delta\omega} A_\ell \right] = - 2\phi(\omega_{K\ell}, t) \left[ \alpha_0 \eta \hbar \omega_{K\ell} \frac{(N_K - N_\ell)}{\Delta\omega} \ell \right] A_c + \frac{N_\ell A_\ell}{\tau \Delta\omega} \dots (2-7)$$

We can now proceed to obtain the last relationship, forming -- together with the relationships (2-6) and (2-7) which we have just derived-- the complete set of rate equations. To this end we write the equation governing the population of level  $\ell$ ,

$$\frac{d}{dt} \left[ \frac{N_\ell A_\ell}{\Delta\omega} \right] = - \frac{N_\ell A_\ell}{\tau \Delta\omega} + \phi(\omega_{K\ell}, t) \left[ \alpha_0 \eta \hbar \omega_{K\ell} \frac{(N_K - N_\ell)}{\Delta\omega} \ell \right] A_c \dots (2-8)$$

Level  $\ell$  is being depopulated by de-excitation to a lower level and by resonant photon absorption transitions to level  $K$ . In addition it is being populated by stimulated transitions from level  $\ell$ . The above equation

quantitatively expresses these processes.

The rate equation for the photon density (2-6) can be rewritten in the following form:

$$\frac{d}{dt} \left[ \phi(\omega_{K\ell}, t) (L + (\eta - 1)\ell) A \right] = \phi(\omega_{K\ell}, t) \left[ \alpha_0 \eta \hbar \omega_{K\ell} \frac{(N_K - N_\ell)}{\Delta\omega} \ell - \gamma \right] A c \quad \dots(2-9)$$

We now make the following substitutions to simplify equations (2-7), (2-8) and (2-9). We let:

$$N = \frac{N_K - N_\ell}{\Delta\omega} \quad \Phi = \phi(\omega_{K\ell}, t) \left( \frac{L + (\eta - 1)\ell}{\ell} \right)$$

$$N_1 = \frac{N_\ell}{\Delta\omega} \quad \beta = \alpha_0 \eta \hbar \omega_{K\ell}$$

$$T_1 = \frac{L + (\eta - 1)\ell}{c}$$

We thus arrive at the following equations governing the photon flux, the population inversion and the laser terminal level population:

$$\frac{d\Phi}{dt} = \frac{\beta N \ell}{T_1} - \frac{\gamma}{T_1} \quad \dots(2-10)$$

$$\frac{dN}{dt} = -2 \frac{\Phi \beta N \ell}{T_1} + \frac{N_1}{\tau} \quad \dots(2-11)$$

$$\frac{dN_1}{dt} = \frac{\Phi \beta N \ell}{T_1} - \frac{N_1}{\tau} \quad \dots(2-12)$$

where  $T_1$  is the time per pass for a coherent photon in the cavity

$N$  is the population inversion per unit volume of the laser material

per unit angular frequency range.

$N_1$  is the population of the terminal level  $l$  per unit volume per unit angular frequency range.

$\phi$  is the coherent photon flux density per unit angular frequency range referred to the volume of laser material in the cavity.

$\beta$  may be considered to be a coefficient of amplification.

At this point we wish to summarize some of the noteworthy approximations involved in deriving equations (2-7), (2-8) and (2-9). The contribution to the laser output from spontaneous emission has been neglected. Spontaneous emission is eventually called upon only to establish the initial value of the photon density in the cavity (see Section 6.1 ).  $\gamma$  has up to this point been assumed to be constant. The following subsection will introduce a time dependence into  $\gamma$ . Further, we have dealt with the case of equal laser level degeneracies -- subsection (2.2-5) will consider the effects on the formulation of any such degeneracies.

The rate equations (2-7), (2-8) and (2-9) have been derived by assuming that the spectral shape of the spontaneous emission line is rectangular.  $\phi$  in equation (2-9) can be interpreted as the number of photons per unit volume of the cavity per unit angular frequency range averaged over the spectral width of the rectangular spontaneous emission line. If there are  $M$  cavity modes within the spectral width of the fluorescent line  $\Delta\omega$ , then

$$\frac{\phi \Delta\omega}{M}$$

is the number of photons per unit volume of the cavity per cavity mode.

For the assumed spectral shape, each cavity mode (on the average) contains the same number of photons. We thus see that, although no mention of cavity modes was made in arriving at equations (2-7), (2-8) and (2-9), the mode structure can nevertheless be accounted for in a first approximation on the basis of those rate equations.

#### 2.3-4 Introduction of A Time Dependent Loss Factor Into the Rate Equations-

In Q-switching experiments one is concerned with an externally controlled time-dependent loss factor; thus, in equation (2-10), we allow  $\gamma$  to become a factor of time and write:

$$\gamma = \gamma(t)$$

For the case of interest, namely Q-switching by employing a rotating Porro prism as one cavity reflector, the above substitution represents an approximation. The nature of the approximation is evident if one recalls that  $\gamma$  arose from considerations of cavity reflector reflectivity. We are assuming therefore that the losses due to reflector misalignment can be accounted for by attributing a variable reflectivity to plane-parallel aligned reflectors. The output of the laser, however, is calculated by taking into account the actual reflectivity of the output coupling reflector and the photon density in the cavity. The output is then proportional through the output reflector reflectivity to the photon density in the cavity. The minimum value of  $\gamma$  is simply  $-\ln R$  where  $R$  is the output reflector reflectivity. This case corresponds to perfect alignment of the Porro prism with respect to the output reflector.

$\phi_0$  changes at a rate given by:

$$\frac{d\phi_0}{dt} = \frac{\phi_0 \ln R}{T_1} \quad \phi_0 \text{ DEFINED ON PAGE 30}$$

due to output coupled into the beam, and changes at a rate given by:

$$\frac{d\phi_0}{dt} = - \frac{\gamma(t)\phi_0}{T_1}$$

due to output coupled into the beam and internal losses owing to Porro prism misalignment. The above assumptions are essential, if one is to proceed with the solution of the problem, since an "exact" formulation would be most difficult to achieve and even more so to solve.

### 2.3-5 The Rate Equations for $Nd^{+3}$ in Glass-

The set of rate equations (2-10), (2-11) and (2-12) have been idealized in more than one respect. Among the idealizations is the assumption that the two energy levels between which lasing takes place are of equal degeneracy or multiplicity. This assumption does not necessarily hold. In fact for  $Nd^{+3}$ -glass lasers it seems unlikely that it does hold. The net degeneracy of the  $Nd^{+3}$  upper level  ${}^4F_{3/2}$  is 4, while the net degeneracy of the terminal level  ${}^4I_{11/2}$  is 12. These two levels are split by interaction with the glass matrix. The upper level splits into two Kramers doublets, each being 2-fold degenerate. The detailed splitting of the  ${}^4I_{11/2}$  level is not clear. In any event, the formulation of the rate equations must take into account the degeneracies of the initial and terminal levels involved in the lasing transition.

If the lasing takes place between two levels, each belonging to a group of closely spaced levels, account must be taken of the fact that

those closely spaced levels may be thermally connected to each other.

In the case of  $Nd^{+3}$ -glass laser material, it is not unreasonable to assume that thermal equilibrium between the thermally connected levels is maintained, from instant to instant, during the period when lasing is taking place. If we attribute the energy level diagram shown in Figure (2-2) to the active ions of the laser material, the laser rate equations governing the system can be easily derived and shown to be:

$$\frac{d}{dt} [\phi(L + (\eta - 1)\ell)A] = \phi [\alpha_0 \eta \hbar \omega_{K\ell} \frac{(N_2/g_2 - N_4/g_4)}{\Delta\omega} \ell - \gamma(t)] Ac \quad \dots(2-13)$$

$$\frac{d[N_\ell/\Delta\omega A \ell]}{dt} = - \frac{N_\ell A \ell}{\tau \Delta\omega} + \phi [\alpha_0 \eta \hbar \omega_{K\ell} \frac{(N_2/g_2 - N_4/g_4)}{\Delta\omega} \ell] Ac \quad \dots(2-14)$$

$$\frac{d \left[ \frac{N_u A \ell}{\Delta\omega} \right]}{dt} = - \phi [\alpha_0 \eta \hbar \omega_{K\ell} \frac{(N_2/g_2 - N_4/g_4)}{\Delta\omega} \ell] Ac \quad \dots(2-15)$$

where

$$N_u = N_1 + N_2 = \text{upper level population}$$

$$N_\ell = N_3 + N_4 = \text{lower level population}$$

$$g_1 + g_2 = g_u = \text{upper level degeneracy}$$

$$g_3 + g_4 = g_\ell = \text{lower level degeneracy}$$

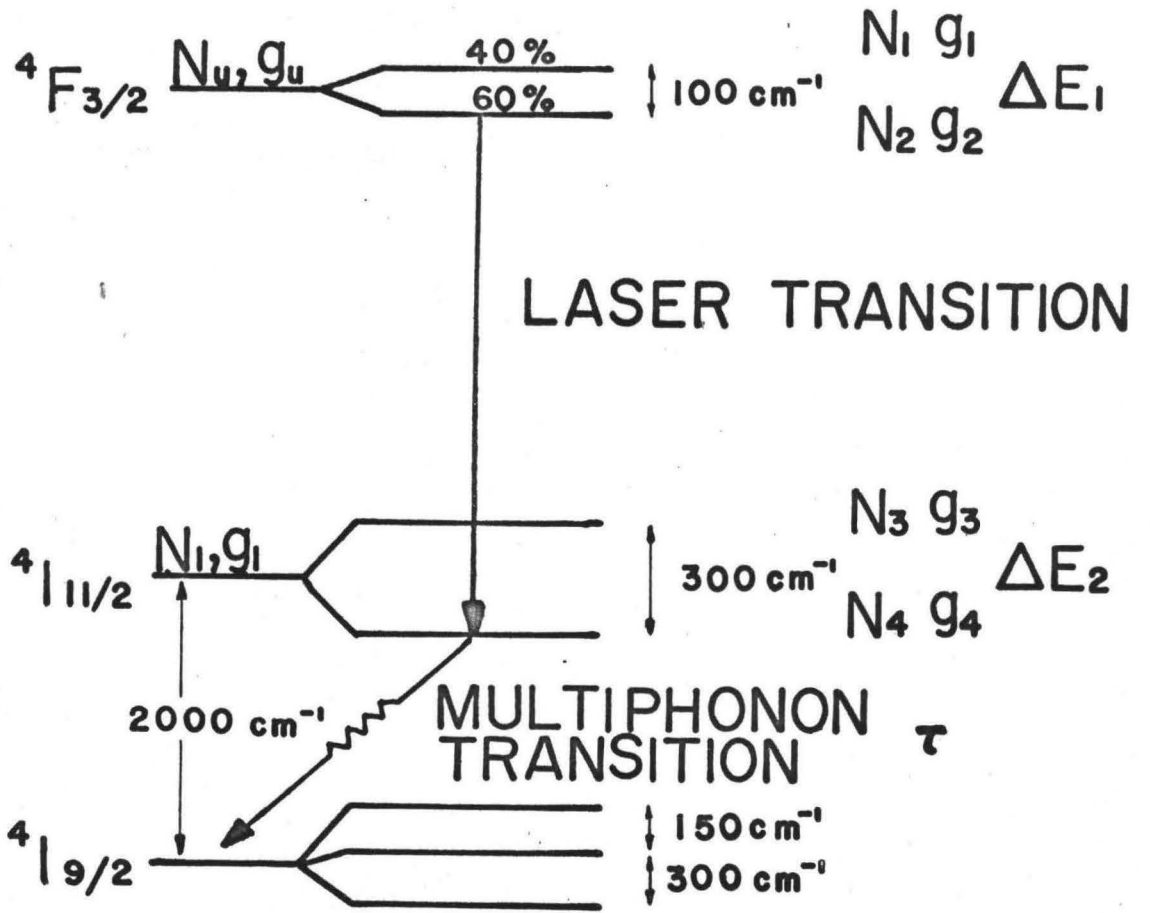
$$\frac{N_1}{g_1} = \frac{N_2}{g_2} e^{-\frac{\Delta E_1}{KT}} = \text{Boltzmann relation between levels } N_1 \text{ and } N_2$$

$$\frac{N_3}{g_3} = \frac{N_4}{g_4} e^{-\frac{\Delta E_2}{KT}} = \text{Boltzmann relation between levels } N_3 \text{ and } N_4$$

Figure (2-2)

The Four Energy Level System Described by the Rate  
Equations

The splittings and spectroscopic labels are those  
of  $\text{Nd}^{+3}$ -in-glass.



In the above equations account has been taken of the degeneracies  $g$  of the levels and it has been assumed that the close lying levels are instantaneously thermally connected to each other.

$\text{Nd}^{+3}$ -glass lasers have the energy level diagram represented in Figure (2-2) and so the rate equations above are applicable to the  $\text{Nd}^{+3}$  in glass system. The 12-fold degenerate terminal level  ${}^4I_{11/2}$  is split into two levels, broadly speaking, by the glass matrix<sup>(27)</sup>. The way in which the degeneracies are distributed among the two levels is not known. Thus, for  $\text{Nd}^{+3}$ -glass laser material, the relevant degeneracies of the terminal level  ${}^4I_{11/2}$  components are not available. It should be pointed out in this respect that in crystal fields of symmetry lower than cubic, all degeneracies of the  ${}^4I_{11/2}$ ,  ${}^4F_{3/2}$  that can be removed by the crystal field are removed<sup>(28)</sup>. It would seem then that the use of the rate equations, including the degeneracies, is foiled by this state of affairs. This is not entirely true, and to demonstrate our point we make the following substitutions into equations (2-13), (2-14) and (2-15):

$$N = \left( \frac{N_2}{g_2} - \frac{N_4}{g_4} \right) / \Delta\omega, \quad N_1 = \left( \frac{N_4}{g_4} \right) / \Delta\omega \quad \phi = \phi \left[ \frac{L + (\eta - 1) \ell}{\ell} \right]$$

$$\beta = \alpha_0 \eta \hbar \omega_{K\ell} \quad T_1 = \frac{L + (\eta - 1) \ell}{c} \quad K_1 = \frac{1}{g_4 + g_3} e^{-\frac{\Delta E_2}{KT}}$$

$$K_2 = \frac{1}{g_2 + g_1} e^{-\frac{\Delta E_1}{KT}}$$

and by making use of the relationships following equations (2-13), (2-14) and (2-15), we arrive at the simplified rate equations applicable to the laser material whose relevant energy levels are shown in Figure (2-2) namely;

$$\frac{d\phi}{dt} = \phi \left[ \frac{\beta N \ell}{T_1} - \frac{\gamma(t)}{T_1} \right] \quad \dots(2-16)$$

$$\frac{dN}{dt} = - \phi \frac{\beta N \ell}{T_1} [K_1 + K_2] + \frac{N_1}{\tau} \quad \dots(2-17)$$

$$\frac{dN_1}{dt} = \phi \frac{\beta N \ell}{T_1} K_1 - \frac{N_1}{\tau} \quad \dots(2-18)$$

The above rate equations are similar in form to the set (2-10), (2-11) and (2-12). The only difference lies in the appearance of  $K_1$  and  $K_2$  to take account of degeneracies and the thermal coupling between the close lying levels. Now, for the case of  $Nd^{+3}$ -glass material we may take:  $g_1 = g_2 = 2$  and  $\Delta E_1 \approx 110 \text{ cm}^{-1}$ . These data, together with the operating temperature, are sufficient to determine  $K_2$ . We can certainly place lower and upper bounds on  $K_1$ . To do this we recall that  $g_3 + g_4 = 12$ . The separation between the two levels originating from the  ${}^4I_{11/2}$  terminal level is  $\Delta E_2 \approx 300 \text{ cm}^{-1}$ . From the above considerations, the smallest possible value of  $K_1$  is  $\frac{1}{10 + 2 \times 0.24} = \frac{1}{10.5}$  where  $e^{-\Delta E_2/KT} = 0.24$  and the largest is  $\frac{1}{2 + 10 \times 0.24} = \frac{1}{4.4}$ . Therefore, a good estimate of  $K_1$  is  $\frac{1}{7.5} = 0.13$ .  $K_2$  has a value given by  $\frac{1}{2 + 2 \times 0.59} = 0.314$ . The estimates are based on room temperature operation. The approximation of instantaneous thermal equilibrium among the close lying sublevels is

valid if the longest relaxation time of the two sets of closely spaced sublevels is shorter than about 1 nsec., a value much shorter than the width of the giant pulse encountered both in theoretical and experimental observations. An estimate of the appropriate thermal relaxation rates is made in the Appendix. The calculation shows that the assumption of instantaneous equilibrium is justified.

## 2.4 Some Properties of the Q-Switched Laser

### Rate Equations:

#### 2.4-1 Normalization of the Rate Equations-

Before entering into a discussion of the properties of the set of rate equations (2-16), (2-17), and (2-18), it is convenient to normalize them. A natural unit for the measurement of the time evolution of the giant pulse is the time per pass of the photon beam in the cavity. It is also convenient to express  $\phi$ ,  $N$  and  $N_1$  in terms of dimensionless variables. To do this we define:

$$\begin{aligned}t &= T_1 T \\ \phi &= \epsilon_1 \phi_0 \\ N &= \epsilon_2 N_0 \\ N_1 &= \epsilon_3 N_{10}\end{aligned}$$

Equations (2-16), (2-17), and (2-18) may thus be reduced to the form:

$$\frac{d\phi_0}{dT} = \phi_0 (\beta \epsilon_2 \ell N_0 - \gamma(T))$$

$$\frac{dN_0}{dT} = -\phi_0 \beta N_0 \epsilon_1 \ell (K_1 + K_2) + \frac{\epsilon_3}{\epsilon_2} \frac{T_1 N_{10}}{\tau}$$

$$\frac{dN_{10}}{dT} = \frac{\epsilon_1 \epsilon_2}{\epsilon_3} \phi_0 \beta N_0 \ell K_1 - \frac{T_1 N_{10}}{\tau}$$

Since  $\epsilon_1$ ,  $\epsilon_2$ , and  $\epsilon_3$  are arbitrary we may choose their value at our discretion. Therefore, let:

$$\epsilon_1 = \frac{2}{\beta \ell (K_1 + K_2)} \quad \epsilon_2 = \frac{1}{\beta \ell} \quad \epsilon_3 = \frac{2K_1}{\beta \ell (K_1 + K_2)}$$

This yields:

$$\frac{d\phi_0}{dT} = \phi_0 (N_0 - \gamma(T)) \quad \dots(2-19)$$

$$\frac{dN_0}{dT} = -2 \phi_0 N_0 + \left( \frac{2K_1}{K_1 + K_2} \right) \frac{T_1 N_{10}}{\tau} \quad \dots(2-20)$$

$$\frac{dN_{10}}{dT} = \phi_0 N_0 - \frac{T_1 N_{10}}{\tau} \quad \dots(2-21)$$

These equations, in terms of normalized variables, are much simpler in form than the equations (2-16), (2-17) and (2-18), from which they result.

We note in particular that the factors  $\beta$  and  $\ell$  occurring in equations (2-16), (2-17) and (2-18), have been absorbed by the transformation and hence no longer appear in the above resulting equations. Further, the factors  $K_1$  and  $K_2$  appeared in equations (2-16), (2-17) and (2-18) as essentially separate entities. However, the transformation used to arrive at equations (2-19), (2-20) and (2-21) in effect groups the degeneracy factors  $K_1$  and  $K_2$  into a single term,  $\left( \frac{2K_1}{K_1 + K_2} \right)$ , appearing solely in equation (2-20). Hence, the effects on the solutions of the above equations, as a result of variations in the factor,  $\left( \frac{2K_1}{K_1 + K_2} \right)$ , are

relatively simple to visualize -- much more so than are the effects of variations in  $K_1$  and  $K_2$  on the solutions of equations (2-16), (2-17), and (2-18). In particular, we note that the term,  $\left(\frac{2K_1}{K_1+K_2}\right)$ , multiplies the quantity  $\frac{T_1 N_{10}}{\tau}$  -- a quantity which may be pictured as reinverting the population,  $N_0$ . Using our estimates of  $K_1$  and  $K_2$ , we see that  $\left(\frac{2K_1}{K_1+K_2}\right)$  is less than unity. We could arrive at the equations describing laser action between non-degenerate energy levels simply by setting the factor  $\left(\frac{2K_1}{K_1+K_2}\right)$  equal to unity in equation (2-20). Hence we may presume that the presence of the term  $\left(\frac{2K_1}{K_1+K_2}\right)$  in equation (2-20) slows down the re-inversion process which would exist in the non-degenerate case.

The equations, as derived above, are in the form that is used for their solution via numerical methods. They represent a description of a Q-switched  $\text{Nd}^{+3}$  in glass laser when appropriate values of  $K_1$ ,  $K_2$  and  $\tau$  are substituted into them.

#### 2.4-2 Behaviour of the Rate Equations Under Limiting

##### Terminal Level Lifetime Conditions -

Equations (2-19), (2-20) and (2-21) reduce, in two limiting cases, to what are essentially the equations of Wagner and Lengyel<sup>(17)</sup>. The first reduction takes place if we let  $\tau \rightarrow \infty$ . Equation (2-21) becomes redundant and we are left with:

$$\frac{d\phi_0}{dT} = \phi_0 (N_0 - \gamma(T))$$

$$\frac{dN_0}{dT} = -2 \phi_0 N_0$$

We now assume  $\gamma(T) = \text{constant} = -\ln R$ , and define the lifetime of a photon in the cavity as  $\tau_c$  where

$$\tau_c = \frac{T_1}{\gamma} = -\frac{T_1}{\ln R}$$

We let

$$\begin{aligned}\phi_0 &= \frac{1}{\eta_p} \frac{T_1}{\tau_c} \phi \\ N_0 &= \frac{1}{\eta_p} \frac{T_1}{\tau_c} n \\ T &= \frac{\tau_c T'}{T_1}\end{aligned}$$

32

and thus obtain:

$$\frac{d\phi}{dT'} = \left( \frac{n}{\eta_p} - 1 \right) \phi$$

$$\frac{dn}{dT'} = - \frac{2n\phi}{\eta_p}$$

The above equations are just those of Wagner and Lengyel<sup>(17)</sup>. The notation is the same as that employed by those authors. We notice that since  $T$  is measured in units of  $T_1$  -- the time per pass of a coherent photon in the cavity --  $T'$  is measured in units of  $\tau_c$  -- the lifetime of a coherent photon in the cavity. The second reduction takes place after replacing  $\phi_0$  by  $2\phi_0$  and allowing  $\tau \rightarrow 0$  in equations (2-19), (2-20) and (2-21). Physically, we know that this implies  $N_{10} \rightarrow 0$ . In fact  $N_{10}$  tends to zero faster than does  $\tau$  since, otherwise, by equation (2-21),  $N_{10}$  would have a finite growth or decay rate, implying that the terminal level, under limiting lifetime conditions, is capable of supporting a population, resulting in a contradiction. In taking the limit  $\tau \rightarrow 0$  we first allow  $N_{10} \rightarrow 0$ , noting that the factor of two in front of the stimulated emission term is now unity. We thus obtain the identical equations given by the case  $\tau \rightarrow \infty$  after replacing  $\phi_0$  by  $2\phi_0$  in the equations which result by letting  $\tau \rightarrow 0$ . In the latter case, the material no longer has gain when the populations of the upper and lower levels for laser action are equal, assuming equal upper

and lower level degeneracies, whereas in the former, the zero gain condition comes when both upper and lower populations are equal to zero. In the zero lifetime case, we obtain twice as much energy output as we do in the infinite lifetime case. In fact, all equivalent quantities of interest behave identically in both cases, except that the output power and energy in the case of  $\tau = 0$  are twice what they are for  $\tau = \infty$ . Note that  $N_0$  in the former case is related to the upper level population whereas, in the latter case, it is related to the difference in populations of the upper and lower levels.

#### 2.4-3 Some Properties of the Rate Equations of Wagner and Lengyel-

Certain useful concepts may be obtained by considering the simplified rate equations, resulting from the above mentioned limiting processes, namely:

$$\frac{d\phi_0}{dT} = \phi_0 (N_0 - \gamma(T)) \quad \dots(2-22)$$

$$\frac{dN_0}{dT} = -2 \phi_0 N_0 \quad \dots(2-23)$$

The quantities  $N_0$  and  $\phi_0$  will not change in time if the initial value of the flux density  $\phi_{oi}$  is zero.  $\phi_{oi}$  in the physical situation arises from spontaneous emission in the laser rod and can be estimated readily<sup>(17)</sup>. The calculation of  $\phi_{oi}$  is carried out in the Appendix.

In the simplest case  $\gamma(T)$  is thought of as a step switch going from a value  $\gamma(T < 0) > N_{oi}$  to a value  $\gamma(T > 0) < N_{oi}$ . An initial value is allocated to both  $\phi_0 = \phi_{oi}$  and  $N_0 = N_{oi}$ . In physical cases of interest  $\phi_{oi}$  is several orders of magnitude less than the peak value of  $\phi_0 = \phi_{op}$ .

Under these conditions  $N_o$  can be considered a constant during the build-up of  $\phi_o$  and equation (2-22) can be readily integrated to yield a pulse build-up time. The pulse build-up time can be arbitrarily defined as the time taken for the pulse to build up from its initial value  $\phi_{oi}$  to one one-hundredth of its peak value,  $\phi_{op}$ .  $N_{oi}$  does not begin to change significantly until  $\phi_o \sim \frac{\phi_{op}}{100}$ . For the pulse build-up region we have immediately:

$$\phi_o = \phi_{oi} e^{[N_{oi} - \gamma(T > 0)] T} \quad \dots(2-24)$$

From (2-22) and (2-23) we can obtain the phase plane equation:

$$\frac{d\phi_o}{dN_o} = - \frac{N_o - \gamma(T > 0)}{2N_o}$$

which can be integrated readily to yield:

$$\phi_o - \phi_{oi} = - \frac{1}{2} (N_o - N_{oi}) + \frac{\gamma(T > 0)}{2} \ln \frac{N_o}{N_{oi}} \quad \dots(2-25)$$

If  $\phi_o = \phi_{op}$  we have from equation (2-22) that

$$N_{op} = \gamma(T > 0)$$

Hence neglecting  $\phi_{oi}$  in comparison to  $\phi_{op}$  in (2-25) we obtain:

$$\phi_{op} = - \frac{1}{2} (N_{op} - N_{oi}) + \frac{\gamma(T > 0)}{2} \ln \frac{N_{op}}{N_{oi}}$$

This last relationship can be used to calculate the build-up time in conjunction with (2-24). The final value of  $N_o = N_{of}$  can also be found using (2-25). It is necessary that  $\phi_o = \phi_{of}$  be assumed close to zero. Since  $\phi_{oi}$  is also small we have immediately:

$$N_{oF} - N_{oi} = \gamma(T > 0) \ln \frac{N_{oF}}{N_{oi}} = N_{oP} \ln \frac{N_{oF}}{N_{oi}} \quad \dots(2-26)$$

The output energy of the pulse is proportional to  $N_{oi} - N_{oF}$ . A more detailed discussion of the coupled pair of differential equations (2-22) and (2-23) may be found in Wagner and Lengyel's paper<sup>(17)</sup>. Equation (2-26) states that the ratio  $\frac{N_{oF}}{N_{oi}}$  depends only on the ratio  $\frac{N_{oP}}{N_{oi}}$ . The energy utilization factor  $\frac{N_{oi} - N_{oF}}{N_{oi}}$  also depends only on  $\frac{N_{oP}}{N_{oi}}$ , the ratio of the loss factor to the initial population inversion.

The set (2-22) and (2-23), assuming a step function switch, is characterized by a single pulse output. On the other hand, the set (2-19), (2-20) and (2-21) can exhibit, for certain switching functions  $\gamma(T)$ , multipulse outputs. We may say quite generally that the multipulse outputs result if the switching function  $\gamma(T)$  is "slow". The multipulsing will be shown to be critically dependent on the relaxation lifetime of the terminal level for laser action. The sensitivity to multipulsing of the equations (2-19), (2-20) and (2-21), arising from a finite lifetime of the terminal level, will be used to advantage in the estimation of the terminal level lifetime of  $Nd^{+3}$  in glass.

#### 2.4-4 Qualitative Behaviour of the Solutions of the $Nd^{+3}$ in Glass Laser Rate Equations-

Let us consider qualitatively the behaviour of  $\phi_o$ ,  $N_o$  and  $N_{oi}$  as governed by equations (2-19), (2-20) and (2-21). From what has been said before about the switching function  $\gamma(T)$  characterizing a laser system using a Porro prism switch, we can assume that  $\gamma(T)$  rises monotonically on either side of the zero reference time point, which is assumed to be

located such that  $\gamma_{\min} = \gamma(0)$ . From symmetry arguments,  $\gamma(T)$  will be an even function of time. At a particular negative time  $T^-$  the condition:

$$N_{oi} = \gamma(T^-)$$

will hold for all non-trivial cases. For times  $T > T^-$  the pulse begins to build up.  $\phi_o$ , however, must reach a certain value before it begins to disturb a lower  $N_{oi}$ . It is only during a time interval  $\Delta T = 2|T^-|$  that an output pulse can occur. Thus, if  $\phi_o$  does not build up to a sufficient amplitude to disturb  $N_{oi}$  significantly in this time interval, no pulse as such will evolve. Switching can then be thought of as occurring too rapidly for the inversion  $N_{oi}$  that is assumed to be present. By decreasing the switching speed, and so increasing  $\Delta T$ , a point will be reached where  $\phi_o$  is given sufficient time to reach a large enough value to disturb  $N_{oi}$  significantly. In this case a pulse will evolve, but it will do so at a time where the losses are high and increasing. The pulse will go through one maximum which will be small in amplitude. A further increase in  $\Delta T$  allows the pulse to occur at a position in time where the losses are lower but still characterized by a positive time slope. The result is an increase in single pulse amplitude and energy. Eventually, if  $\Delta T$  is increased to approximately twice the value necessary just to obtain high switching speed cut-off, the pulse will evolve when  $\gamma(T) = \gamma_{\min} = \gamma(0)$  and the result will be the highest output energy and power content achievable in the pulse for the given initial inversion  $N_{oi}$ . A further increase in  $\Delta T$  results in a single pulse appearing before the switch has had the opportunity to decrease the losses to a minimum. The pulse then reverts to a situation characterized by lower energy and power content.

The pulse is now occurring at a time when the losses are decreasing but relatively high. If the losses are high enough and the lifetime of the terminal level short enough -- though longer than the giant pulse width -- we have a situation where the available energy will not be entirely released after the initial pulse. Because the losses are decreasing and re-inversion is taking place due to terminal level de-excitation, a time will come, as  $\Delta T$  continues to increase, when a secondary pulse will appear following the initial pulse. This pulse will carry energy and so the net output energy contained in both pulses will show an increase over the energy output obtained just prior to double pulse operation.

The value of  $\Delta T$  in a Porro prism Q-switched laser system is controlled by the rotational rate of the prism. For a given excitation of the laser rod a set value of  $N_{oi}$  is established. Upon monitoring the output energy content of the giant pulse for varying Porro prism rotational rates and constant laser rod excitation, we expect to observe the behaviour we have discussed above. This expectation is borne out by experiment.

## 2.5 Determination of the Population Inversion

### Necessary to Maintain Laser Action:

The expression derived in Section 2,3-2 for the condition met at threshold by a laser system contains the product of two unknowns: these are the population difference,  $N_K - N_\ell$ , and the dipole matrix element for the  $K \leftrightarrow \ell$  transition, hidden in the term  $\alpha_0$ . In order to calculate the inversion necessary to maintain laser action, we must determine the value of the dipole matrix element in terms of a directly measurable quantity.

Rearranging the expression for the spontaneous transition probability it follows that

$$|(\bar{r})_{K\ell}|^2 = \frac{1}{\tau_r} \frac{3\hbar c^3}{4e^2 \omega_{K\ell}^3 \eta^3} \quad \dots(2-27)$$

where  $\tau_r$  is the spontaneous radiative lifetime of level K, which is directly measurable in some cases<sup>(26)</sup>. Also, from equation (2-5) after substituting in for  $\alpha_0$  and rearranging terms, we can calculate  $|(\bar{r})_{K\ell}|^2$  in an alternate fashion to arrive at the expression:

$$|(\bar{r})_{K\ell}|^2 = - \ln r_1 r_2 \frac{3\hbar c \Delta\omega}{\ell \omega_{K\ell} \eta (N_K - N_\ell) 4\pi^2 e^2} \quad \dots(2-28)$$

The quantity  $\frac{N_K}{\Delta\omega}$  can be interpreted as the number of atoms or ions in stationary state K per unit angular frequency range per unit volume.  $E_K$  is thought of as varying slightly from atom to atom due to different environmental conditions acting on each particular atom or ion. A similar interpretation mutatis mutandis can be attached to  $\frac{N_\ell}{\Delta\omega}$ . With these interpretations, equation (2-28) can be used for calculations relating to a resonant transition exhibiting a relatively wide profile in angular frequency space, since  $\Delta\omega$  becomes the spontaneous line width of the transition.

The application of (2-28) to a  $\text{Nd}^{+3}$  in glass laser is particularly simple since, under normal lasing conditions, as opposed to Q-switched conditions, level  $\ell$  can be assumed to be essentially empty allowing one to set  $N_\ell \sim 0$  in equation (2-28);

Equations (2-27) and (2-28) provide us with two separate approaches for the calculation of the magnitude of the matrix element for electric dipole transitions. Alternately, if the radiative lifetime is known, and the reflectivity losses are the main contribution to the losses in the laser cavity and are also known, an estimate of the number of excited ions per unit angular frequency range in the upper state  $K$ , at threshold, may be obtained. This estimate can then be used to obtain an approximate value of stored energy in the rod as a function of pump energy, if the relation between pump energy and fluorescent output intensity is first determined experimentally. The stored energy estimate can then be used to determine the output energy in the case pertaining to Q-switched operation of the laser system. Eliminating  $|\langle \mathbf{r} \rangle_{K\ell}|^2$  by combining expressions (2-27) and (2-28) we obtain the threshold value of  $\frac{N_K}{\Delta\omega}$ , after setting  $N_\ell = 0$  -- a condition applicable to  $\text{Nd}^{+3}$  in glass laser material -- namely:

$$\left(\frac{N_K}{\Delta\omega}\right)_{\text{THRESHOLD}} = -\ln(r_1 r_2) \frac{\tau_r \omega_{K\ell}^2 \eta^2}{c^2 \pi^2 \ell} \dots (2-29)$$

The fact that the terminal level is assumed to be empty is responsible for the lack of dependence of the threshold condition on the level degeneracies. An interesting point is brought out by equation (2-29) namely, that the longer the radiative lifetime, the greater the number of atoms that need to be excited into the upper level for laser action by the pump source. The reason for this result is that the matrix element involved in stimulated emission is the same one which arises in spontaneous emission; therefore, the shorter the spontaneous lifetime the

larger will be the stimulated emission matrix element. A laser system can thus afford to lose more coherent photons per second the shorter the radiative lifetime, while still maintaining oscillation, since coherent photons will then be created by stimulated emission at a faster rate. Alternately, with equal losses, the shorter lifetime results in a lower requirement on the degree of excitation. The pumping requirements, however, will be more stringent for the case of a short spontaneous lifetime, since spontaneous emission can then become significant as a mechanism for losing excited ions. Thus, given a pump pulse of time half-width  $T_p$ , the optimum spontaneous lifetime would be close to  $\tau_r \approx 3T_p$ , approximately. This condition would allow adequate integration of the pump pulse by the upper level for laser action, without destroying the advantages of a short radiative lifetime. It is also evident from equation (2-29) that a narrow fluorescent line width is desirable. Doubling the width of the fluorescent line requires twice as many atoms or ions to maintain the system at threshold. The fluorescent line becomes in essence a gain profile as a function of wavelength. Equation (2-29) also indicates that ideal geometry is obtained by having a long laser rod with a small cross-sectional area. This result will hold as long as diffraction losses are not overly increased due to the decrease of the cross-sectional area. The angular frequency dependence indicates that threshold is easier to achieve at low laser operating frequencies. From a pumping standpoint it is also desirable to operate at low frequencies and between deep lying levels.

An application of equation (2-29), employing experimentally determined values of threshold and mirror reflectivity applicable to the laser

system used for the work presented in this thesis yields a Q-spoiled output energy prediction in good agreement with that obtained experimentally. The output energy calculation, based on equation (2-29), will be demonstrated at a later stage in this thesis.

The derivation of equation (2-29) follows similar lines to those employed by Yariv and Gordon<sup>(29)</sup> to calculate the threshold condition for both Gaussian and Lorentzian line-profiles. Those authors find that somewhat different inversion requirements are to be met in each case. For equal line widths, the Gaussian line-profile requires an inversion which is less by a factor of  $\sqrt{\pi \ln 2}$  than does the Lorentzian line-profile. Our calculation of the inversion requirement to just maintain oscillation was based on a rectangular line-profile and the result of the calculation falls between the results for the Gaussian and Lorentzian line-profiles as obtained by Yariv and Gordon<sup>(29)</sup>.

## CHAPTER 3

### MODES IN ANGULAR LIMITED RESONATORS

#### 3.1 Introduction:

In Section 1.3 we indicated that this Thesis would be partly concerned with the electromagnetic field distribution within a symmetrical two reflector cavity containing an angular selective device. In this Chapter the relationship governing the field distribution in such a cavity will be developed and solutions based on it obtained. In particular, the case of rectangular and also circular interferometer geometry will be treated. The problem, though not directly pertinent to the experimental work leading to this Thesis, is of considerable interest in situations where it is desired to discriminate against competing transverse modes in a laser system. The solution will indicate a means by which the diffraction losses, for all modes but one, may be increased over those which would exist in an identical cavity without an angular selective device within it. The increased losses, for all but one transverse mode, make it more likely that only this unperturbed mode will build up in such a laser cavity containing an appropriately-adjusted angular selective device. An idea of the desirability of single transverse mode operation of a laser system may be gained by noting that the transverse modes in a laser beam govern the distribution of energy in the far-field pattern of the beam. The larger the number of transverse modes forming

the beam, the greater will be the spread of the beam as it travels in space. Thus, for example, in long range communications systems using laser beams for transmitting information, it is desirable to operate in the single transverse-mode configuration. This will allow more efficient concentration of the available energy onto the receiver entrance pupil. In the field of optical harmonic generation, such single transverse-mode operation may also be desirable, since in certain cases a well-collimated beam leads to increased conversion efficiency from fundamental to harmonic<sup>(30)</sup>.

### 3.2 Rectangular and Circular Plane Parallel

#### Symmetric Resonators with Angular Limiting

##### Devices - Formulation of the Problem:

#### 3.2-1 Rectangular Plane Parallel Resonators-

In order to proceed with the formulation of the problem presented, namely, when it is desired to find the steady state field distribution and the propagation constant of the field within symmetrical cavities containing an angular limiting device, it is necessary to consider some relations obeyed by waves in three-dimensional space. It is well known<sup>(31)</sup> that waves in three-dimensional space may exist as plane waves, cylindrical waves with the motion and space dependence in planes perpendicular to the cylinder axis, and in addition more general waves where the variation in space is neither linear nor planar. All these waves may be built up by a superposition of plane waves. For simple harmonic waves  $\Psi = \psi e^{-i\omega t}$ , with  $\psi$  a solution of the three-dimensional Helmholtz equation,

$$\nabla^2 \psi + K^2 \psi = 0$$

it can be shown that the most general solution  $\psi_K(x, y, z)$  of the Helmholtz equation can be written (31):

$$\psi_K(x, y, z) = \int_0^{2\pi} dv \int \sin u \, du \, A(u, v) e^{i\mathbf{K} \cdot \mathbf{r}}$$

where the spherical angle  $u$  is the angle between the propagation vector  $\mathbf{K}$  and the  $z$ -axis, and the spherical angle  $v$  is the angle between the  $\mathbf{K} - z$  plane and the  $x - z$  plane.  $A(u, v)$  is a function to be determined from the conditions imposed by the particular problem being considered. Its dimensions are field amplitude per unit solid angle.  $\mathbf{r}$  is the radius vector to the observation point and  $\mathbf{K}$  is the propagation vector with magnitude  $|\mathbf{K}| = \omega/c$ . The integration is carried out over the surface of the unit sphere in  $\mathbf{K}$ -space since the magnitude of  $\mathbf{K}$  is fixed. The integration over  $u$  may be from 0 to  $\pi$  or it may extend into the complex  $u$  plane. The latter situation takes account of the possibility of the existence of evanescent waves which may be necessary for the fitting of boundary conditions (32). These waves are of little interest to us because they only exist close to current sources and carry away no energy from those sources. In what follows we will assume that the integration over  $u$  is from 0 to  $\pi$  and, by so doing, neglect the presence of evanescent waves. We will drop the subscript  $K$  from  $\psi$ , it being implicitly assumed that we are dealing with field distributions created by single frequency sources.

We may expand the term  $\mathbf{K} \cdot \mathbf{r}$ ; the result, after expressing  $\mathbf{r}$  in

cartesian co-ordinates, is:

$$\underline{K} \cdot \underline{r} = |\underline{K}| (x \sin u \cos v + y \sin u \sin v + z \cos u)$$

The field distribution then becomes:

$$\psi(x,y,z) = \int_0^{2\pi} dv \int_0^{\pi} \sin u \, du \, A(u,v) e^{iK(x \sin u \cos v + y \sin u \sin v + z \cos u)}$$

where

$$|\underline{K}| = K \quad \dots(3-1)$$

Let us consider a well collimated beam traveling along the positive z-axis. The function  $A(u, v)$ , for such a beam, is non-zero only close to  $u = 0$ . It is assumed to be collimated well enough so that we may set  $\sin u = u$  and  $\cos u = 1 - \frac{u^2}{2}$  in equation (3-1) without significantly affecting the result of the integration. Furthermore,  $A(u, v)$  is assumed to decrease rapidly enough to allow the limits of integration of  $u$  to be replaced by  $(0, \infty)$ . It follows that:

$$\psi(x,y,z) = \int_0^{2\pi} dv \int_0^{\infty} u \, du \, A(u,v) e^{iK(xu \cos v + yu \sin v + z(1 - \frac{u^2}{2}))}$$

We now let

$$X = u \cos v, \quad Y = u \sin v$$

Hence:

$$\psi(x,y,z) = \int_{-\infty}^{\infty} \int_{-\infty}^{\infty} dXdY \, A(X,Y) e^{iK(xX + yY + z(1 - \frac{X^2 + Y^2}{2}))} \quad \dots(3-2)$$

We now consider the field distribution in the x-y plane. In order to do so let us put  $z = 0$  in equation (3-2) to obtain:

$$\frac{\psi(x, y, 0)}{2\pi} = \frac{1}{2\pi} \int_{-\infty}^{\infty} \int_{-\infty}^{\infty} dXdY A(X, Y) e^{iK(xX + yY)} \quad \dots(3-3)$$

The above integral is a two-dimensional Fourier integral relating the field distribution on the x-y plane to its angular spectrum A(X, Y).

Inverting equation (3-3) we have for A(X, Y):

$$A(X, Y) = \frac{K^2}{(2\pi)^2} \int_{-a}^a \int_{-b}^b dx dy \psi(x, y, 0) e^{-iK(xX + yY)} \quad \dots(3-4)$$

The limits a and b arise, rather than the usual infinities, because the field distribution is thought of as being zero outside the rectangular aperture defined by those limits. We may think of the aperture as a rectangular opening in a completely absorbing screen located in the x-y plane. The aperture is considered to be illuminated by a well-collimated beam traveling in the positive z-direction and incident on the aperture from the negative z-portion of space. The field distribution in the positive z-portion of space is then given by equation (3-2) where A(X, Y) is defined by equation (3-4).  $\psi(x, y, 0)$  becomes the field amplitude on the aperture seen from the positive z-portion of space and is limited by the aperture boundaries.

If we locate an identical screen parallel to and a distance d away from the first screen along the positive z-axis, and further position the second screen symmetrically with respect to the first screen, we obtain the amplitude of the field at the second aperture as:

$$\psi(x, y, d) = \int_{-\infty}^{\infty} \int_{-\infty}^{\infty} dXdY A(X, Y) e^{iK(xX + yY + d(1 - \frac{X^2 + Y^2}{2}))}$$

for

$$-a \leq x \leq a, \quad \text{and} \quad -b \leq y \leq b$$

The above equation was obtained under the assumption that all the plane-wave components propagating through the first aperture are allowed to contribute to the field amplitude at the second aperture. However, if we consider that a device is introduced between the two screens which strongly attenuates any plane-wave with a propagation vector whose direction is not contained within the square,

$$-\Delta_1 \leq X \leq \Delta_1, \quad -\Delta_2 \leq Y \leq \Delta_2$$

we may write for the field amplitude at the second aperture:

$$\psi(x, y, d) = \int_{-\Delta_1}^{\Delta_1} dX \int_{-\Delta_2}^{\Delta_2} dY A(X, Y) e^{iK(xX + yY + d(1 - \frac{X^2 + Y^2}{2}))}$$

for

$$-a \leq x \leq a, \quad \text{and} \quad -b \leq y \leq b$$

The above expression simply assumes complete attenuation outside the square.

Let us assume that we may write:

$$A(X, Y) = B(X) C(Y)$$

It follows that:

$$\psi(x, y, d) = \psi_B(x, d) \psi_C(y, d)$$

where

$$\psi_B(x, d) = \int_{-\Delta_1}^{\Delta_1} dX B(X) e^{iK(xX + d(\frac{1 - X^2}{2}))}$$

$$\psi_C(y, d) = \int_{-\Delta_2}^{\Delta_2} dY C(Y) e^{iK(yY + d(\frac{1 - Y^2}{2}))}$$

....(3-5)

Also from equation (3-4):

$$B(X) = \frac{K}{2\pi} \int_{-a}^a dx \psi_B(x, 0) e^{-iK(xX)}$$

$$C(Y) = \frac{K}{2\pi} \int_{-b}^b dy \psi_C(y, 0) e^{-iK(yY)} \quad \dots(3-6)$$

The manipulations undertaken above allow the separation of the two-dimensional rectangular aperture problem into two one-dimensional problems. It is not difficult to show that each of the one-dimensional problems is in fact the formulation that results from considering the case of infinite strip apertures of dimensions  $2a$  and  $2b$  respectively, and an appropriate angle limiting device.

At this point we impose on the field distribution  $\psi_B(x, d)$  the following restriction:

$$\psi_B(x, d) = \lambda \psi_B(x, 0) \text{ for } -a \leq x \leq a \quad \dots(3-7)$$

This implies, if we allow  $\lambda$  to be a complex number, as we must, that the acceptable field distributions are those which propagate from the first infinite strip aperture, and arrive at the second infinite strip aperture, to create the same field distribution present at the first infinite strip, except for an overall phase shift and some attenuation. A similar argument and restriction can be applied to considerations of the  $y$ -co-ordinate variations of the field.

The restriction on the field distribution introduces the concept of cavity transverse modes<sup>(33)</sup>. It can be shown that a cavity, produced by two plane-parallel infinite and symmetrically-placed strip reflectors,

has the same effect on a propagating beam's field distribution, as does an infinite number of geometrically identical apertures cut in absorbing screens, separated from each other by the distance separating the reflectors<sup>(33)</sup>. It follows mutatis mutandis that the same is true for the cavity containing an angular selective device. Furthermore, condition (3-7), together with equations (3-5) and (3-6), defines the cavity modes of an infinite strip cavity containing an angular selective device having the properties assumed in the derivation of equation (3-5). The property attributed to the angular selective device of allowing only those plane-wave components, whose propagation vectors have directions in the range  $-\Delta_1 \leq X \leq \Delta_1$ , to contribute at the second aperture, is a special case of optical filtering<sup>(34)</sup>. This particular type of filtering is of interest because it results in high losses for those cavity transverse modes having field distributions that have off-axis propagation vector bundles not falling within the bandpass,  $-\Delta_1 \leq X \leq \Delta_1$ , of the filter. In general, the higher the order of the transverse mode, the more off-axis its propagation vector bundles become. Hence, by judicious choice of the filter bandpass, it is possible to allow only the lowest order mode to propagate essentially unattenuated by the low pass filter. The filtering action of the angular selective device leads, then, to transverse mode selection. It is this property that makes the consideration of cavities containing angular selective devices worthwhile.

Combining equations (3-5), (3-6) and (3-7) we arrive at the following equality after dropping from the notation the distance dependence of the field amplitudes:

$$\lambda\psi(x) = \frac{K}{2\pi} \int_{-\Delta_1}^{\Delta_1} dX \int_a^a dx' \psi(x') e^{-iK(X(x-x') + d(\frac{1-x^2}{2}))}$$

We assume that we can change the order of integration and by so doing write:

$$\lambda\psi(x) = \frac{K}{2\pi} e^{iK\frac{d}{2}} \int_a^a \psi(x') K(x, x') dx' \quad \dots(3-8)$$

where

$$K(x, x') = \int_{-\Delta_1}^{\Delta_1} e^{iK(X(x-x') - \frac{dX^2}{2})} dX \quad \dots(3-9)$$

Equation (3-8) is a homogeneous linear integral equation of the second kind and has the properties thereof<sup>(35)</sup>. Non-zero solutions of equation (3-8) result only for certain complex values of the quantity  $\lambda$ . Those values are the characteristic numbers, or eigenvalues, of the kernel  $K(x, x')$ . The solution corresponding to a particular eigenvalue is the eigenfunction associated with that eigenvalue. The eigenfunctions associated with different eigenvalues are linearly independent.

The expression for the kernel equation (3-9) can be obtained explicitly by performing the appropriate integration<sup>(36)</sup>. The result is:

$$K(x, x') = \sqrt{\frac{\pi}{Kd}} \{ C[\alpha] - C[\beta] - i(S[\alpha] - S[\beta]) \} e^{\frac{iK(x'-x)^2}{2d}} \quad \dots(3-10)$$

where,

$$\alpha = \sqrt{\frac{1}{\pi Kd}} (Kd\Delta_1 + (x' - x) K)$$

$$\beta = \sqrt{\frac{1}{\pi Kd}} (-Kd\Delta_1 + (x' - x) K)$$

The functions  $C(z)$  and  $S(z)$  are defined by:

$$C(z) = \int_0^z \cos\left(\frac{\pi t^2}{2}\right) dt, \quad S(z) = \int_0^z \sin\left(\frac{\pi t^2}{2}\right) dt$$

and will be recognized as the Fresnel integrals.

It can be shown quite simply that the integral equation (3-8) has solutions which depend only on two dimensionless parameters. One of these parameters is the Fresnel number<sup>(33)</sup> given by:

$$N = \frac{a^2}{d\lambda}$$

The other is a dimensionless number,  $A$ , given by the expression:

$$A = \frac{2\pi d\Delta_1^2}{\lambda}$$

which we may call the angular number of the angular selective device.

At this point we estimate the minimum value of  $\Delta_1$  that results in low losses for the lowest order propagating mode. Let us call that value  $\Delta_{1c}$ . Recalling the diffraction limit of an infinite strip aperture we can write for the critical angle  $\Delta_{1c}$  the following expression:

$$\Delta_{1c} \approx \frac{\lambda}{2a}$$

where we have assumed that the angular width of the lowest-order even mode of the infinite strip cavity is not significantly different from the diffraction limit of a strip aperture of width  $2a$ . If  $\Delta_1$  is made smaller than  $\Delta_{1c}$  we begin to introduce strong attenuation of the lowest order mode. On the other hand, if  $\Delta_1$  is made larger than  $\Delta_{1c}$  we may begin to allow the propagation of higher order modes without attenuating them significantly.

The critical product of N and A is obtained if A is evaluated using  $\Delta_1 = \Delta_{1c}$ . The critical product is estimated to be  $(NA)_c \approx \frac{\pi}{2}$  which is independent of the cavity parameters.

If  $\Delta_1$  is allowed to tend towards infinity the kernel of the integral equation (3-8) yields the kernel obtained by Fox and Li, for the infinite strip cavity, as it should.

### 3.2-2 Circular Plane Parallel Resonators-

We now consider in less detail the problem of a cavity formed by two identical plane-parallel circular reflectors placed symmetrically with respect to each other, with an angular selective device introduced between them. This case presents a complication. The indefinite integral required to undertake the step equivalent to that which we took in the case of the rectangular resonator, to arrive from equation (3-9) to equation (3-10) is not available in closed form. However, we will be able to derive the result obtained by Fox and Li for the circular plane-parallel cavity as a limiting case. We may write:

$$\psi(x,y,z) = \int_0^{2\pi} dv \int_0^{\infty} u du A(u,v) e^{iK(xu \cos v + yu \sin v + z(1 - \frac{u^2}{2}))}$$

by proceeding as we did previously in considering the case of the rectangular cavity. We introduce the change of variables;

$$x = r \cos \theta$$

$$y = r \sin \theta$$

and consider the field distribution in the  $r - \theta$  plane and so obtain:

$$\underline{\psi}(r,\theta,0) = \int_0^{2\pi} dv \int_0^{\infty} u du A(u,v) e^{iKur \cos(v - \theta)} \quad \dots(3-11)$$

We write:

$$A(u, v) = U(u) e^{-inv} \quad \text{with } n \text{ an integer,}$$

and we employ the following integral relation for the Bessel functions<sup>(35)</sup>:

$$J_n(Kr_1 r_2) = \frac{1}{2\pi} e^{-in(\frac{\pi}{2} - \phi_2)} \int_0^{2\pi} e^{iKr_1 r_2 \cos(\phi_1 - \phi_2) - in\phi_1} d\phi_1$$

Where  $J_n$  is the Bessel function of the first kind of integer-order  $n$ .

Equation (3-11) then reduces to:

$$R(r, 0) = 2\pi e^{in\frac{\pi}{2}} \int_0^\infty u du U(u) J_n(Kur)$$

Where

$$\psi(r, \theta, 0) = R(r, 0) \theta(\theta) \quad \text{and} \quad \theta(\theta) = e^{-in\theta}$$

We are now in a position to solve for  $U(u)$  by making use of the Fourier Bessel formula<sup>(37)</sup>.

$$f(\rho) = \int_0^\infty S J_n(S\rho) dS \int_0^\infty t f(t) J_n(St) dt$$

We obtain, on applying it to the expression for  $R(r, 0)$ :

$$U(\rho) = \frac{K^2}{2\pi} e^{-in\frac{\pi}{2}} \int_0^a R(r, 0) J_n(Kr\rho) r dr$$

The upper limit of the integral has been changed to  $a$  since  $R(r)$  is non-zero only for  $r \leq a$ . The  $\theta$  variation of the field is independent of  $z$  and is given by  $\theta(\theta) = e^{-in\theta}$ . It follows that we need to solve only for  $R(r, d)$  where  $d$  is the distance separating the two reflectors. As before, we assume that an angular selective device is introduced in the cavity

which attenuates completely those plane wave components whose propagation vectors  $\underline{k}$  have directions not falling within the range  $u \leq \Delta$ . Therefore:

$$R(r,d) = K^2 \int_0^{\Delta} u du J_n(Kur) e^{iKd(1 - \frac{u^2}{2})} \int_0^a R(r',0) J_n(Kr'u) r' dr'$$

We assume further that we can change the order of integration without affecting the final result and so obtain:

$$R(r,d) = K^2 e^{iKd} \int_0^a R(r',0) r' dr' \int_0^{\Delta} u du J_n(Kur) J_n(Kr'u) e^{-iKd \frac{u^2}{2}}$$

We now require that

$$R(r, d) = \lambda R(r, 0)$$

We thus obtain:

$$\lambda R(r, 0) = K^2 e^{iKd} \int_0^a R(r', 0) K(r', r) r' dr' \quad \dots (3-12)$$

where

$$K(r', r) = \int_0^{\Delta} u du J_n(Kur) J_n(Kr'u) e^{-iKd \frac{u^2}{2}}$$

Equation (3-12) is the integral equation governing the allowed steady state field distribution on the surface of the reflectors of the circular plane parallel cavity containing an angular limiting device. If we let  $\Delta \rightarrow \infty$  the integral expression for the kernel can be obtained in closed form. (38)

The result, in this limiting case, is that equation (3-12) becomes the Fox and Li result for the circular plane parallel cavity, as it should.

To show this we must use the following expression:

$$\int_0^{\infty} u du J_n(Kur) J_n(Kr'u) e^{-iKd \frac{u^2}{2}} = \frac{e^{-i \frac{\pi}{2} (n+1)}}{Kd} J_n\left(\frac{Kr'r}{d}\right) e^{iK \left[ \frac{(r^2+r'^2)}{2d} \right]}$$

which is not available as an indefinite integral. It yields immediately on substitution into equation (3-12)

$$\lambda R(r,0) = \frac{K}{d} e^{i \left[ Kd - \frac{\pi}{2} (n+1) \right]} \int_0^a R(r',0) r' dr' J_n\left(\frac{Kr'r}{d}\right) e^{\frac{iK}{2d} [r^2+r'^2]}$$

The above integral equation is the Fox and Li result governing the modes of the circular plane parallel cavity. The derivation undertaken above differs considerably from that of those authors.

### 3.3 Solution of the Integral Equation Governing the Steady State Field Distribution in a Cavity Formed by Two Infinite Strip Reflectors and an Angular Limiting Device:

The solution of equation (3-8) has been carried out numerically with the aid of a high-speed digital computer. The solution has been taken only up to the point necessary to demonstrate the transverse mode selecting properties of an angular limiting device introduced within a cavity. In particular, the Fresnel number range ( $1 < N < 15$ ) has been covered. The angular numbers used in the calculations were allowed to vary on either side of the critical product  $(NA)_c$  for  $N \sim 3$ . Only the lowest-order even transverse mode field distributions, together with the corresponding power losses per transit and phase shifts per transit, were obtained. The solution of equation (3-8) is discussed in this Section.

We intend to consider now some of the properties possessed by the

integral equation (3-8). It is not difficult to see from physical arguments, or from the fact that the kernel being considered is the sum of an odd and an even function of  $x'$ , that the eigenfunction solutions are either odd or even.

It is also not difficult to show that the kernel of equation (3-8) is symmetric:

$$K(x, x') = K(x', x)$$

The eigenfunctions of symmetric kernels have important properties. In particular, when the kernel is continuous and symmetric the eigenfunctions are orthogonal to each other over the range  $(a, b)$  where  $a$  and  $b$  are the limits of integration in the linear homogeneous Fredholm integral equation of the second kind<sup>(39)</sup>.

The orthogonality condition for equation (3-8) can be written:

$$\int_{-a}^a \psi_m(x) \psi_n(x) dx = 0 \quad m \neq n$$

We have assumed that to each eigenvalue,  $\lambda$ , there corresponds one and only one eigenfunction. Physically, the assumption is not unreasonable. We also have at our disposal the following theorem: "Any function which can be generated from a continuous function  $\phi(x)$  by the operation

$$\int_{-a}^a K(x, \epsilon) \phi(\epsilon) d\epsilon \quad \text{where } K(x, \epsilon) \text{ is continuous and symmetric}$$

so that

$$f(x) = \int_a^b K(x, \epsilon) \phi(\epsilon) d\epsilon$$

for some continuous function  $\phi$  can be represented over  $(a, b)$  by a linear

combination of the eigenfunctions  $\psi_1, \psi_2, \psi_3, \dots$  of the homogeneous Fredholm integral equation of the second kind with  $K(x, \epsilon)$  as its kernel"<sup>(39)</sup>

Furthermore if the kernel is non-separable, hence yielding an infinite number of eigenfunctions, the resultant infinite series converges absolutely and uniformly in the interval  $(a, b)$ <sup>(39)</sup>. This theorem is directly applicable to equation (3-8) if we assume that the kernel is non-separable. We make the assumption purely on physical grounds, basing it on the infinite number of degrees of freedom that the field distribution on the aperture may possess. It follows then that we may expand any continuous function in the interval  $(-a, a)$  in terms of the eigenfunctions of the kernel of equation (3-8) which are assumed to form a complete set.

We can define the mode content of a field distribution as the value of the coefficient multiplying the particular mode of interest in the series expansion of the field in terms of the eigenfunctions of the kernel. From physical arguments, the magnitudes of the eigenvalues of equation (3-8) are all less than unity. The largest eigenvalue corresponds to the lowest-order mode since it will be by definition the mode with the lowest amplitude at the reflector edges and hence, will be characterized by the lowest "spill over" losses. It follows immediately that any arbitrary field distribution, initiated at the first aperture, yields a field distribution at the second aperture whose lowest-order mode content is enhanced relatively to the higher order mode contents. It has been implicitly assumed that the field distribution at the first aperture does, in fact, have lowest-order mode content.

If we now imagine that the field distribution at the second aperture is transposed to the first aperture and again calculate the

effect of this distribution on the second aperture we conclude that we can continue to enhance the lowest order mode content of the resultant distribution by repeating the process several times. Physically, this represents the behaviour of the field distribution as the electromagnetic energy in the cavity travels back and forth between the two infinite strip reflectors suffering, in each pass, the effects of the angular limiting device. In the limit of an infinite number of passes, the only mode content that will remain will be the lowest order one.

The above description is directly applicable to the numerical solution of the integral equation (3-8) and the method was first used by Fox and Li to solve for the lowest-order even and the lowest-order odd modes of the infinite strip cavity without an angular selective device<sup>(33)</sup>. We have used the same method of solution to obtain the lowest-order even mode of the infinite strip cavity with an angular limiting device. Any initial field distribution may be used. However, it is advantageous to start with an even field distribution since odd-mode contents are then excluded automatically and hence the solution will converge faster to the lowest-order even mode.

The orthogonality relation satisfied by the modes can be used to advantage in seeking, for instance, the second-lowest-order even mode. We have not used that relation, but it is worth while sketching the method to be used for higher order mode calculations. From an exact mathematical point of view, given an even field distribution, it is sufficient by means of the orthogonality relation to erase the lowest-order even mode content from the given field distribution and then simply proceed with the calculation by iterating the resulting field distribution. However, from a

numerical method's point of view, we need repeatedly to erase any lowest-order even mode content that enters from numerical inexactitude after each pass of the field distribution. The solution will then converge to the next lowest-order even mode because the resultant field distribution will be the even-field distribution obtained having the lowest losses, with the restriction that it has no lowest-order even mode content. The argument can be extended to apply to higher and higher even-order mode solutions; but the calculations become lengthier the higher the order of the mode desired. The argument applies mutatis mutandis to odd modes after one has obtained the lowest-order odd mode solution.

Some details of the calculations will now be outlined. The range  $(-a, a)$  of the field distribution was sampled uniformly at 81 points. The kernel of equation (3-8) was also evaluated at  $81^2 = 6561$  points. Each point on the uniform grid had associated with it the real and the imaginary portion of the quantity of interest. The larger the number of samples within the range, the larger the value of Fresnel number that can be covered in the calculations since the magnitude of the Fresnel number determines the number of periodic fluctuations of the kernel in the range of integration. The ultimate limitation on the sampling frequency is the storage capacity of the computer since to speed up the numerical calculation the kernel should only be calculated once at the appropriate points of interest and the values obtained stored. The numerical integrations were carried out employing the closed type eleven-point Newton-Cotes Formula eight times, thus covering the entire range of integration  $(-a, a)^{(36)}$ . In this type of formula the error vanishes if the function being integrated is a polynomial of degree not greater than 10.

The overall features of the solutions of the infinite strip cavity with an angular selective device are best presented in graphical form. The eigenvalues corresponding to the lowest-order even modes of the cavity are particularly amenable to this type of presentation. In Figure (3-1) we have plotted the power loss per transit, as a function of the Fresnel number of the cavity for three values of the angular number. We define the power loss per transit by the relationship:

$$\begin{aligned} \text{Power loss per Transit} &= \frac{\text{Input Power} - \text{Output Power}}{\text{Input Power}} \times 100\% \\ \text{(percent)} & \\ &= (1 - |\lambda|^2) \times 100\% \end{aligned}$$

The Fox and Li results for an infinite strip cavity without an angular limiting device (angular number  $\rightarrow \infty$ ) are shown for comparison. The corresponding phase shifts per transit have been plotted in Figure (3-2) in a similar manner. The Fox and Li results are again plotted for comparison. The phase shift per transit is the phase shift in addition to the geometrical phase shift suffered by the field distribution and is hence just the phase angle of the eigenvalue of the mode of interest.

The power loss per transit plot shows some interesting features associated with the presence of the angular selective device in the cavity. First of all we note that a break point in the angular number 0.566 curve appears at a point given approximately by formula  $(NA)_c = \pi/2$ , as predicted. The break point for the angular number = 0.141 curve also correctly appears at a Fresnel number of roughly 11. The break point for the angular number = 2.26 would have appeared at a Fresnel number of roughly

Figure (3-1)

Power Loss Per Transit of the Lowest-Order Mode of  
an Infinite Strip Resonator as a Function of the  
Fresnel Number for Three Values of the Angular Number

The Fox and Li results are shown for comparison.

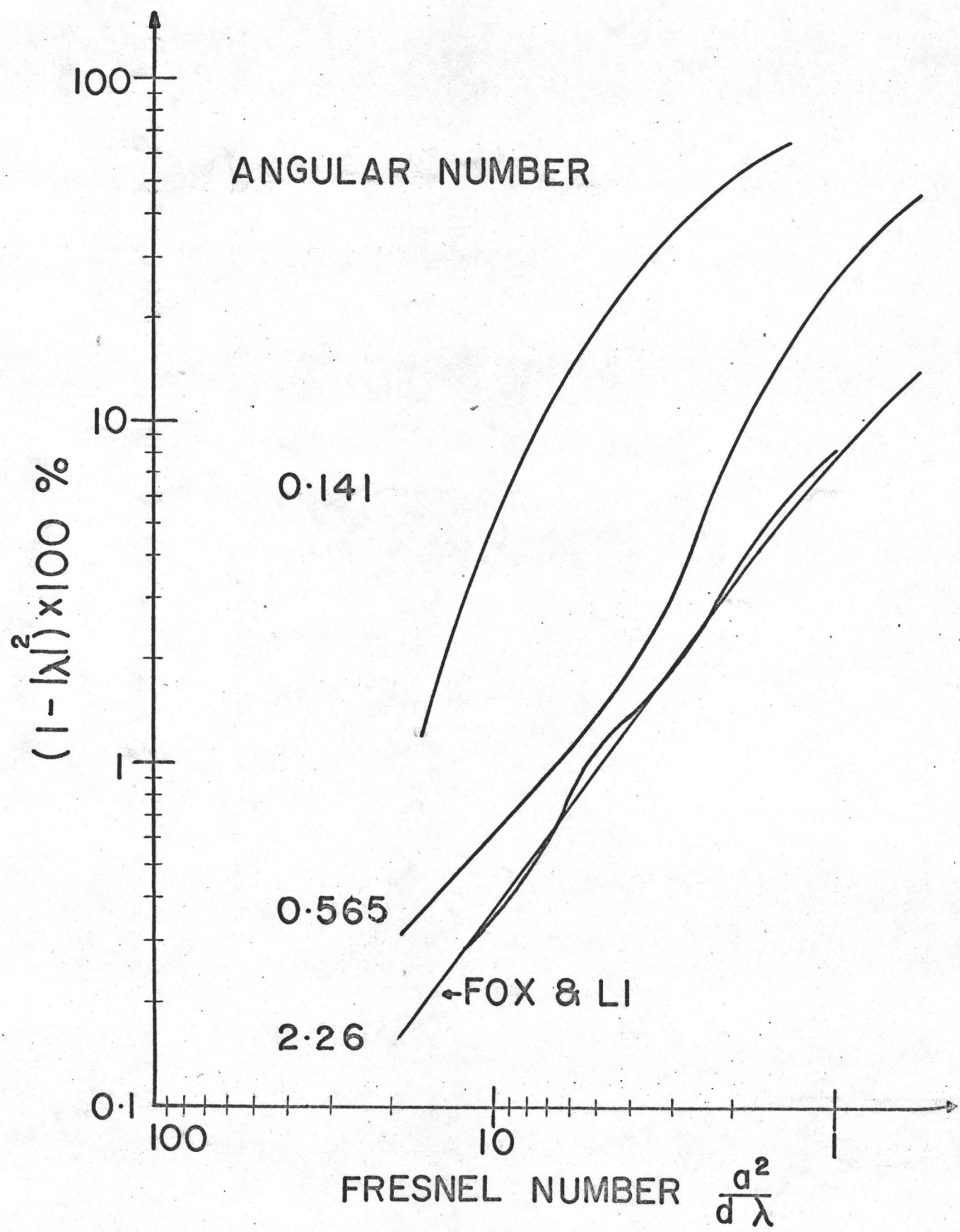
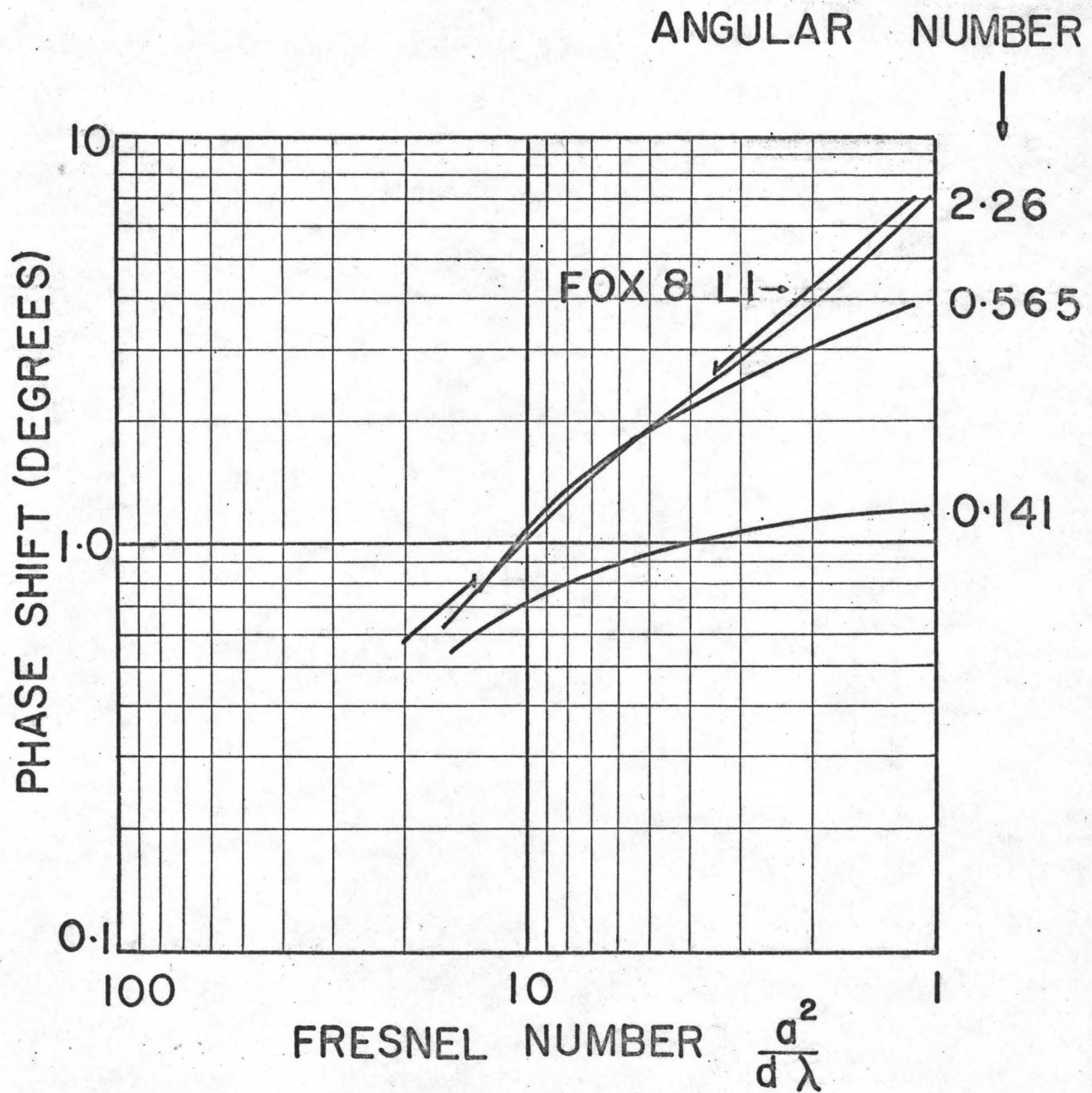


Figure (3-2)

The Phase Shift per Transit of the Lowest-Order Mode  
of an Infinite Strip Resonator as a Function of the  
Fresnel Number for Three Values of the Angular Number

The Fox and Li results are shown for comparison.



0.7, had we taken the calculations far enough to show it. Secondly, we see that the curve for the angular number = 2.26 coincides for all practical purposes with that of the unrestricted cavity, for the range of Fresnel numbers covered in the calculations. A similar comment applies to the case pertaining to the corresponding phase shift per transit curves. This result implies that the angular selective device is not significantly perturbing the lowest-order even mode field distribution of the infinite strip cavity without an angular selective device, for the range of Fresnel numbers considered. We should bear in mind in relation to the point just mentioned that in general, to evaluate an eigenvalue of the integral equation (3-8) to second order of exactness, the field distribution corresponding to that eigenvalue need only be known to first order of exactness.

As less and less of the plane wave components, into which the steady state field distribution at the first aperture breaks up, are allowed to contribute to the field distribution at the second aperture -- by narrowing the acceptance angle of the angular selective device - the losses corresponding to the lowest-order even mode increase. This behaviour is shown graphically in Figure (3-1). For a given Fresnel number, the losses increase as the angular number decreases. The phase shift per transit is also seen in Figure (3-2) to decrease as the angular number decreases. Physically, we can explain this behaviour by considering the limiting case: angular number  $\rightarrow 0$ . We see that only those plane-wave components in the immediate vicinity of normal emergence from the first aperture, contribute to the field distribution at the second aperture. It follows that as the angular number is made smaller and smaller, the

field distribution at the second aperture becomes closer and closer to what it would be if only a single normally incident plane wave illuminated that aperture. Hence, the phase shift per transit (i.e. that phase shift in addition to the geometrical phase shift) tends to zero. It also follows that the phase shift per transit has as its origin the off-axis plane waves that are allowed to contribute at the second aperture. Arguing further, we can state that the higher the order of the mode the larger is the additional phase shift per transit that it suffers on propagating back and forth between the two reflectors.

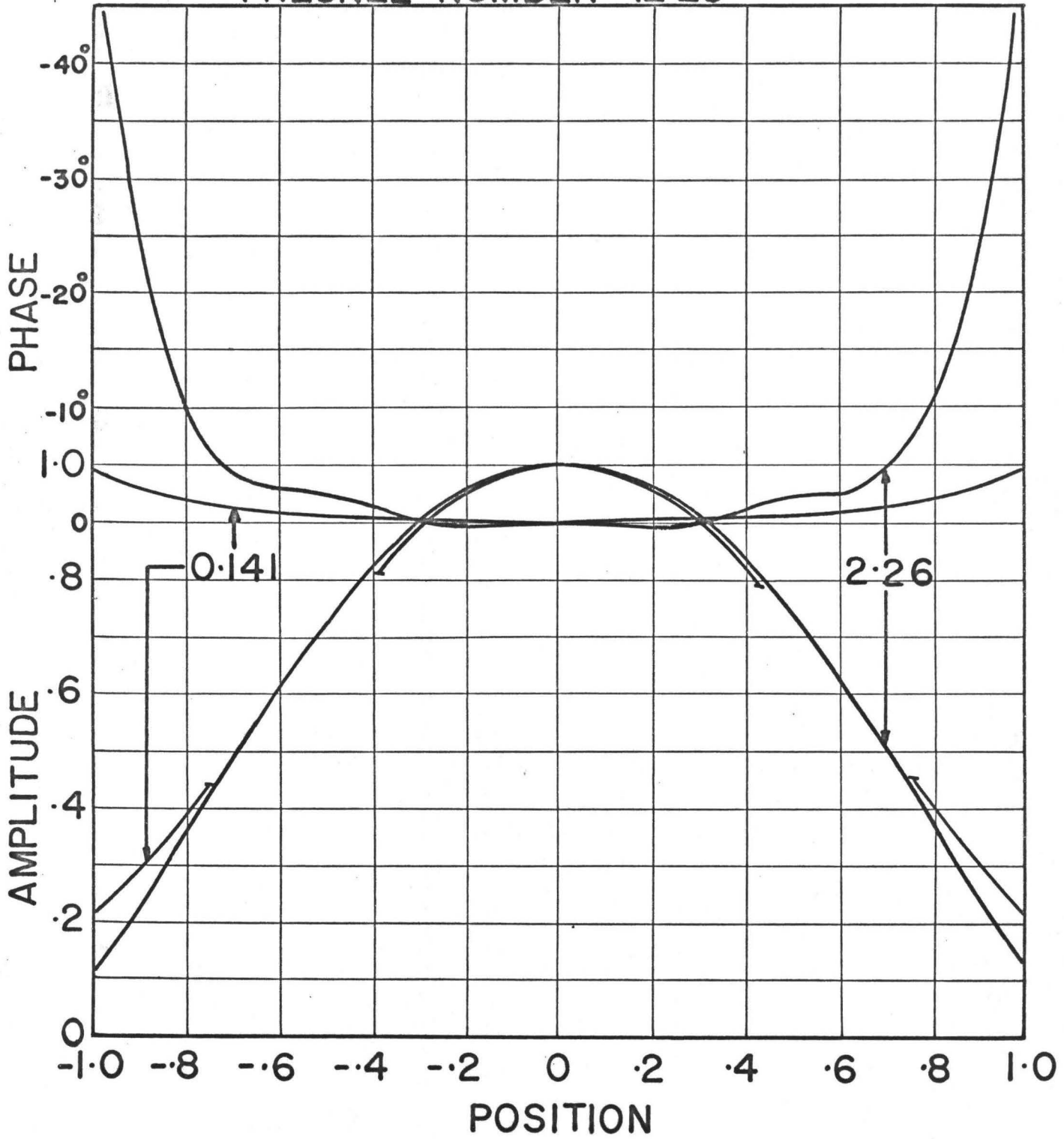
As the angular number is decreased, keeping the Fresnel number constant, one expects to find a tendency on the part of the lowest-order even mode magnitude to "flatten" out. The value of the field magnitude at the edge of the reflector will increase, giving rise to higher "spill over" losses. This behaviour of the eigenfunction solutions is, in general, found to take place. The phase of the field along the reflector short dimension also tends to flatten out with decreasing angular number. A "flat" phase front would have to be considered a desirable feature of a laser beam—indicating a possible use for an angular selective device. Figure (3-3) shows the behaviour outlined above for two lowest-order even eigenfunctions.

The smoothness of the phase and amplitude functions of the modes shown in Figure (3-3) contrasts with the solutions of Fox and Li, which show a superimposed low amplitude ripple on both the phase and amplitude functions. The ripple can be explained in terms of the magnitude of the Fresnel number<sup>(33)</sup>. The fact that it is not present in the solutions shown in Figure (3-3) is due to the presence of the angular selective

Figure (3-3)

The Amplitude and Phase of the Lowest Order Even  
Mode of an Infinite Strip Cavity for Angular Numbers  
of 0.141 and 2.26

FRESNEL NUMBER = 12.25



device which "filters out" the high-frequency field variations. The ripple would eventually appear for an angular number large enough to let through the off-axis plane-wave packets needed to account for the fluctuations.

The behaviour for infinite angular number of the solutions of the integral equation governing the steady state field distribution in an infinite strip cavity has been discussed by Fox and Li. The behaviour for constant angular number of the solutions is essentially the same and will not be discussed here.

We have indicated earlier that the numerical method process of starting with an aperture restricted plane wave field distribution and iterating it by calculating the resultant field distribution at the second aperture and then repeating the process several times, corresponds, physically, to launching a plane wave excitation into the equivalent cavity and letting diffraction continually reshape the field distribution until a steady state field distribution is obtained. There is no a priori reason to believe that the aperture-restricted plane wave does not contain to some extent all the even-order modes. In particular, it should have a fair amount (greater than  $\frac{1}{10}$  of the lowest-order even mode content) of second-order even mode content. As the iterative procedure is carried to its limit, the last surviving mode contents in the transient field distributions, to all intents and purposes, will be the lowest-order even and the second-order even modes, with the second-order even mode content decreasing rapidly relative to the lowest-order mode content. If, instead of launching a plane-wave field distribution, we chose to launch the field distribution having only the lowest-order even and

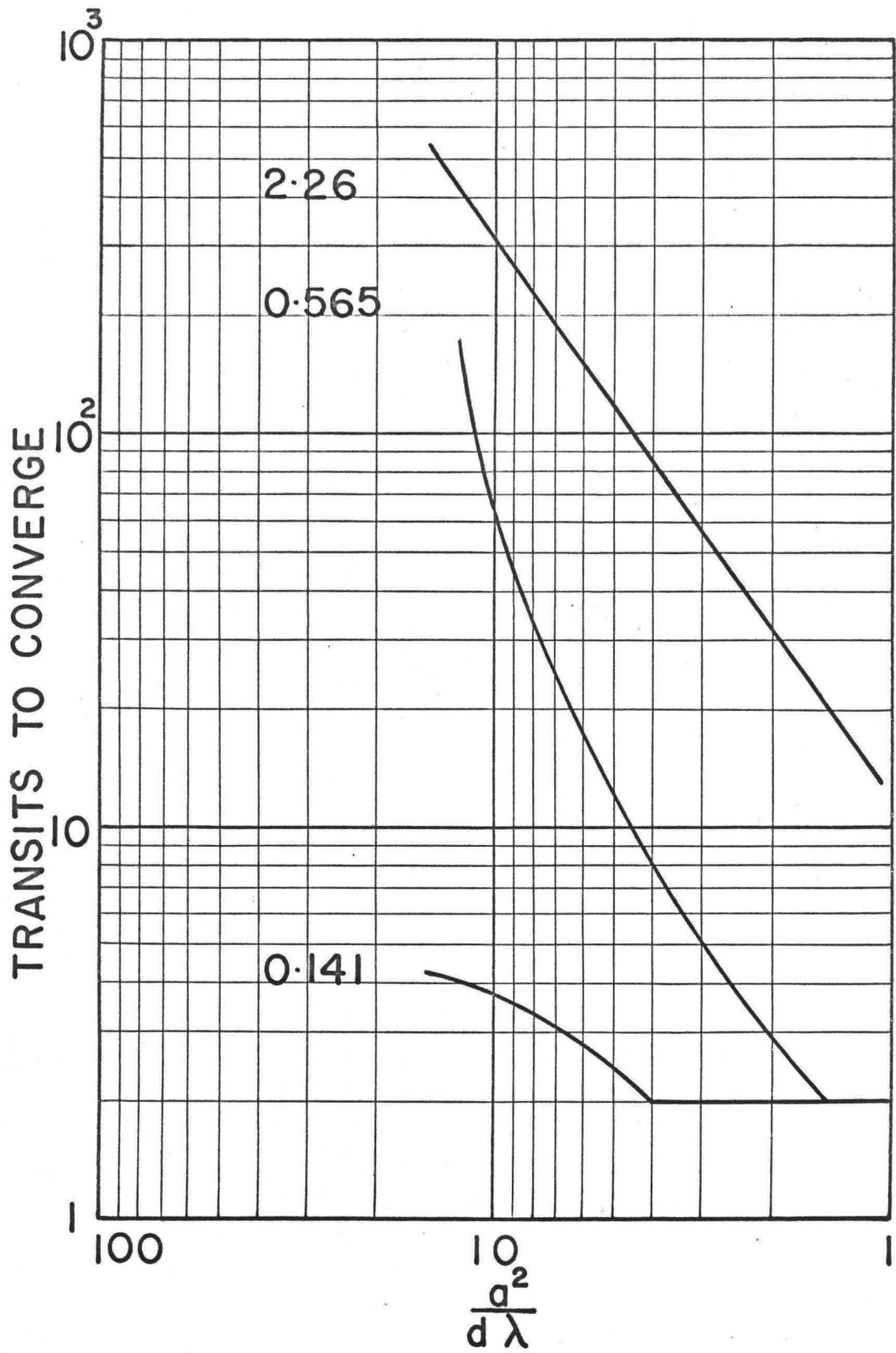
second-order even mode contents in the same proportions as the equivalent plane-wave contents, the solution would converge to a given degree of accuracy in the same number of iterations as the plane-wave initiated solution. We emphasize that the above result does not follow in general and is a fact established through observation of the convergence of the solutions. This point will become clearer below.

It follows from the above arguments that the number of iterations required to determine the eigenvalue of the lowest-order even mode to a prescribed degree of accuracy, starting from a plane wave, is a measure of the relative magnitudes of the eigenvalues corresponding to the lowest-order even and second-order even eigenfunctions. If, for a particular cavity configuration and cavity angular number, the solution converges more rapidly than it does for the same cavity configuration and different cavity angular number, we can say that the ratio,  $\left| \frac{\lambda_0}{\lambda_2} \right|$ , of the eigenvalue magnitudes of the two lowest-order even modes in the former case is greater than that in the latter case. This is the same as saying that the ratio of the diffraction losses, with the angle limiting device, of the second order even mode to the lowest order even mode is greater in the former case than in the latter. The former cavity configuration offers increased mode selection properties over the latter.

A plot of the number of transits required to determine the lowest-order even eigenvalue magnitude to a particular and sufficiently fine degree of accuracy ( $\pm \frac{1}{10^5}$ ) starting from an aperture restricted plane wave field distribution, is shown in Figure (3-4). The plot can be used to give a relative idea of the high order mode rejection properties of cavity configurations under comparison. When used together with the

Figure (3-4)

The Number of Transits Required for an Aperture Limited  
Plane Wave to Converge to the Lowest Order Even Mode for  
an Infinite Strip Cavity as a Function of the Fresnel  
Number for Angular Numbers of 2.26, 0.565 and 0.141



power loss per transit plot, a happy medium of balancing lowest order mode losses against mode rejection properties can be attained. It appears that, if one can tolerate a certain loss, the best mode rejection is obtained by decreasing the angular number and increasing the Fresnel number commensurate with the allowable losses as much as practically possible. It should be pointed out that, ideally, if the losses of all the modes were available, the number-of-transits-to-converge plot would be superfluous.

We can show the behaviour of the converging solutions graphically by plotting the power ratio:

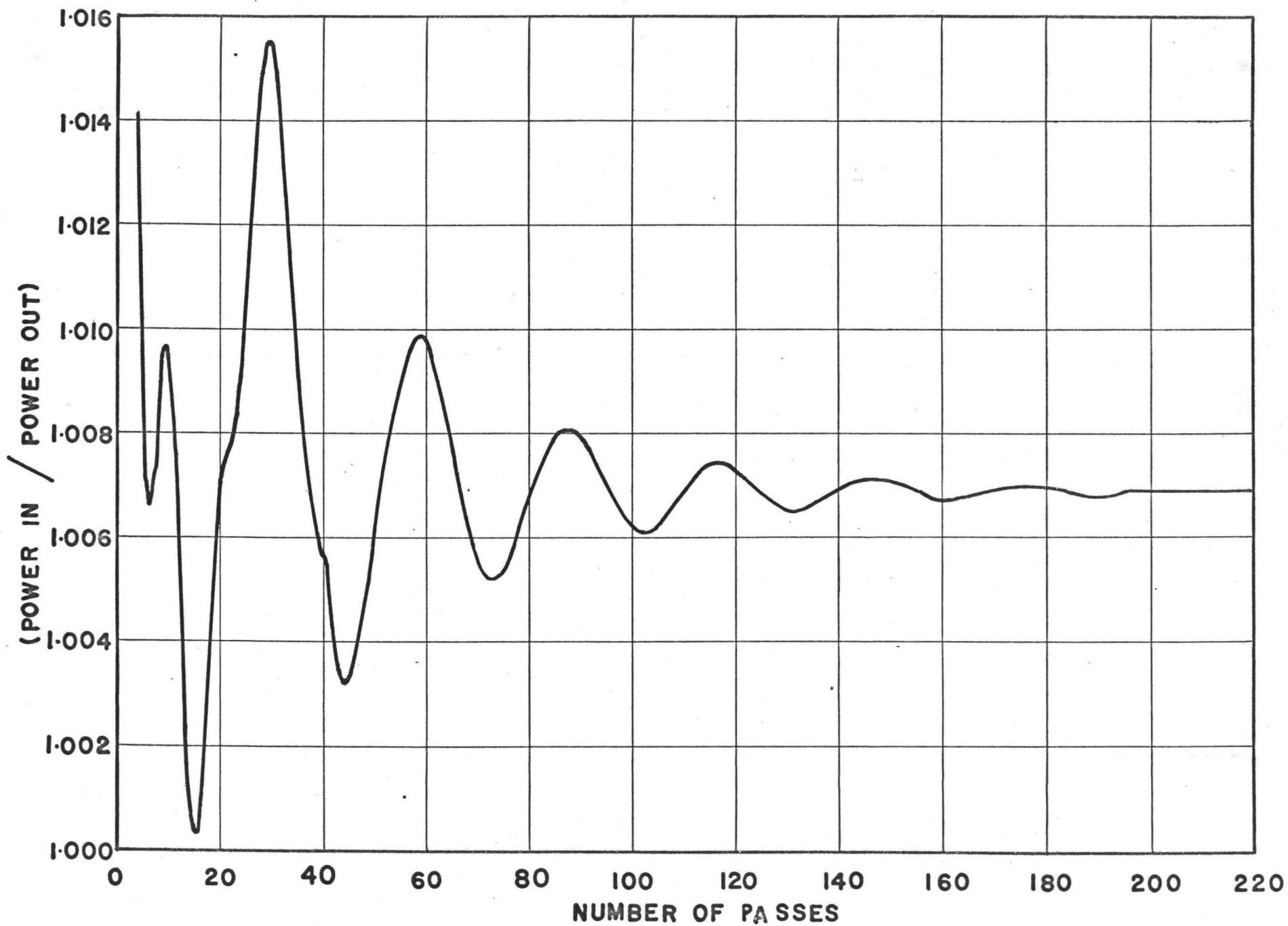
$$\frac{\text{Power Input}}{\text{Power Output}}$$

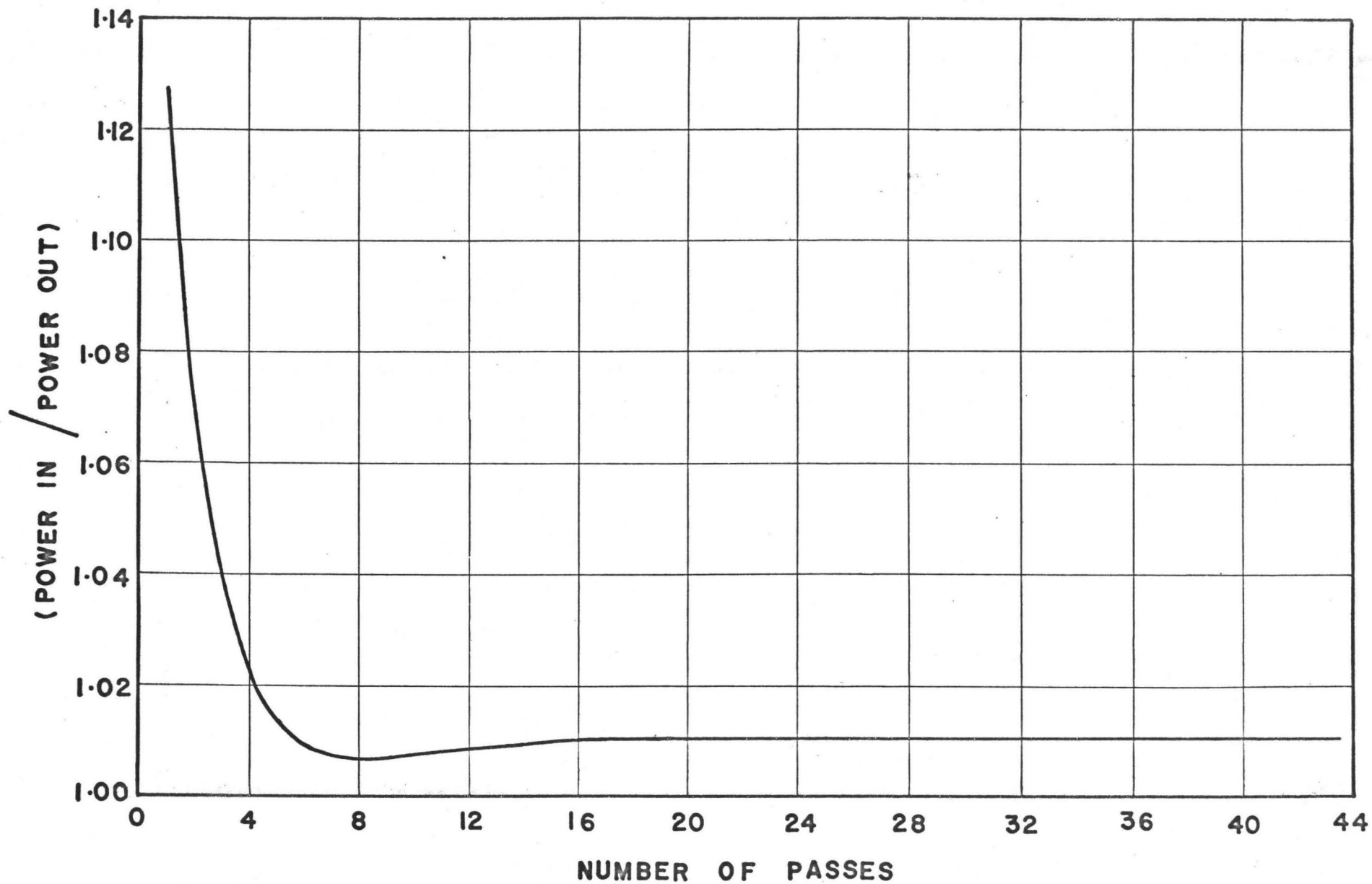
as a function of the number of passes. In Figure (3-5) we show three plots of this quantity each for a Fresnel number of 6.25. As the angular number decreases, the convergence becomes more rapid. For the largest angular number it is seen that the power ratio at first oscillates irregularly, gradually going into a damped sinusoid about 1.0069. The initial irregular behaviour is associated with the presence of several modes in the transient field distributions<sup>(33)</sup>. As diffraction takes its toll of the higher order modes only two modes, having the lowest losses, remain. These give rise to the damped sinusoid. The phase shifts per transit of the two modes, being different, periodically concentrate to a certain extent the net field distribution on and off the second aperture, giving rise to fluctuating diffraction losses. The second-lowest-order even mode has higher losses than the lowest-order mode, resulting in the

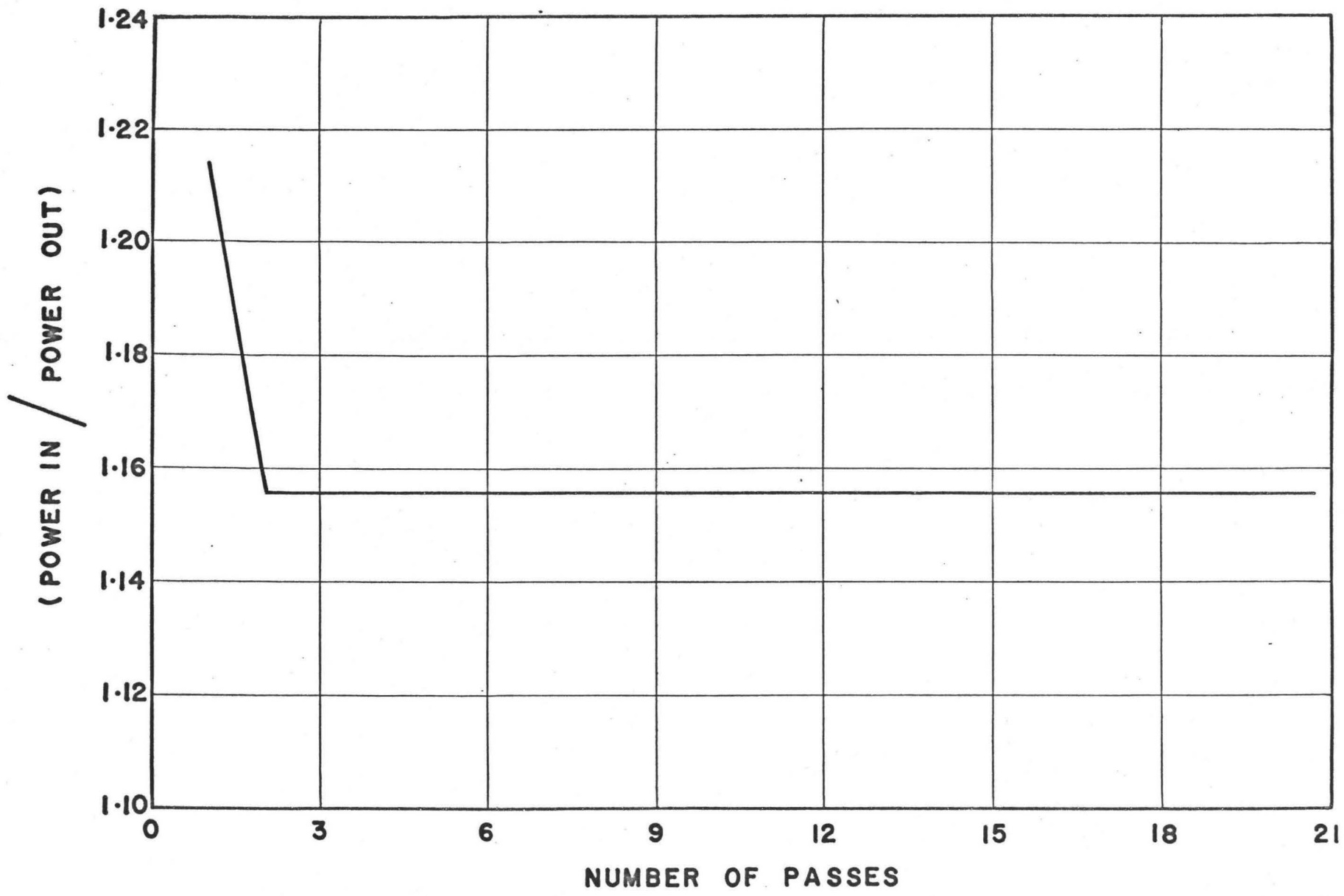
Figure (3-5)

Power Ratio as a Function of the Number of Passes

The power input divided by the power output is plotted as a function of the number of passes, starting from a plane wave. The Fresnel number is 6.65 in each of the three cases corresponding to angular numbers of 2.26, 0.565 and 0.141.







damping which, in this case, will be almost exponential. As the angular number is decreased to 0.565, the second-lowest-order even mode damps out much more rapidly relative to the lowest-order mode and convergence is thus approached faster. The higher order modes, needless to say, damp out even sooner. For the smallest angular number considered, the limit  $\frac{1}{|\lambda_0|^2}$  is approached even more rapidly. A similar behaviour is observed for other values of the Fresnel number.

In summary, we have shown that an angular selective device, which restricts some of the plane wave components of a propagating field distribution in a cavity from contributing to the field distribution at the second reflector, is capable of mode selecting. The purpose of a mode selecting device is to leave essentially unperturbed the lowest-order mode of the cavity without a mode selecting device, while increasing the losses of all the other modes. For an appropriately adjusted angular number, the lowest-order even mode will bear a close resemblance to the lowest-order even mode for infinite angular number and the same Fresnel number. The other equivalent modes, however, will be quite different for the two cases.

Mode selection is an important aspect of laser cavity design. Several methods of realizing an angular selecting device are available. The simplest consists of two lenses and a pin-hole. Another such device is the Lummer Gehrcke plate. The operation of the plate will be explained at a later stage in this Thesis in connection with its capacity to increase the apparent switching speed of a rotating prism Q-switch.

## CHAPTER 4

### EXPERIMENTAL APPARATUS AND PROCEDURE

#### 4.1 Introduction:

This Chapter will deal with the details of the experimental apparatus employed during the course of this work to observe those aspects of a Q-switched laser system of direct interest to us here. The method of extracting meaningful physical data from the system will be clarified. In relation to the first instance, the general features of a Q-switched laser system as well as the role of supporting equipment will be described. A detailed characterization of the various individual components of the particular system used will follow, and some of the design considerations involved in the realization of an efficient Q-spoiled laser system will be presented. In the second instance, the specific experimental methods used to extract information about the system behaviour relevant to this Thesis will be outlined in detail. The type of measurements required for the comparison of theoretical predictions with experimental results will show the necessity of having a versatile laser system on which to undertake those measurements. It is this requirement that rules out as impractical the "off-the-shelf" commercially available units.

## 4.2 Experimental Apparatus:

### 4.2-1 The Q-Switched Laser System-

A schematic diagram of a Q-switched laser with subsidiary equipment for observation of the time evolution of the giant pulse, as well as its energy content, is shown in Figure (4-1). A photograph of the system is shown for reference in Figure (4-2). The laser itself consists of two plane parallel reflectors between which is placed a material capable of providing gain at some optical frequency. The laser material is usually shaped in the form of a long cylinder with optically polished ends. The ends, in the case when the cavity is formed by external mirrors, may be plane parallel and normal to the axis of the rod. It is then advantageous to have anti-reflection end coatings. Brewster angle ends can alternately be used, in which case the component transverse vibrations of the electromagnetic field in the plane of incidence are transmitted through the interface without reflection loss -- for a beam propagation vector parallel to the rod axis. Brewster angle ends may thus serve in lieu of antireflection coatings.

The cavity formed by the output reflector and the Porro prism has as its purpose the providing of sufficient optical feedback to form, together with the laser material amplifier, a laser oscillator. The Q of the cavity can be switched, periodically, by rotating the Porro prism (Section 4.2-2) at a uniform rate. It is only when the Porro prism is aligned parallel to the output reflector to within a rather narrow tolerance angle, that gain in the excited laser crystal can overcome inherent cavity losses. Lasing can occur, then, only within a very small fraction of the time required for the rotor to complete a full revolution.

Figure (4-1)

Schematic of the Giant Pulse Laser System

1. Energy Detecting Thermopile head
2. Back-Biased Light Sensitive Diode
3. Diode Load
4. Diode Power Source
5. Oscilloscope
6. Microvoltmeter
7. Capacitor Bank Power Supply
8. Synchronizing Unit
9. Fire Button
10. Pick-up Coil
11. Porro Prism
12. Xenon Flashlamp
13. UV Reflection Filter
14. Cooling Fan
15. Nd<sup>+3</sup>-in-glass Laser Rod
16. Output Reflector

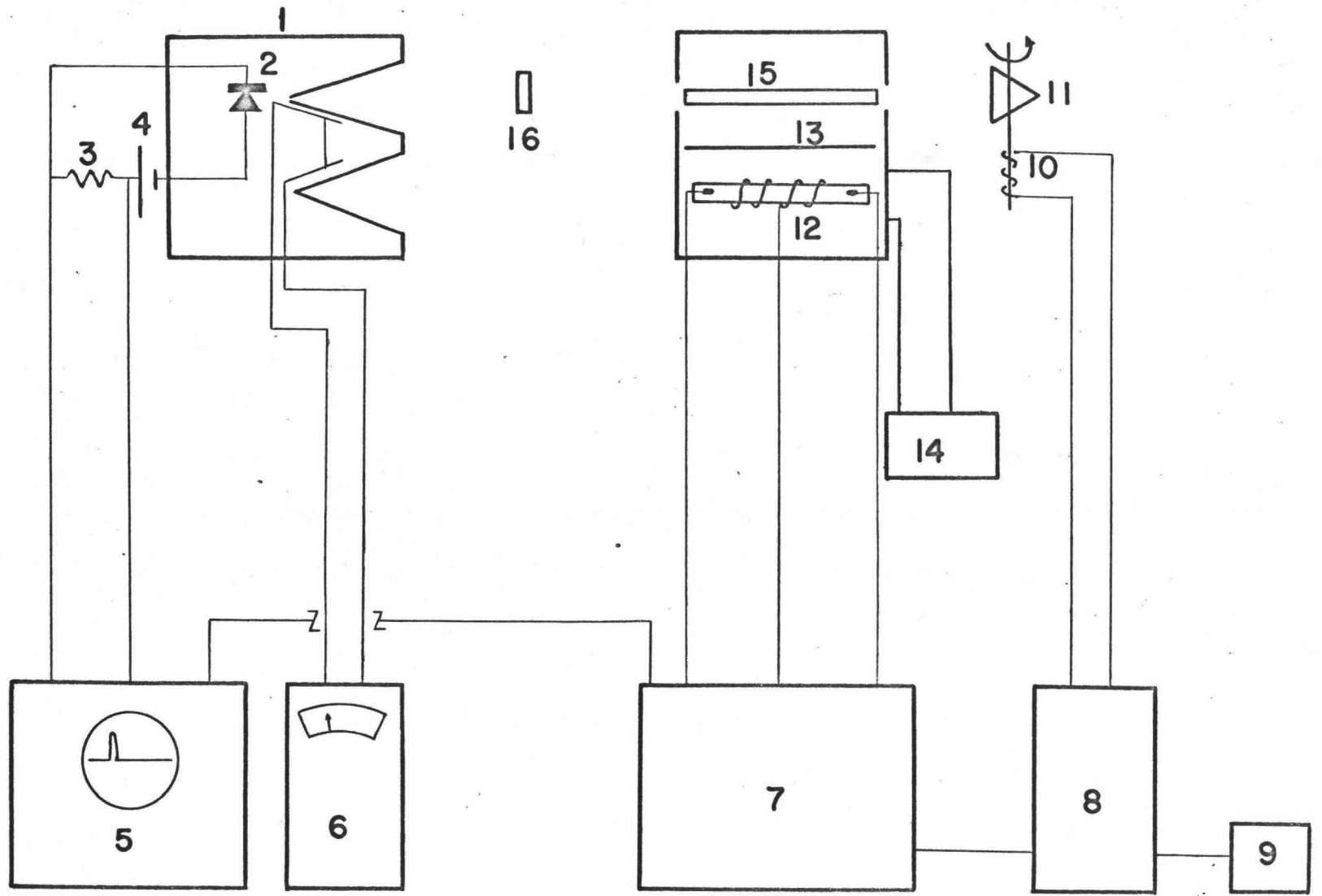
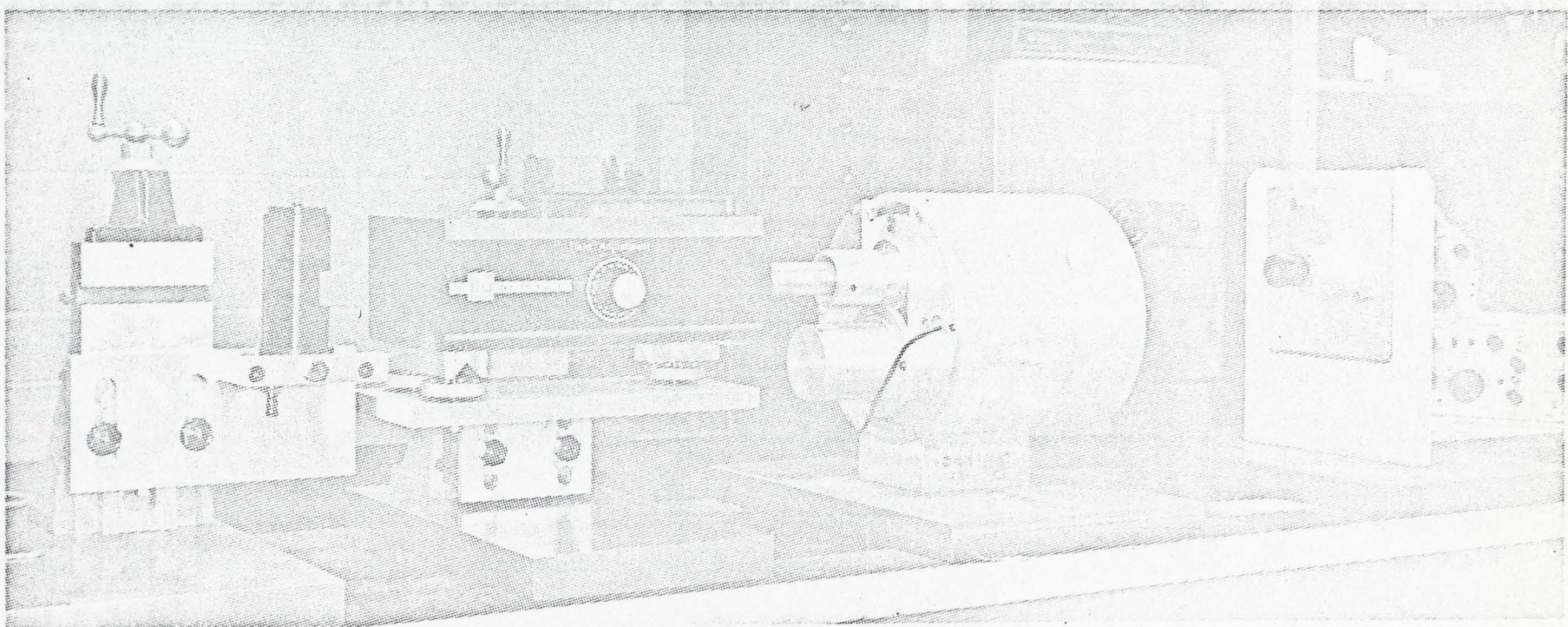


Figure (4-2)

Photograph of the System



Excitation of the laser rod itself is accomplished by optically pumping it with the aid of a pulsed linear flashlamp, located along one focus of an elliptical housing (Section 4.2-5) which has highly polished inner metal surfaces acting as reflectors. The rod is located along the other focus of this elliptical housing, assuring good coupling for optical excitation transfer from the flashlamp to the rod.

The flashlamp is driven by a capacitor-bank power-supply (Section 4.2-5), and is triggered by a high-voltage ionizing pulse from a trigger coil. In practice, the duration of the pumping pulse from the flashlamp is much longer than the time interval during which the  $Q$  of the cavity is high enough to allow oscillation of the system. The pump will establish a laser level population inversion which grows to a maximum at some time during the pumping pulse, and it is desirable that the  $Q$  of the cavity be switched at a time when this population inversion is a maximum. The requirement is, therefore, that the rotor shall bring the Porro prism into alignment with the output reflector at the appropriate time during the flashtube cycle. This state of affairs is accomplished by synchronizing the rotor to the power supply. The rotor position, under steady state conditions, is determined by the phase of an AC signal from the pickup coil located in the rotor housing. This information is used by the synchronizing unit (Section 4.2-7) to trigger the flashlamp, through the power supply, in such a way that the Porro prism comes into alignment when maximum inversion in the crystal has been established by the pump. The laser is fired by activating the synchronization unit which in turn triggers the flashlamp at the appropriate time.

The phase of the AC signal may be varied coarsely with respect

to the Porro prism orientation by rotating the pickup coil with respect to the rotor housing. It is thus possible to synchronize the rotor to the flashlamp pulse in spite of the varied range of conditions that can arise in practice. Fine phase control is accomplished electronically within the synchronization unit proper.

The output pulse from the laser is monitored in two ways. In ~~the first of these, the energy content of the pulse is converted into~~ heat at the input cone of the energy monitoring thermopile (Section 4.2-6) thus raising its temperature. The cone has a long taper making its aperture appear like a black-body to an incident beam. Identical reference and input cones absorb roughly the same amount of non-collimated radiation. The maximum temperature difference reached by the two cones ~~is then proportional to the energy content of the pulse.~~ The temperature difference is measured by means of a thermopile -- the "hot" junctions being those attached to the input cone and the "cold" those attached to the reference cone. The maximum voltage generated by the thermopile is monitored by a DC microvoltmeter and is associated, by ~~calibration of the device, with the joule content of the laser pulse.~~ A small pin-hole, bored through the end of the input cone, provides a means of extracting a minute fraction of the power of the pulse which is then collected at the surface of a fast response photodiode. The output of the photodiode is coupled to an oscilloscope (Tektronix 555) and thus ~~provides a means of observing the time development of the giant pulse.~~

Some subsidiary equipment, not shown in Figure (4-1) completes the laser system. This subsidiary equipment consists of a high-resolution autocollimator which may be used to measure the degree of parallelism

of a surface's unit normal with respect to the optic axis of the auto-collimator. A transit-type optical telescope, with the capability of focusing on close lying planes, also forms part of the system. These optical tools may be used, in conjunction, to align the optics of the laser system.

#### 4.2-2 Rotating Prism Laser Q-Spoiler-

The Q-spoiling was accomplished with the aid of a Beckman and Whitley Model 402 rotating-prism laser Q-spoiler. The device is driven by compressed air. The maximum applicable drive pressure is 80 psi resulting in a turbine rotational rate of 1500 rps. The device accommodates 5/8" maximum diameter laser beams. To eliminate critical alignment problems, the device employs a Porro prism, rotated about an axis parallel to the prism hypotenuse and perpendicular to the prism roof edge. Synchronization of the Q-spoiler with the flashlamp pumping pulse is accomplished through the signal coming from a built-in pickup coil in the turbine housing. The signal frequency is a direct measure of the prism rotational rate. Its phase with respect to the prism position is continuously variable through  $360^\circ$  by rotating the pickup coil with respect to the rotor housing. The prism roof edge width is less than 0.1 mm and the prism roof angle tolerance is better than 1 minute of arc.

The manufacturer claims light losses for the device at least five times less than those incurred with Kerr cell Q-spoilers. The Porro prism results in cavity lengths which are effectively about twice those which would result if an ordinary mirror were mounted on the rotor turbine.

The upper bound on the rotational rate of the device results from tensile strength limitations of the materials used in its construction. The lower bound of 50 cps, achieved by us, is mainly limited by jitter in the synchronization between the rotor and the flashlamp pump pulse. Also, at lower switching speeds, the percent random fluctuations in the rotational rate of the device are larger than they are at higher speeds. At low switching speeds, there is some difficulty involved in setting the phase of the signal from the pickup coil for correct synchronization. It is not difficult to understand the reason for this if one considers that the optimum time for Q-switching our laser lasts at best 0.1 milliseconds. At 50 cps, 0.1 msec. corresponds to an angle sweep of 1.8 degrees. The phase must therefore be set to within 1.8 degrees. The scale monitoring the position of the pickup coil is readable to 1% or 3.6 degrees.

A Hewlett Packard digital frequency counter was used in the "Period" mode to measure the time required by the rotor to complete a revolution. This procedure yields a periodically sampled "instantaneous" rotor rotational rate. Since the stability of the rotational rate was thus readily monitored, it was possible to keep the long term rotational rate of the Q-spoiler within tolerance.

#### 4.2-3 Nd<sup>+3</sup> In Glass Laser Rods-

The laser rods used for the experimental work of this Thesis were Type ND-11 as supplied by the Eastman Kodak Company. The doping of all the rods was nominally 3% by weight Nd<sub>2</sub>O<sub>3</sub> in EK silicate glass. The relatively long lifetime of the metastable <sup>4</sup>F<sub>3/2</sub> state of Nd<sup>+3</sup> in this host material makes it particularly useful in Q-spoiling applications and

is recommended in this regard by the Eastman Kodak Company. The metastable lifetime of  $\text{Nd}^{+3}$  in silicate glass is 360 microseconds at room temperature as compared with the 51 microsecond lifetime of the  $\text{Nd}^{+3}$  ion in borate-base rare earth optical glass - a laser material manufactured by the same company.

A large majority of the experimental results were obtained using 3" x 1/4" rods with plane parallel ends normal to the rod axis. The rods were supplied by the manufacturer with antireflection coatings on both ends peaked for 1.06  $\mu$  operation. One 3" x 1/4" rod was purchased with Brewster angle ends and some fluorescence observations were made employing it.

Kodak quotes end-flatness better than  $\frac{\lambda}{10}$  and end-parallelism better than 6 seconds of arc for its glass laser rods. In order to evaluate the tolerances, note that a 1/4" aperture has a diffraction limit of approximately 30 seconds of arc and that  $\frac{\lambda}{10}$  in 1/4" corresponds to about 3 seconds of arc of "roughness". Thus the end faces are to all intents and purposes optically perfect, since the quoted tolerances are well within the diffraction limit of the 1/4" aperture used. Homogeneity of the glass laser rods as checked by us with the aid of a He-Ne laser, appears to be excellent -- a fact that is not surprising since optical quality glass is being employed as the host material for the  $\text{Nd}^{+3}$  ions. It might seem that accurate measurements of the parallelism of two surfaces are limited by the diffraction limit of the smaller of the two surfaces. However, one may use large-diameter optical flats placed in intimate contact with the surfaces being measured and so avoid the limitations placed on the parallelism measurement by Rayleigh's criterion.

#### 4.2-4 Optical Mounts-

That part of the system comprising the laser head, the rotating prism Q-switch, the output reflector mount and the high resolution autocollimator as well as the energy monitoring head was mounted on a 2.5 m lathe bed. The rigidity of the lathe bed resulted in a relatively vibration-free optical cavity.

The mount for the Q-switch was a 1" thick plate made of mild steel which could be pulled firmly onto the two horizontal flat rails of the lathe bed by means of a crossbar and bolt assembly. Vertical height adjustment of the Q-switch, which is desirable, was made possible by mounting a machinist's slide onto the plate and bolting the Q-switch firmly on the carrier of the slide. Vertical positioning of the Q-switch to 1/1000" could thus be accomplished without difficulty. The mount of the Lummer Gehrcke device was similarly constructed. In the latter case, however, an aluminum plate was horizontally mounted on the carrier of a machinist's slide. Three adjusting screws, symmetrically located and passing through the plate, (each having been provided with a ball-end), fitted onto V-cut strips on the Lummer Gehrcke device, thus giving the necessary freedom to control the attitude of the device.

Lateral attitude was accomplished in both cases by appropriately orienting the mild steel base of the mounts with respect to the lathe bed. This adjustment was undertaken with the aid of an optical alignment telescope and autocollimator. Precision alignment of the Lummer Gehrcke device and the Q-switch rotor with respect to the axis of the cavity was thus made possible.

The reflector mount was of kinematic design. A vertical holder

mounted on a steel base plate, similar to those already described, coupled a plate to the lathe bed. The plate itself could be slid vertically on the holder and secured to it at will. Another plate, to which a reflector could be attached, had three screws passing normally through it. The screws formed the vertices of a right angle triangle. One of the screws had a ball end--the other two had fine point ends. The ball end screw rested against the plate held by the holder, while one of the point-end screws rested in a V-cut groove on the holder plate. The point end of the last screw rested in a conical indentation of the holder plate. Two strong springs, within the triangle formed by the three screws, were mounted in such a way that the two plates were always held in contact through the screws by pressure from the springs. The V-cut groove was oriented to prevent rotation of the actual mirror mount about the conical indentation. This design gives reflector tilt about two independent axes. The three inch closest-neighbour separation of the screws together with their fine thread allowed accurate control of the reflector tilt. In practice, and with some care, it was possible to set angles to within one second of arc.

The autocollimator was placed on a rigid platform located at one end of the lathe bed. The platform's height relative to the lathe bed was adjustable. Precision height and lateral adjustment was not required because the exit pupil of the autocollimator was 5 cm in diameter. The autocollimator's tilt attitude could be controlled precisely using the three support screws provided on the instrument for that purpose.

The laser head was bolted to a plate which in turn was held securely to the lathe bed by a cross-bar and bolt assembly. All

adjustments were made with respect to the laser crystal axis and so only lateral translation and rotation of the laser head with respect to the lathe bed needed to be controlled to align the laser crystal axis, initially and appropriately, with respect to the lathe bed. No height adjustment was necessary and adequately machined laser head parts assured that the laser crystal was horizontal, within necessary tolerance, to the lathe bed rails.

The energy meter optical-head was placed on a bellows type mount whose height could be readily adjusted.

#### 4.2-5 Laser Head and Power Supply-

The laser head used to optically pump the laser crystal was of the elliptic type. A pumping system must be capable of coupling light from the pump source to the laser crystal as efficiently as possible. The elliptical cylinder type of laser head, when used in conjunction with a linear flashlamp, constitutes such a system. If the laser crystal is supported along one focus of the ellipse and the flashlamp along the other, a degree of concentration of the light emanating from the flashlamp on the crystal is realized. That degree is strongly dependent on the quality of the reflectors forming the closed elliptical cylinder and on the geometry of the ellipse. The present trend is to have the crystal and the flashlamp close together in an appropriate elliptical cavity. Two partial sections of an elliptical cylinder are very often used to form a symmetrical three-focus system with the crystal located between two linear flashlamps. The ellipse in the present case had the following dimensions:

Major Axis	5"
Minor Axis	4 1/2"
Distance Between Foci	2 1/8"

Using the calculations of Schuldt and Aagard<sup>(40)</sup>, which assume a Lambert's Law pump and define the efficiency of the system in terms of the relative percentage of rays which travel from the source to the laser crystal and reach there--suffering no more than one reflection by the cylinder--one obtains an efficiency of 50% for the above geometry.

The flashlamp used as the pump source was a Edgerton, Germeshausen and Grier FX-42 linear xenon flashtube. It was excited by a GNB Model 20-002 power supply and capacitor bank. This unit is composed of 8 separate capacitor units, each capable of storing 250 joules of energy at 2200 volts: This being the maximum rated voltage of the power supply. At the other extreme the minimum output energy obtainable is 62.5 joules at 1100 volts. The individual capacitor units are easily connected in parallel to cover this output energy range of 62.5 - 2000 joules.

The stored energy is controlled by the controller module in the GNB unit. The flashtube easily supports a potential difference of 2200 volts across its terminals until a 20,000 volt trigger pulse is supplied to a coarse 1/2 inch conducting grid surrounding the flashtube. The trigger pulse ionizes the xenon in the flashtube, resulting in a main breakdown of the gas by the energy stored in the capacitor banks. This energy is converted into useful light output as well as into heat. Part of the role of the controller module can now be appreciated; it can control the trigger pulse in any of three ways, namely:

- (1) Manually
- (2) Automatically with a period ranging from 0.01 sec. to 100 sec.
- (3) By an external +10 volt pulse into 4000 ohms.

The controller module also sets the energy stored in the capacitor to the value required by a manually adjustable control which is of the on-off type. To offset the accuracy limitations of such a control, we incorporated an error monitoring meter into the power supply, which allowed for 1:1000 energy reset-ability from firing to firing. We note that the average output power of the GNB unit may not exceed the rated linear charging rate of 200 joules per second. The pulse from the thyatron that generates the flashtube trigger pulse via a pulse transformer, is also used to generate a +2 volt pulse from 100 ohms which is useful for external synchronization purposes.

The energy module is used to generate a linear charging rate of 200 joules per second until a predetermined voltage across the capacitor banks is reached. This voltage is controlled from the panel of the controller module. A pointer and scale on that module is calibrated to read directly in joules. The scales may be interchanged with one of several others which are available in order to allow direct energy settings to be made for different capacitor bank interconnections.

An inductance module is provided consisting of two 800 millihenry coils each tapped at 100, 200, and 400 millihenries. This permits interconnections to be made between the chokes and the capacitor banks in order, for instance, to give the resulting circuit current limiting properties, or to simulate the discharge from a transmission line and so approach a

rectangular shaped light output pulse from the flashtube. In general, only the current limiting aspects of a single choke (200 millihenry) in series with the flashtube were exploited in this Thesis work.

#### 4.2-6 Detectors-

Three different types of detectors were essentially used in performing the experimental measurements. The first of these was an energy detector, while the second and third were a fast response solid state photodiode and photomultiplier respectively.

The energy detector (TRG Model 102) consists of a ballistic thermopile which measures the temperature rise of a nickel-plated silver input-cone resulting from absorbed incident radiation, with respect to the temperature rise of a second identical reference cone. The input cone receives the laser beam together with non-collimated background radiation, while the reference cone receives only the non-collimated background. The thermopile consists of ten series-connected iron-constant thermocouples. Radiant energy, which is directed into the aperture of the input cone, is almost totally absorbed due to the Mendenhall wedge effect. The temperature rise of the input cone with respect to the reference cone causes an emf to be generated in the thermopile, which can be monitored by an externally-connected microvoltmeter. The peak emf measured is linearly related by a known calibration factor (206  $\mu\text{v}/\text{joule}$ ) to the total input energy, as long as that energy is incident on the input cone in a time short compared to the response time of the instrument ( $\sim 10$  seconds).

The radiant power of the laser beam is monitored by a fast response (rise time = 4 nsec.) photodiode located in an enclosure immediately behind the input-cone. A small pin-hole at the vertex of the input-cone allows a small fraction of the power in the beam to be incident on the photosensitive area of the diode detector. The diode is backbiased with a 90 volt battery across whose terminals is connected a 0.1  $\mu$  farad capacitor. The capacitor serves to maintain the bias voltage when current is drawn by the photodiode and also reduces external transients from the signal picked up by the battery-leads. The photodiode is loaded by a 200 ohm resistor and it is across this resistor that a voltage signal, proportional to the laser beam incident power, is monitored by a Tektronix 555 oscilloscope. The connection between the oscilloscope and the photodiode is made using 100 ohm coaxial cable, terminated at the input of the vertical amplifier of the oscilloscope with a 100 ohm load. This procedure ensures a fast response time for the system free from degrading capacity-loading effects. The system comprising the photodiode circuitry and the oscilloscope was estimated to have an impulse response time of roughly 20 nanoseconds.

From the point of view of Q-spoiled pulse detection, noise considerations take a secondary place to response time. This is, of course, due to the strength of the signals being detected.

In order to make observations on the fluorescent  $1.06\mu$   ${}^4F_{3/2} \rightarrow {}^4I_{11/2}$  transition of  $Nd^{+3}$ , a Dumont 6911-S1 photomultiplier tube was used in conjunction with a grating spectrograph. The circuit for the photomultiplier was designed using the relevant principles outlined in reference 41. The S-1 photocathode response is the only response

characteristic commercially available in photomultiplier tubes which is satisfactory in the  $1\mu$  region of the electromagnetic spectrum. Even so, at  $1.06\mu$  the quantum efficiency is down to 0.04% corresponding to a photocathode sensitivity of 0.004 amperes/watt. The only alternate choice to the S-1 photomultiplier at  $1\mu$  is a silicon photodiode or a Riese p-i-n junction photodiode<sup>(42)</sup>. The availability of the S-1 photomultiplier forced the choice in this instance.

The photomultiplier circuitry was designed to provide a  $0.5\mu\text{sec}$ . response time. A faster response time would have been desirable and could have been obtained by cooling the photomultiplier tube to  $77^{\circ}\text{K}$ . The response time was limited by the necessity of minimizing the noise-bandwidth. The limited response time of the photomultiplier and associated circuit simply puts an upper limit on the speed of the transients of the signal being detected which can be observed. To be more specific: If one observes fluorescence from a laser rod in a narrow frequency range and then, by some means or other, is able to burn a hole in the fluorescent line, the equilibrium line shape will be restored after a certain time. If the time required for this process to take place is shorter than the detector response time, the hole burning will not be detected.

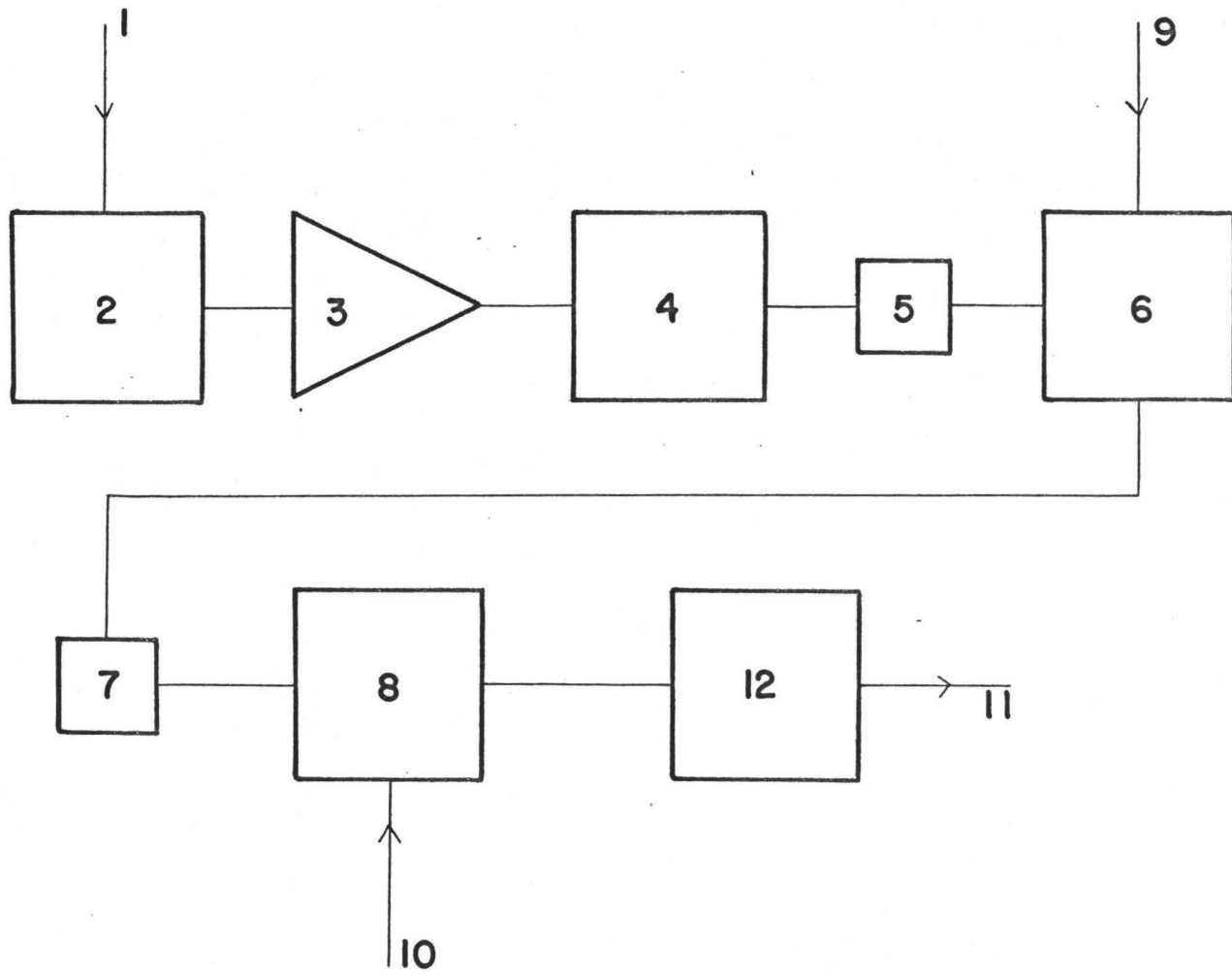
#### 4.2-7 The Synchronization Unit-

A schematic diagram of the synchronization unit is shown in Figure (4-3). The sinusoidal signal from the pickup coil of the rotor Q-switch is clipped symmetrically and then amplified. This procedure assures that faster rise-times than would be obtained with a sinusoidal signal will characterize the resultant waveform. Fast rise-times at the input of the

Figure (4-3)

Schematic of the Synchronization Unit

1. Input Signal from Pick-up Coil
2. Symmetric Clipper
3. Amplifier
4. Schmitt Trigger Circuit
5. Differentiator and Clipper
6. Monostable Multivibrator
7. Differentiator and Clipper
8. Connecting Circuit
9. Delay Control
10. Fire Button
11. Output Synchronizing Pulse
12. Binary



Schmitt trigger circuit result in a rectangular waveform output from that circuit with less phase jitter than would be obtained with a sinusoidal input signal.

The rectangular waveform output of the Schmitt trigger circuit is differentiated and clipped to allow only the positive going spikes to arrive at the monostable multivibrator input. The spikes trigger the monostable multivibrator thus changing its state. That state lives for a time determined by the RC time-constant of the multivibrator. Control of the RC time-constant of the device allows one to obtain a delayed signal. Thus, the spike train output from the differentiator and clipper following the multivibrator is delayed by a controllable time interval with respect to the spike train output of the first differentiator and clipper. By making contact with the aid of the control release switch between the terminals from the second differentiator and clipper and those of the binary, one is able to obtain a change in state of the binary. The switching action initiated in the binary by the pulse just following the contact instant, gives rise to that change of state. The result is a step output from the binary which is used to automatically trigger the power supply. The circuit is readied for the next laser pulsing cycle on reversing the state of the binary by means of a switch.

The synchronization unit we have described is capable of providing a trigger pulse whose phase can be varied within a certain range (0.5msec) with respect to a reference sinusoidal signal. The 0.5 msec electronic phase control proved to be adequate in practice. A maximum  $360^{\circ}$  phase control could be obtained mechanically by rotating the pickup coil in its mounting on the Q-switch housing. The electronic phase control could then be used as a trimmer.

#### 4.2-8 The Lummer-Gehrcke Plate-

A modification of the Lummer Gehrcke interferometer<sup>(32)</sup> results in an optical device useful as a one-dimensional angle-limiting filter. The device is available commercially from TRG Inc. under the name Daly-Sims accessory. It makes use of the phenomenon of total internal reflection in a multiple-reflection plane-parallel optical plate.

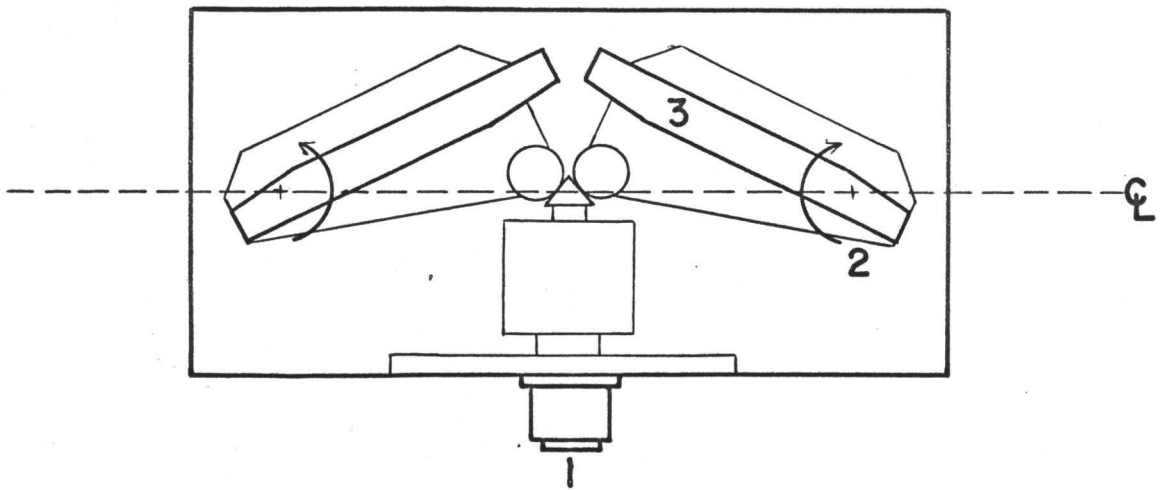
To understand the operation of the Lummer Gehrcke plate as an angular limiting filter, we consider a beam of monochromatic light propagating within a plane-parallel non-absorbing plate with a given angle of propagation measured with respect to the unit normal of the plate. We further limit our discussion to a plate whose thickness is large compared to the width of the beam being considered. This restriction allows us to neglect the effects of vignetting on the plane-wave components of the beam after it is allowed to exit from the interior of the plate. Those plane-wave components of the beam, whose angles of incidence are greater than the critical angle of the medium in which the plane-waves are propagating, will be totally internally reflected. In contrast, those plane-wave components whose angles of incidence are smaller than the critical angle will, in part, be refracted at the boundary and, in part, be reflected. The net result is that such reflected plane-waves have suffered attenuation. After a large number of passes the angular content of the beam will essentially be the same as the angular content before the first reflection--except that now the angular content is truncated on one side by the loss mechanism described.

A schematic of the Daly-Sims accessory is shown in Figure (4-4). The diagram shows the way in which the ideas just outlined are implemented

Figure (4-4)

Schematic of Daly-Sims Accessory

1. Field Control
2. Axis of Rotation of the Plates
3. Brewster Angle Multireflection Plates.



to yield a practical device. The arrangement shown in the Figure has the advantage of having the entrance and exit pupils on line. The Brewster angle ends allow those plane-wave components, polarized with the electric vector in the plane of incidence, to cross the boundaries without suffering a reflection. The angular field of acceptance can be varied by simultaneously rotating the two component plates about the axes shown in Figure (4-4). In the device proper an arbitrary scale is provided to allow the monitoring of the field of acceptance of the device.

To gain an idea of the sharpness of the cut off of the device it is perhaps useful to quote the results of some of our calculations on a 12-reflection plate made from a medium of index of refraction  $n = 1.46$ . The calculations assume a plane-wave polarized in the plane of incidence and are based on the Fresnel formulae<sup>(32)</sup>, and the law of refraction. The restriction on the polarization takes account of the fact that when the device is placed inside a laser cavity, the losses for the two linearly independent polarizations are different. Due to the Brewster angle windows of the plate, the losses for those plane-waves polarized in the plane of incidence are the smallest, and hence the output beam will be polarized accordingly. For small deviations from the critical angle,  $\theta_c$ , given by  $\Delta > 0$  we can easily arrive at the formula:

$$R = \left[ 1 - \frac{2 \sqrt{2} n(n^2-1)^{\frac{1}{4}}}{\left(1 - \frac{1}{n^2}\right)^{\frac{1}{2}}} \Delta^{\frac{1}{2}} \right]^2$$

where  $R$  is the reflectivity for one reflection and  $\eta$  is the index of refraction of the plate. For a 12-pass plate with  $\eta = 1.46$  and  $\Delta = 10^{-3}$  radians = 3.4 minutes,  $R^{12} = 0.01$ . For the same plate with  $\Delta = 0.5 \times 10^{-3}$  radians,  $R = 0.04$ . These figures, applicable to this Daly-Sims accessory, give an idea of the sharpness of the cut-off of the device for plane-waves incident at angles smaller than the critical angle.

As long as the main lobes of the plane-wave components of a given beam fall within the band-pass of the device, the beam will propagate through the device essentially unattenuated. To be more specific, we focus our attention on the lowest order transverse mode of the cavity in which the device is assumed to be located. The lowest order mode has its main angular lobe symmetrically located about the axis of the cavity. We further assume that the angular width of the main lobe is narrow enough to be allowed to propagate through the device essentially unattenuated. The device then has no apparent effect on that cavity mode. Assume now that the previously well-aligned cavity has one of its reflectors tilted with respect to the other. The lowest-order mode of the new configuration, if it exists, can be considered to be made up from a mixture of modes of the unperturbed cavity. Some of these component modes which normally would give rise only to extra diffraction losses are now also attenuated by the device since they will fall outside its bandpass. Bearing this picture in mind it is not difficult to understand that the losses associated with the misaligned cavity containing the device will be higher than the losses for the misaligned cavity without the device. On the other hand, for the case of the aligned cavity with and without the device, the losses can, under certain circumstances, be made approximately equal.

One of the uses of the Lummer Gehrcke plate is to increase the effective switching speed of a rotating reflector Q-switch. The effective switching speed may be increased by narrowing the loss vs angular-misalignment function of the cavity. This narrowing may be accomplished by introducing the Lummer Gehrcke device into the cavity. The largest increase in effective switching speed is obtained when the angular bandpass of the device is adjusted to the minimum value that results in essentially identical losses for the aligned cavity with and without the device.

#### 4.2-9 Reflectors:

The cavity in a laser system is formed by two reflectors. In Q-spoiling applications these are usually plane parallel. If Q-spoiling is accomplished using a rotating totally internally reflecting prism, one of the reflectors forming the cavity is the prism itself, the other one being the output reflector.

The output reflector can be made from a metallic thin film deposited by vacuum-evaporation techniques on a dielectric substrate, such as fused quartz or glass polished to optical tolerances. This type of reflector is highly unsuitable for Q-spoiling applications since it may become irreparably damaged after a single operation of the laser in the giant pulse mode.

Multiple dielectric coated optical flats provide a much more satisfactory answer to the search for a suitable output reflector. It has been observed experimentally by us that they may become damaged by the output giant pulse of the laser for output pulse power densities of the order of 0.3 joules in 25 nanoseconds over a 0.05 in<sup>2</sup> area.

By far the most suitable type of reflector for O-spoiled operation is of the resonant type. This type of reflector has a wavelength-dependent reflectivity. For normal incidence an  $n$  platelet resonant reflector formed from a medium of index of refraction  $\eta$  has reflectivity  $R$  given by:

$$R = \left[ \frac{(\eta)^{2n-1}}{(\eta)^{2n+1}} \right]^2$$

at optimum resonance. The derivation of the formula follows from the Fresnel laws<sup>(32)</sup>.

For a three platelet resonant reflector made from sapphire ( $\eta = 1.76$ )  $R = 87\%$ . The separation and thickness of the platelets are such that the spacing between the resonant electromagnetic wavelengths is  $1 \text{ cm}^{-1}$ . Since the fluorescent line width of  $\text{Nd}^{+3}$  in glass for the  ${}^4F_{3/2} \rightarrow {}^4I_{11/2}$  transition is about  $300 \text{ cm}^{-1}$  at room temperature, we see that there are many resonant wavelengths within the fluorescent line width for which the reflectivity is high.

Most of the experiments were performed using dielectric reflectors of either 50% or 80% reflectivity. An 87% resonant reflector was available but was not used except in making some energy utilization measurements. The reason for not using it more extensively was that it was found to be defective in its alignment when it was checked out using a high resolution autocollimator. The resonant reflector was later realigned with the aid of a He-Ne gas laser and subsequently used in some of the energy utilization factor measurements. It performed in a similar manner to the 80% dielectric coated reflector, as far as could be determined from observations

of the output energy level of the beam and the energy utilization factor.

#### 4.3 Procedure:

##### 4.3-1 Alignment Techniques-

The alignment problem in laser systems lies in the requirement that cavity reflectors be parallel and that all optical apertures be centered on the optical cavity axis. The optical cavity axis need not be a straight line. This case obtains when a Brewster angle laser rod is used as the drive element in a cavity.

The solution to the alignment problem may be found in the use of a single optical-tooling telescope and autocollimator combination. This solution is adequate when high resolution is not demanded from the autocollimation process. High resolution autocollimators ( $\Delta\theta \sim 0.5$  seconds of arc) are only available as fixed focus instruments. They do not perform the function of a telescope. However, when used in conjunction with a transit type telescope they may be used to effectively solve the alignment problem. We will now briefly indicate the method employed to realize the solution.

The projection of the cross-over point of the autocollimator cross hairs defines a direction in space within the circumference of autocollimator beam. A telescope focused at infinity with its axis parallel to the direction defined by the autocollimator and whose objective receives the beam from the autocollimator will form a real image of the autocollimator cross-hairs at its focal plane. If the axis of the telescope is marked by cross-hairs located in its focal plane, then the cross-over point of the imaged cross-hairs will coincide with the telescope cross-hairs. Imagine

that the telescope is now refocused at a point intermediate between it and the autocollimator. The output reflector is placed at that point and is then tilted in its mount until its reflected cross-hairs, as viewed in the autocollimator, indicate parallelism of its unit normal to the axis of the autocollimator. The reflector is now aligned when one has made certain that the image of the reflector centre falls on the cross-over point of the telescope cross-hairs.

The next step is to refocus the telescope at a closer point on the front face of the laser rod which, held in the elliptical pumping housing, has been moved into the line of sight of the telescope. The axis of the laser rod is made to coincide with the imaginary line segment traced in space by the cross-over point of the telescope cross-hairs as the telescope is first focused on the front end of the laser rod and then on the back end.

If it is desired to make use of the Lummer-Gehrcke plate, the same technique may be applied to align it as was used to align the laser rod, after placing the plate between the telescope and the laser rod. However, one must now check the position in angular space of the angular field of acceptance of the device with respect to the autocollimator axis. To this end the telescope is refocused on the autocollimator cross-hairs. The field of the plate is then closed almost completely. The previously circular field of view of the telescope as illuminated solely by the autocollimator beam is now a single vertical band. If this band is located symmetrically about the vertical cross-hair of the telescope the Lummer-Gehrcke plate is perfectly aligned. If not, a slight adjustment of the attitude of the plate is made until this situation obtains. For this procedure to be successful the Lummer-Gehrcke plate must be in perfect adjustment.

The Q-switching rotor may now be placed in the desired location closest to the telescope. It is positioned with the  $90^\circ$  edge of the Porro prism in the imaginary plane traced out by the horizontal cross-hairs of the telescope as it is focused over its range. This is accomplished by means of a previously-placed accurate mark on the back of the rotor housing.

If it is desired to operate the laser in its normal mode, the prism must be fixed in position and the whole rotor housing rotated until the prism is normal to the output reflector. The existence of this condition may be monitored with the aid of the autocollimator.

#### 4.3-2 Q-Spoiled Pulse Output Energy Measurements

##### and Complementary Measurements:

A set of Q-spoiled output energy measurements consists of those values obtained experimentally for the output energy content of the Q-spoiled laser beam for various Q-switch rotor speeds and laser rod excitations. Those measurements must be complemented by a knowledge of the values of other variables of interest.

The aim of making output energy measurements, together with measurements of other relevant data, on a Q-switched laser system is to obtain sufficient quantities to allow a complete description of that system.

At this point, therefore, it is perhaps worth while to recall those quantities which are complementary to the output energy measurements. Cavity configuration measurements are thought of as yielding values of the physical cavity length,  $L$ , the laser rod length,  $\ell$ , the index of refraction of the rod,  $\eta$ , and the rod end face area,  $A$ . Measurements on the physical properties of the laser rod are similarly thought of as yielding the value of the

magnitude of the electric dipole matrix element for the transition in question, which has already been related directly to  $\alpha_0$ , by measurements on the decay time constant and the branching ratio of the upper level for laser action. Such measurements are also thought of as yielding the operating angular frequency of the device,  $\omega_{k\ell}$ , the half-width of the fluorescent transition,  $\Delta\omega$ , the relevant level degeneracies,  $g$ , the operating temperature,  $T_0$ , and the splittings of the upper and lower levels for laser action,  $\Delta E$ .

By referring to the equations for  $\text{Nd}^{+3}$  ions in a glass matrix (2-13), (2-14), (2-15) we see that a knowledge of the above listed quantities - together with a knowledge of  $\gamma(T)$ ,  $\tau$ , and the initial conditions - are sufficient to enable us to predict the behaviour of the laser system by solving those equations. In particular it is possible to predict the output energy characteristics of the Q-switched laser system under consideration. The complementary measurements yield, through the rate equations, predicted output energy characteristics which may be compared with the experimentally observed characteristics.

In practice, the situation is not quite as simple as that described above. In the first place the level degeneracies are not known; this obtains because of experimental difficulties in their measurement. Secondly, the relaxation time constant,  $\tau$ , of the lower level for laser action is also not directly known. In Section 2.3-5, however, we have indicated how to deal approximately with those unknown level degeneracies. On the second point, however, if we assume that the rate equation model is valid, we may fit the predicted output energy characteristics to those observed experimentally if we treat  $\tau$  as an adjustable parameter in the solution of those

rate equations. This procedure allows us to obtain an approximate value for  $\tau$ . The overall validity of the model can then be judged by the measure of agreement between the experimental and theoretically fitted output energy characteristics.

The problem is simplified somewhat if one considers the normalized rate equations (2-19), (2-20), (2-21). The solution of those equations is determined by a knowledge of the switching function,  $\gamma(T)$ , the time per pass of a photon in the cavity,  $T_1 = \frac{l + (\eta - 1)l}{c}$ , the degeneracy factor,  $\frac{2K_1}{K_1 + K_2}$  and the relaxation lifetime of the terminal level,  $\tau$  - taken together with the imposed initial conditions. The output energy,  $E_o$ , of the laser system model being considered will certainly be proportional to:

$$\int_{T=0}^{\infty} \phi_o \, dT$$

The proportionality constant may be determined by fitting that point of maximum experimentally observed output energy, (for single laser-pulse action at a particular constant excitation energy), to the corresponding point of the theoretical characteristic. Once this constant is determined it should be applicable to all excitations of the laser rod. The fit further enables one to determine  $\phi_{oi}$  - which is the initial condition on  $\phi_o$ . The quantity  $\phi_{oi}$  can also be obtained from theoretical calculations and thus a comparison may be made with the fitted  $\phi_{oi}$ . The validity of the rate equations can therefore be determined in respect to their ability to predict the relative behaviour of the output energy characteristics. To validate the rate equations as far as the prediction of the absolute energy output is concerned we need to use the results of Section 2.5. It may be noted at this time that a very satisfactory agreement of predicted output

energy with experimentally observed output energy results (see Section 6.2). The fitted  $\phi_{oi}$  is also found to be in good agreement with the corresponding predicted value.

The method just outlined is, in fact, the one used to test theoretical predictions against experimental results. We have indicated that the first step in the procedure to apply the method consists in determining the switching function,  $\gamma(T)$ , the degeneracy factor,  $\frac{2K_1}{K_1 + K_2}$ , and the time per pass of a photon in the cavity  $T_1$ . Of these, the degeneracy factor and  $T_1$  are easily arrived at. The problem is then to determine  $\gamma(T)$  and the initial conditions. Since  $\phi_{oi}$  is fitted to experiment we need only determine  $N_o$  (recall that  $N_{o1} = 0$  initially) to be able to find the solutions of equations (2-19), (2-20), (2-21). We naturally need the experimentally determined output energy characteristics to determine the quantity  $\phi_{oi}$ , and the output energy constant of proportionality. Later (see Section 6.1) we will see that in fact  $\phi_{oi}$  can be estimated theoretically. The result of such an estimate will be shown to be in good agreement with the experimentally fitted value.

#### 4.3-3 Determination of The Loss Function $\gamma(T)$ :

In this Section the method of evaluating the loss function  $\gamma(T)$ , associated with the prism switch, will be described. To begin with, the laser system is first aligned for normal operation without Q-spoiling and the cavity length is noted. The threshold energy for laser action is then measured by observing the minimum pump energy required to bring about the onset of laser relaxation oscillations. That value of the pump energy is recorded.

Referring to equation (2-19) we see that the threshold condition is simply:  $N_o = \gamma(T)$  Since we make the measurements with a static aligned Porro prism, the threshold condition becomes:

$$[N_o]_{\theta = 0, \text{ Threshold}} = \gamma(0) = - \ln R$$

This result obtains since for high quality  $Nd^{+3}$  in glass rods, and large cavity Fresnel numbers, the only significant losses arise from the fractional reflectivity of the output reflector. We are consequently able to associate a particular value of the quantity  $N_o$  with the threshold pump energy. Now, experimental evidence indicates (see Section 4.1) that  $N_o$  for our laser system, (assuming for the moment that positive feedback is being prevented), is to a good approximation, proportional to the pump energy for the entire range of flashlamp input energies. It follows that if the output reflector is misaligned by an angle  $\theta$ , and the threshold pump energy is once again measured and recorded we immediately obtain  $[N_o]_{\theta, \text{ Threshold}}$  which we can then equate to  $\gamma$  as follows,

$$[N_o]_{\theta, \text{ Threshold}} = \gamma(\theta)$$

Repeating the measurements for various degrees of misalignment,  $\theta$ , we obtain the angular dependence of  $\gamma$ . This information together with an assumed given rotational rate of the Q-switch determines the time dependence of the switching function,  $\gamma(T)$ . In these measurements it is evident that we have made use of an approximation; namely, that it does not particularly matter which reflector - the output reflector or the Porro prism - is made

responsible for the misalignment. For small angles,  $\theta$ , this conclusion will certainly follow. We may in a similar manner determine  $\gamma(\theta)$  for a cavity containing a Lummer-Gehrcke plate. In this case we can arrive at a family of curves each of which corresponds to a particular field opening of the device.

#### 4.3-4 Measurement of The Q-Spoiled Output Energy

##### Characteristics of a Mechanically Switched Laser:

Once the switching function  $\gamma(T)$  has been determined by the method outlined in the previous Section it only remains to determine the output energy characteristics of the device. To this purpose the rotor is allowed to come to a fixed rate of rotation, following which the energy content of the Q-switched output pulse is monitored for certain pump-drive energies. The synchronization of the Q-switch is set to assure that the giant pulse appears when the laser rod is at peak excitation. This requirement maintains the linear relationship between the inversion,  $N_0$ , prior to giant pulse evolution and the energy input into the flashlamp. It is also the condition for obtaining maximum inversion prior to the appearance of the giant pulse, for a given pump excitation.

The output energy measurements are made for various rotational rates of the Q-switch rotor. These measurements are continued until enough data points are secured to determine the functional dependence of the output energy content of the beam on the rotational rate of the prism. The result is several energy output constant-excitation characteristics, distinguishable from each other by the particular input energy to the flashlamp used in the observation of each one of them.

In practice, the range of switching speeds of the rotor must be such as to allow cut-off of the laser giant pulse to be reached at the maximum excitation of the laser rod. The origin of cut-off has been explained. For a given laser rod, cut-off is a function of laser rod excitation, cavity length and output reflector reflectivity. The higher the excitation of the rod the greater will be its gain, and consequently the shorter will be the build-up time of the pulse; thus in order to reach cut-off one will be required to employ a faster switching speed.

Increasing the cavity length results in two effects. The first of these is due to the increase in the transit time per pass of a photon in the cavity. This increase, in fact, slows down events taking place in the cavity by the ratio of the old transit time to the new. In turn, cut-off will occur at a slower switching speed. Experimentally it has been observed that longer cavity lengths have a narrower switching function  $\gamma(\theta)$ . Thus at a given rotor speed it will appear to the photons in the cavity that switching is taking place faster when longer cavity lengths are employed. The two effects taken together result in a higher apparent switching speed, and cut-off will consequently occur at slower switching speeds for the longer cavity. The higher the reflectivity of the output reflector, the faster will be the pulse build-up and consequently higher switching speeds will be required to cut off the pulse.

For 50% and 80% output reflector reflectivities it was found that the interesting portion of the output energy characteristics could be observed employing a cavity length of 45 cm separating the Porro prism and the output reflector. The experimental output energy characteristics presented in this Thesis were in general measured using 50 joule flashlamp

excitation energy intervals to approximately cover the 250-550 joule range. The procedure can be extended to the measurement of energy characteristics for the case of a rotating prism Q-switched laser containing a Lummer-Gehrcke plate with its field of acceptance held constant.

One serious experimental difficulty arises from these measurements. At peak output powers and high excitations any damage that occurs to either the Porro prism or the output reflector, from the high power densities of the beam, will change  $\gamma(\theta)$  irreversibly. On various occasions measurements had to be halted because of radiation damage sustained by the dielectric coated output reflector. The damage may be sensed by observing any drop in output energy - for constant excitation and switching speed. To avoid the detrimental effects of such damage the characteristics were measured by starting the run at low switching speeds and finishing it at high switching speeds. Thus relatively high power densities were only encountered at the end of the run when most of the measurements had been completed. The results presented in this thesis were obtained with minimal resultant damage to the laser system components and it is therefore felt that they are a good measure of the actual characteristics of the system.

#### 4.3-5 Fluorescence Measurements and the

##### Energy Utilization Factor:

The determination of the fluorescent line width,  $\Delta\omega$ , for the  ${}^4F_{3/2} \rightarrow {}^4I_{11/2}$ , 1.06 $\mu$  transition of  $Nd^{+3}$  in glass, as well as the line shape of the transition, was ascertained with the aid of a concave cylindrical grating spectrograph. (1.5 meter Bausch and Lomb Model 11 stigmatic grating spectrograph). The required setting of the grating was determined with the

aid of a mercury source by observing in second order the two mercury yellow lines ( $\lambda_1 = 5791$ ,  $\lambda_2 = 5770 \text{ \AA}$ ) as well as the mercury green line ( $\lambda = 5461 \text{ \AA}$ ). Use was made of the fact that a grating will not distinguish spatially between spectral lines satisfying the condition  $n\lambda = \text{constant}$ , where  $\lambda$  is the wavelength of the lines under observation and  $n$  the spectral order in which they are observed. Observations on the above mercury lines thus provided markers in first order at  $\lambda = 1.1582\mu$ ,  $1.1540\mu$  and  $1.0922\mu$  respectively. The dispersion of the grating in first order could thus be calculated and the position determined at which to expect the  $1.06\mu$  transition of  $\text{Nd}^{+3}$ .

A photo multiplier with an S1 spectral response was used to monitor the wave length dependence of  $1.06\mu$  fluorescence transition, for various pulsed excitations of the laser rod. The fluorescence was guided into the entrance slit of the grating spectrograph with the aid of fibre optics. Visible radiation was excluded from the spectrograph by an appropriately located Wratten 87C filter.

The fluorescent strength of the  $1.06\mu$  transition is a direct measure of the number of ions in the excited  ${}^4F_{3/2}$  state of  $\text{Nd}^{+3}$ . By measuring the drop in fluorescent strength at the time the giant pulse occurs, one obtains the fraction of the available ions which have in fact contributed to the energy of the output pulse. This quantity is just the energy utilization factor. The value of such a factor may also be obtainable from solutions of the rate equations; thus a further check is possible on the validity of those equations.

Energy utilization factor measurements were made on the system and the results of those measurements are in good agreement with the values predicted by the rate equations (see Section 5.7).

## CHAPTER 5

### EXPERIMENTAL RESULTS

#### 5.1 The Fluorescent Output Strength of the ${}^4F_{3/2} \rightarrow {}^4I_{11/2}$ Transition of $Nd^{+3}$ as a

##### Function of the Pump Input Energy:

Figure (5-1) presents the functional dependence on wavelength of the fluorescent strength of the  ${}^4F_{3/2} \rightarrow {}^4I_{11/2}$  transition of  $Nd^{+3}$ -in glass for Kodak type ND11 laser rods at room temperature, and under pulsed excitation conditions. The energy input into the flashlamp is the variable parameter labeling the family of curves obtained experimentally.

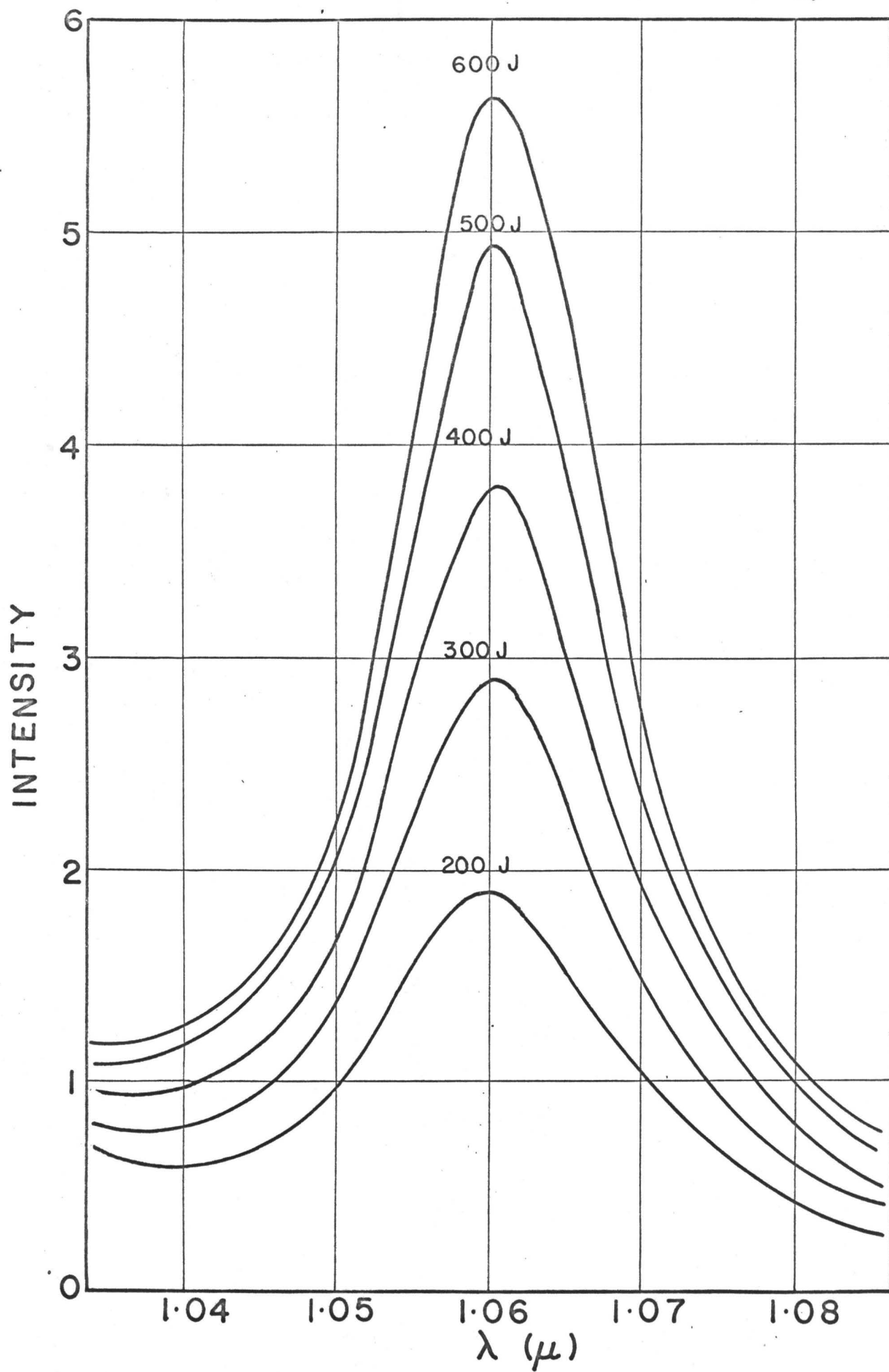
A background signal, which is dependent on flashlamp excitation and wavelength, is clearly visible on the wings of the fluorescence response curves. The background is attributed to the flashlamp output in that region of the infrared spectrum. The output from xenon flashlamps extends well into the infrared and certainly into the  $1\mu$  region of the spectrum.<sup>†</sup> We note, in particular, that the background signal increases by a factor of approximately two for a change by a factor of three in the excitation energy into the flashlamp. This observation may result from the increase in voltage across the flashlamp which was employed to gain the increase in excitation energy, since xenon flashlamps tend to give proportionally less output in the infrared at higher operating voltages<sup>(43)</sup>. The background is

---

<sup>†</sup> General Electric Flashtube Data Manual

Figure (5-1)

Intensity of the  ${}^4F_{3/2} \rightarrow {}^4I_{11/2}$  Transition  
of  $Nd^{+3}$ -in-glass as a Function of Wavelength  
for Various Values of the Pulsed Input Energy  
into the Flashlamp



not constant with wavelength, but drops as one approaches the long wavelength side of the electromagnetic spectrum. This result cannot be attributed to a variation of the infrared output of the flashlamp with wavelength, since we are dealing with a relatively narrow spectral band. The cause of such a dependence lies in the spectral response characteristic of the S1 photo surface of the photomultiplier, which drops rapidly with increasing wavelength in this region of the spectrum<sup>(42)</sup>. Finally, we should note that it is important to consider the presence of flashlamp background in the fluorescent signal when energy utilization measurements are made.

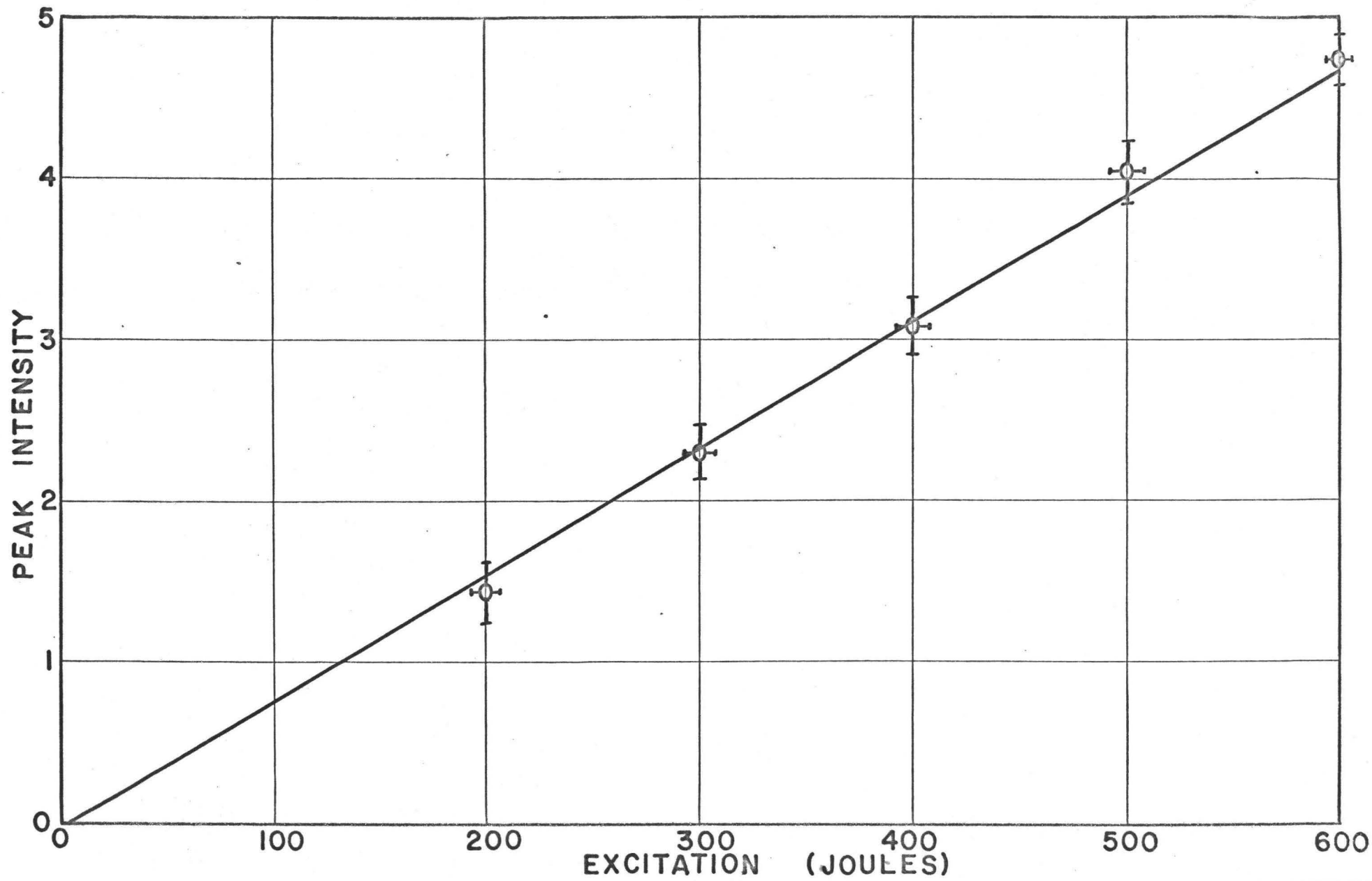
In Figure (5-2), the peak fluorescent intensity has been plotted as a function of excitation energy into the flashlamp. The data used to obtain the plot were obtained after subtracting out the background contribution from the fluorescent signals. It is evident that the dependence of fluorescent output on the flashlamp input energy is linear, and that the extrapolation of the plot to low flashlamp energies goes through the origin. Thus, in the calculations based on the rate equations, it is correct to assume that the initial inversion just prior to switching is proportional to the input energy into the flashlamp. These results hold as long as switching takes place at a time when peak inversion has been reached.

Referring back to Figure (5-1), we observe that the measurement of the fluorescent line half-width yields a value for that width of about  $180\text{\AA}$ ; this is somewhat low. Kodak quotes a fluorescent line width for its ND 11 laser rods of approximately  $300\text{\AA}$ . Recall that the response curves of Figure (5-1) have not been corrected for the spectral characteristics of the S1 photo surface used for their measurement. Also, the observations of

Figure (5-2)

Peak Fluorescent Intensity of the  ${}^4F_{3/2} \rightarrow {}^4I_{11/2}$   
Transition of  $Nd^{+3}$ -in-glass as a Function of Pulsed  
Excitation Energy

The peak fluorescent intensity is a measure of the maximum gain of the laser rod obtained with the given excitation. It depends strongly on pumping geometry.



the fluorescence were made on axis, and at 600 joules excitation the gain of the laser rod is significant - so that one may be observing a degree of fluorescent line narrowing due to stimulated emission taking place in the laser rod.<sup>†</sup>

As a final note, it may be pointed out that the slope of the straight-line relationship between fluorescent strength and excitation energy will depend strongly on the condition of the reflectors of the elliptical pumping housing, as well as on the relative alignment of the linear flashlamp and the laser rod within the pump housing. Thus, the use of newly buffed pump reflectors will yield a steeper slope for the above relationship than reflectors that have experienced the effects of a deteriorating environment. The slope will evidently also depend on the  $\text{Nd}^{+3}$  concentration present in the laser rod.

## 5.2 The Experimental Determination of the Switching Function $\gamma(\theta)$ :

Figure (5-3) shows the dependence of the threshold energy for normal laser action upon the tilt angle of the output reflector, which is of 75% reflectivity. We have indicated previously that the same dependence would result if we held the output reflector fixed, and tilted the Porro prism about its axis of rotation in the turbine housing. The plot is for a separation of 46 cm between the Porro prism and the output reflector. Because of the optical properties of a Porro prism, this distance corresponds

---

<sup>†</sup> Fluorescent measurements made under very low excitation conditions on a  $\text{Nd}^{+3}$ -in-glass sample at room temperature yielded a fluorescent line half-width of 230 Å.

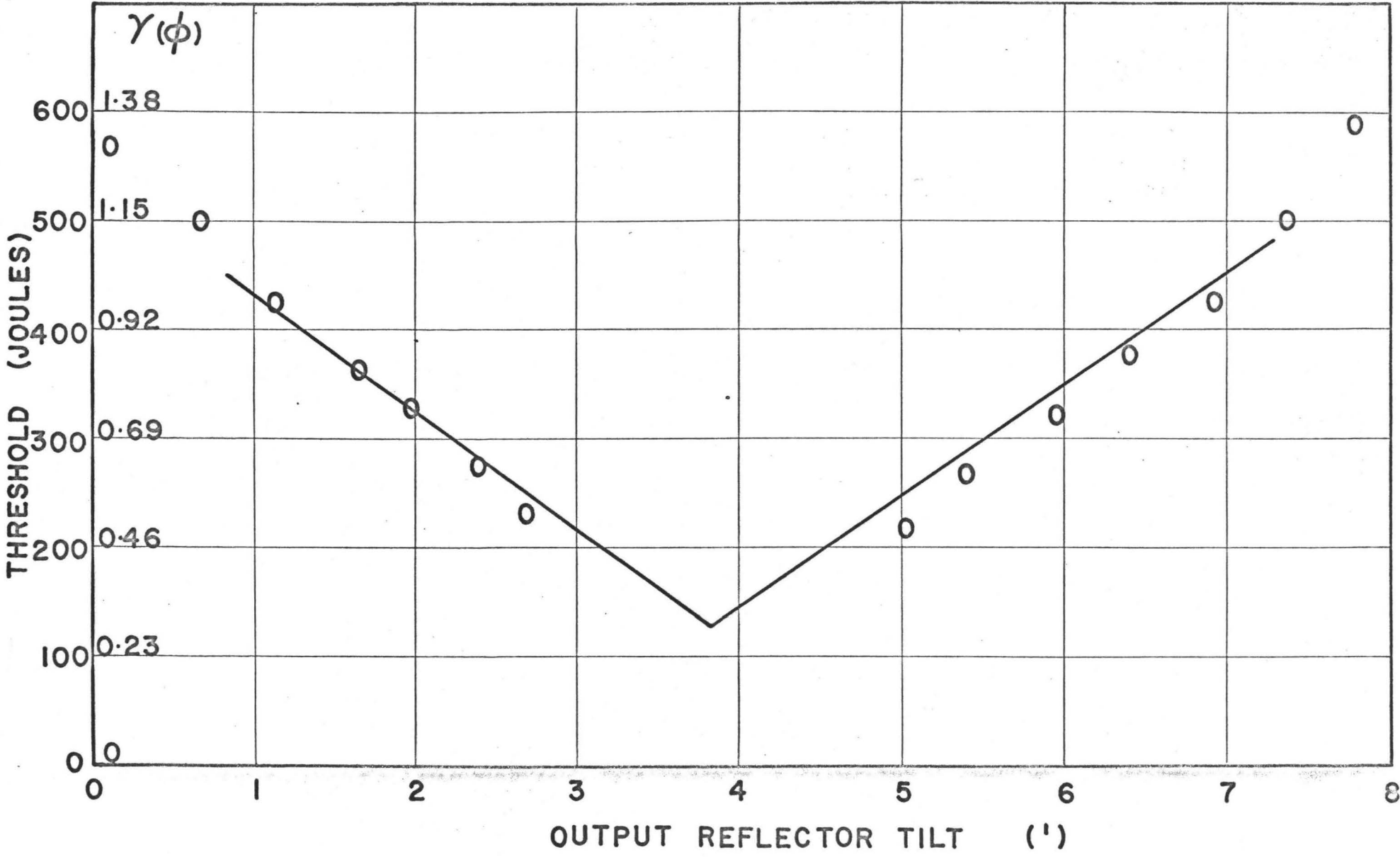
Figure (5-3)

Threshold as a Function of Output Reflection Tilt

Cavity Length = 46 cms.

Output reflector reflectivity = 75%

At 100 rps sweeprate is 2.16 minutes/ $\mu$ sec.



to a cavity length of approximately 92 cm.

The plot in Figure (5-3) is quite symmetric about the position 3' 50". This dependence may be described - up to 450 joules excitation - by two straight lines, one valid for  $\theta \geq 3' 50''$  and  $E \leq 450$  joules and the other valid for  $\theta \leq 3' 50''$  and  $E \leq 450$  joules. If we change the scale of the dependent variable in Figure (5-3) so that in terms of the new scale the functional dependence becomes  $\gamma(\theta)$  we need to keep in mind the reflector reflectivity ( $R = 0.75$ ) which was used to obtain the measurements. We know that the minimum threshold for a high quality laser rod and a large enough cavity Fresnel number is governed entirely by the cavity reflector reflectivities. In the case being considered, there is only one such reflectivity to take into account. This may be done by recalling that

$$\gamma_{Th} = - \ln R = 0.286 \quad \text{for } R = 0.75$$

We thus arrive at the correspondence: 125 joules excitation is needed to overcome losses characterized by a loss function value  $\gamma_{Th} = 0.286$ . We see that if, say, 250 joules are now assumed to be needed to overcome the losses,  $\gamma$  must be equal to  $2 \times \gamma_{Th} = 0.572$ . The dependence is linear. Both scales are shown in Figure (5-3) for ease of reference.

We now clarify a small point in order to avoid confusion. The roof edge of the Porro prism in the experimental apparatus lies in a horizontal plane. The angle  $\theta$  in  $\gamma(\theta)$  is a rotation about a vertical axis. A rotation about a horizontal axis does not change the losses significantly if the angle of rotation is kept small, a consequence of the optical properties of the Porro prism. Thus only one angle of rotation needs to be specified.

Many loss-function dependences on tilt angle were measured. It was observed, experimentally, that the widths of the loss functions vary with cavity length. For long cavities the loss function is narrow. The loss function is also critically dependent on the condition of the optical components within the cavity. A damaged output reflector or faulty dielectric antireflection coatings on the laser rod faces, as well as chipped Porro prisms, increase the losses at a given angle and generally change the function  $\gamma(\theta)$ .

The loss function  $\gamma(\theta)$  depends somewhat more subtly on cavity alignment. The position of the Porro prism roof edge with respect to the cavity axis passing through the centre of the laser rod end-faces is critical. A variation of as little as 0.040 in. Porro prism height changes the response of the laser system significantly. This is a result of variations in the loss function brought about by the change of the prism roof edge height.

### 5.3 The Switching Function $\gamma(\theta)$ with the Lummer Gehrcke

#### Angular Limiting Device Present in the Cavity:

The methods for the determination of the loss function for a cavity containing the Lummer Gehrcke device, are exactly the same as those employed to determine that function for the case without the device. One can now determine, however, a family of loss functions, each member of which corresponds to a particular field opening of the device.

Figure (5.4) shows the results of measurements yielding the family of loss functions for various arbitrary field openings of the device. The degree to which the field has been opened is monitored on a scale provided

Figure (5-4)

Threshold as a Function of Output Reflector Tilt  
with the Lummer Gehrcke Plate in the Cavity

Cavity Length = 40 cms.

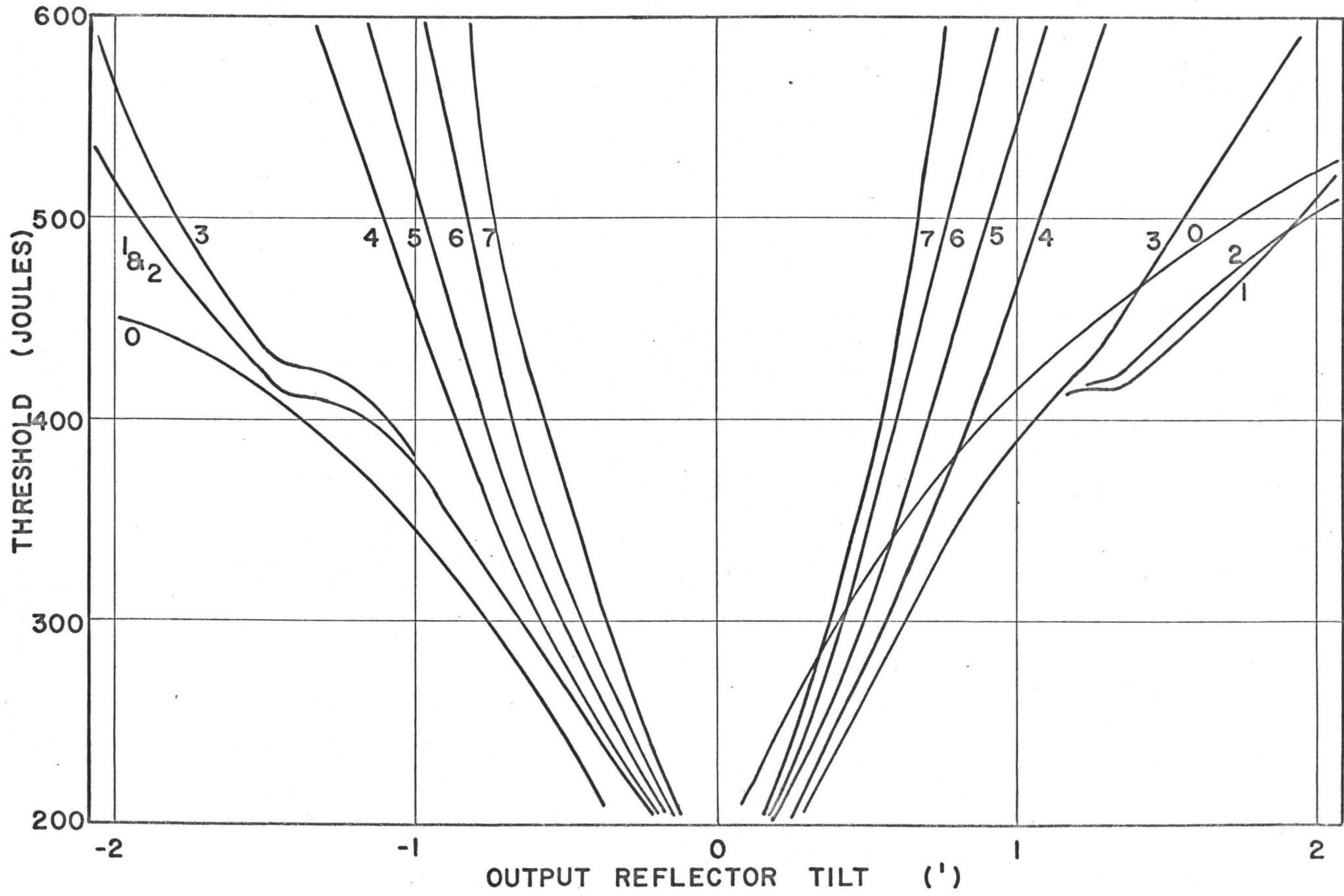
Output Reflector Reflectivity = 55%

The arbitrary field setting is the parameter for the family of loss functions.

FIELD SETTING

- 0 - No Lummer Gehrcke in the cavity
- 1 - 320
- 2 - 340
- 3 - 300
- 4 - 280
- 5 - 270
- 6 - 260
- 7 - 245

(Experimental points not shown in order to avoid clutter  
of the diagram)



on the device for that purpose. The loss function obtained by simply removing the device from the cavity, is also shown for comparison.

The family of loss functions is characterized by various noteworthy features. It is evident that the threshold energy for the aligned configuration is essentially independent of the field opening and furthermore of whether or not the device is present in the cavity. On the other hand, the angular width of each loss function is strongly dependent on the particular field opening - as monitored on the scale provided for that purpose - that characterizes each of those functions. The Lummer Gehrcke angular limiting device provides a means, then, of increasing the effective switching speed of a Porro prism Q-switched laser.

Before proceeding further, an apparent discrepancy will be pointed out, and an explanation removing it given. The reflector reflectivity used to obtain the measurements of the loss functions was 55%. Using the data of the previous section, we would expect threshold for the aligned cavity to have occurred at joules excitation. Threshold, however, occurred at 175 joules excitation. The apparent discrepancy will be resolved with the following additional information. In particular, the measurements on the system containing the angular selective device were carried out under ideal conditions. A new flashtube had just been installed and the elliptical cylinder reflector surfaces polished to a fine finish. A new laser rod had been inserted accurately along the appropriate focal line of the elliptical cylinder pump housing. These conditions combined to obtain an ideal situation which would tend to minimize threshold, in contrast to the measurements described in the last Section which were not carried out under quite such ideal circumstances. The differences in the system, from one set of measurements to

another make analytical comparisons meaningless.

The results of Figure (5-4) were not easy to obtain. Many attempts to make similar measurements were frustrated by incorrect results. In particular, it was observed on numerous occasions that, rather than narrowing the loss function, closing the field of the angular limiting device simply resulted in an apparent upward displacement of the loss function  $\gamma(\theta)$ . The correct results depicted in Figure (5-4) were obtained after careful alignment of the Lummer Gehrcke device with respect to the axis of the cavity, and also after careful alignment of the two component plates of the device with respect to each other.

The device plates must be positioned in such a manner that on a double pass through the system by a beam, well spread in angular space, the two resulting cut-off angles of one plate coincide with the appropriate cut-off angles of the other plate. In this configuration, the cut-off is as steep as can be obtained with the given device. Inspection of the characteristics of Figure (5-4) tells us that the above mentioned condition must be met within approximately ten seconds of arc.

With reference to the alignment of the cavity axis with respect to the axis of the device, the condition to be met can be formulated as follows. The cavity axis must coincide in direction with the propagation vector of one of the "plane-waves" which will be allowed to propagate, unattenuated, through the device when the acceptance angle of the device tends to zero. Inspecting once more the magnitude of the angles involved in Figure (5-4), we see that the above restriction can be violated by not more than ten seconds of arc without impairing system performance.

From such tolerance restrictions, therefore, it is evident why success did not arrive immediately on the first attempt at measuring the characteristics with the device in the cavity.

Output energy characteristics were obtained from the laser using a field setting of 270 as determined from the arbitrary scale of the Lummer-Gehrcke device. The results of those measurements will be presented in Section 5.6.

#### 5.4 The Output Energy Characteristics:

Figure (5-5) shows graphically the results of output energy measurements on our Q-spoiled laser system for a cavity configuration without an angular limiting device. The output reflector reflectivity was 75%. The cavity configuration which was used in the measurement of the output energy characteristics shown in Figure (5-5) was identical to that used to determine the switching function shown in Figure (5-3). The appropriate switching function to use, in calculations attempting to predict the energy characteristics of Figure (5-5), is thus the switching function depicted in Figure (5-3).

Each member of the family of characteristics of Figure (5-5) is distinguished from all other members by a label giving the energy input into the flashlamp which was used in obtaining the particular characteristic. One could just as easily label each characteristic by the maximum population inversion obtained for the particular flashlamp input energy. To avoid cumbersome numbers one could, alternately, use the value of  $N_0$  corresponding to the flashlamp energy. The procedure is already familiar to us. Corresponding to the aligned threshold value of 125 joules, we can

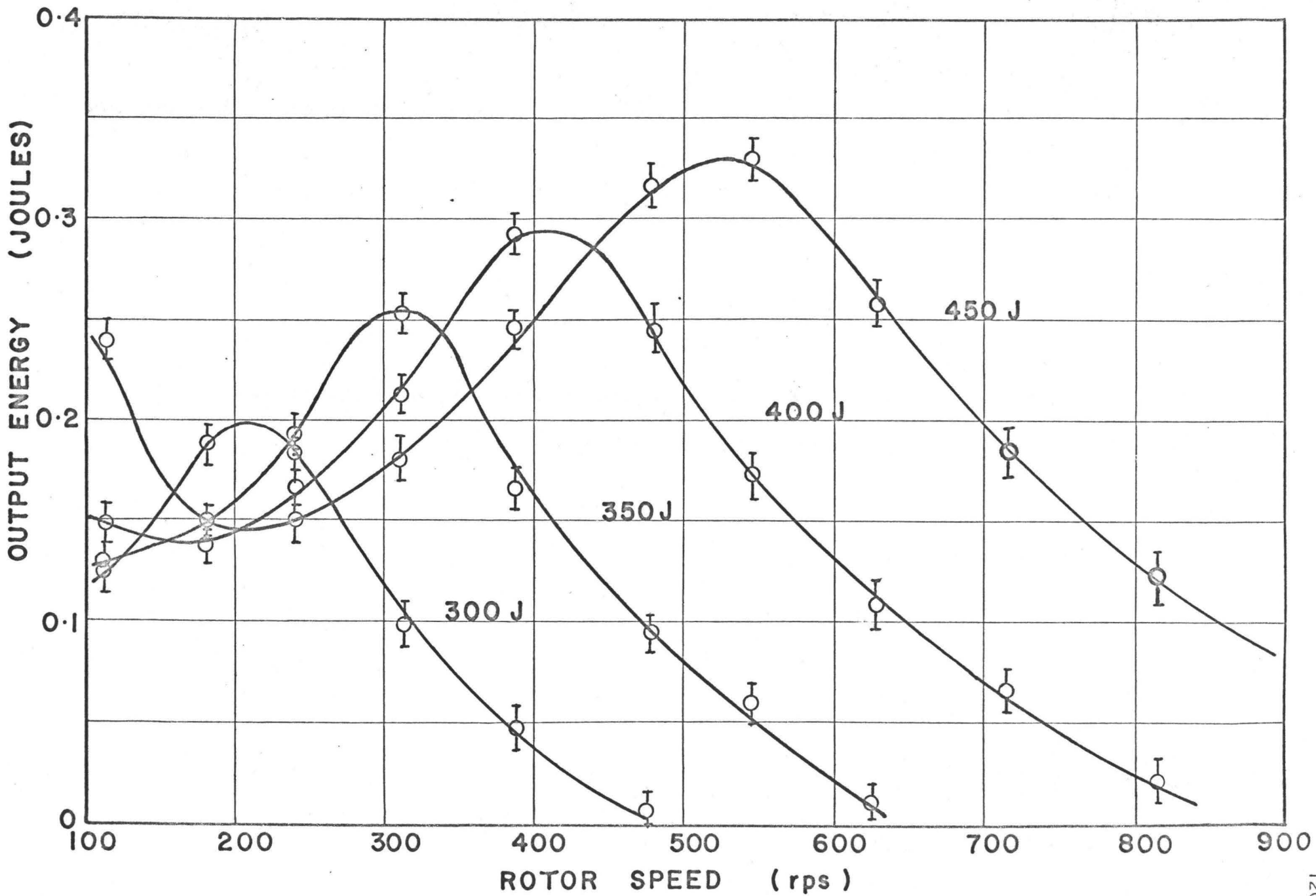
Figure (5-5)

Experimental Output Energy Characteristics

Cavity length = 46 cms.

Output reflector reflectivity = 75%

Excitation energy into the flashlamp is the family parameter.



calculate the appropriate value of  $N_0$  given by  $N_0 = \ln R$  - which for  $R = 75\%$  gives  $N_0 = 0.286$ . The relationship between  $N_0$  and input energy into the flashlamp is linear; thus, for 450 joules, the corresponding value of  $N_0$  will be  $\frac{450}{125} \times 0.286 = 1.03$ . The value of  $N_0$  so obtained will be the normalized inversion just prior to the start of positive feedback in the cavity for 450 joules excitation into the pumping flashlamp. Since all measurements refer to that time during the pulsed pumping cycle when the fluorescent strength is at its maximum, the value of  $N_0$  which we have arrived at for 450 joules excitation is the maximum normalized inversion obtained during the pumping cycle. Since we now know how to relate the input energy into the flashlamp to the normalized initial peak inversion,  $N_0$ , we henceforth may label the characteristics by the input energy into the flashlamp.

The characteristics of Figure (5-5) have some noteworthy features. In particular, we see that each characteristic of the family cuts off at sufficiently high switching speeds. There also exists a maximum for each characteristic, (corresponding to the largest energy output obtainable from the laser system for a given excitation), which occurs at a switching speed roughly one half that of the corresponding cut-off speed. We have indicated earlier that this is just the behaviour one would expect in the presence of a symmetric switching function,  $\gamma(\theta)$ . If we restrict our attention to that portion of the 450 joules characteristic relating to switching speeds slower than the optimum, we note that the output energy first decreases and eventually reaches a minimum at about 200 rps.

The increase in output energy, upon continuing to still slower switching speeds, would finally saturate, resulting in a new energy maximum.

The 450 joules characteristic of Figure (5-5) unfortunately does not show this behaviour, because sufficiently low switching speeds were not reached during the experimental run.

If we refer now to Figure (5-6), we note the clear evidence for a secondary maximum in the case of the 550 joule and 600 joule characteristic. The characteristics of Figure (5-6) were obtained with a 75% reflectivity output reflector employing a similar cavity configuration as that which was used to obtain the results represented by Figure (5-5). On making a comparison between the two sets of characteristics, it is evident that the characteristics of Figure (5-6) have shifted towards lower switching speeds with respect to the characteristics of Figure (5-5). The shift is due to somewhat different cavity configurations used in obtaining the two sets of characteristics. The second cavity configuration either because of the positioning of the laser rod in the elliptic pumping housing or because of slight maladjustment of the Porro prism height with respect to the cavity axis, was not quite as efficient as it could have been made. We conclude that about 50 joules of excitation were "lost".

The characteristics of Figure (5-6) clearly show the effects of reflector damage, which probably occurred at 460 rps and 500 joule excitation, and this fact was confirmed visually. The result of the damage was to make the high excitation energy ( $> 350$  joules) characteristics cut-off much quicker than they would have done had damage to the output reflector not occurred.

The two sets of characteristics we have been discussing show clearly that the optimum switching speed depends strongly on the excitation

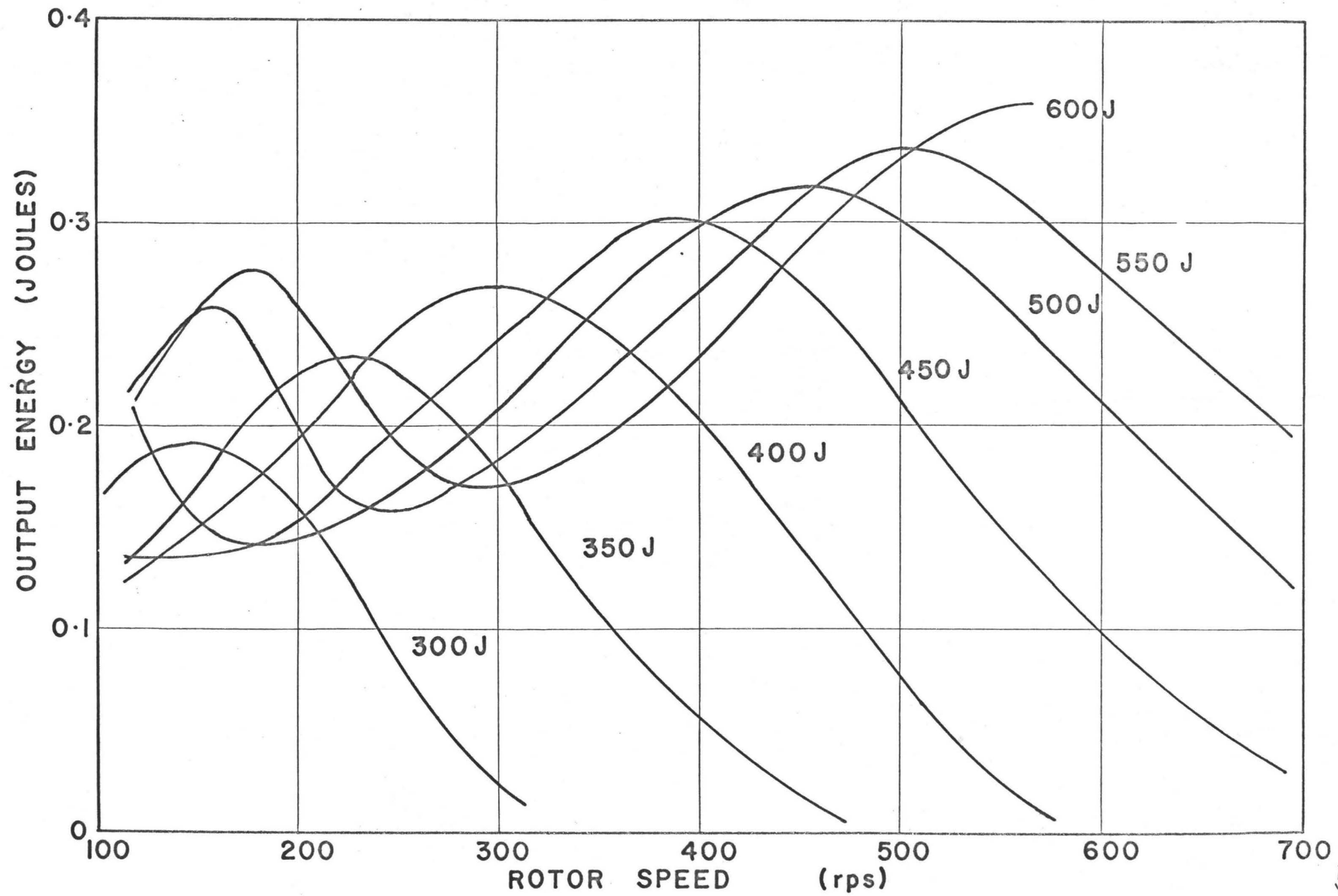
Figure (5-6)

Experimental Output Energy Characteristics

Cavity length = 46 cms.

Output reflector reflectivity = 75%

Excitation energy into the flashlamp is the family parameter.



of the laser rod. In particular, the lower the laser rod excitation, the slower will be the optimum switching speed required to yield maximum energy-content in the pulse. We should, at this point, specify that we are speaking of the optimum switching speed as determined from the maximum in the output energy characteristic for the excitation of interest. We shall see later that maximum pulse energy and maximum pulse power are not necessarily obtained simultaneously.

Together with the output energy measurements presented in Figure (5-6), time evolution observations on the development of the giant pulse(s) were made. The results of those measurements are presented in the next Section.

#### 5.5 Relation of the Time Evolution of the Giant Pulse to the Output Energy Characteristics:

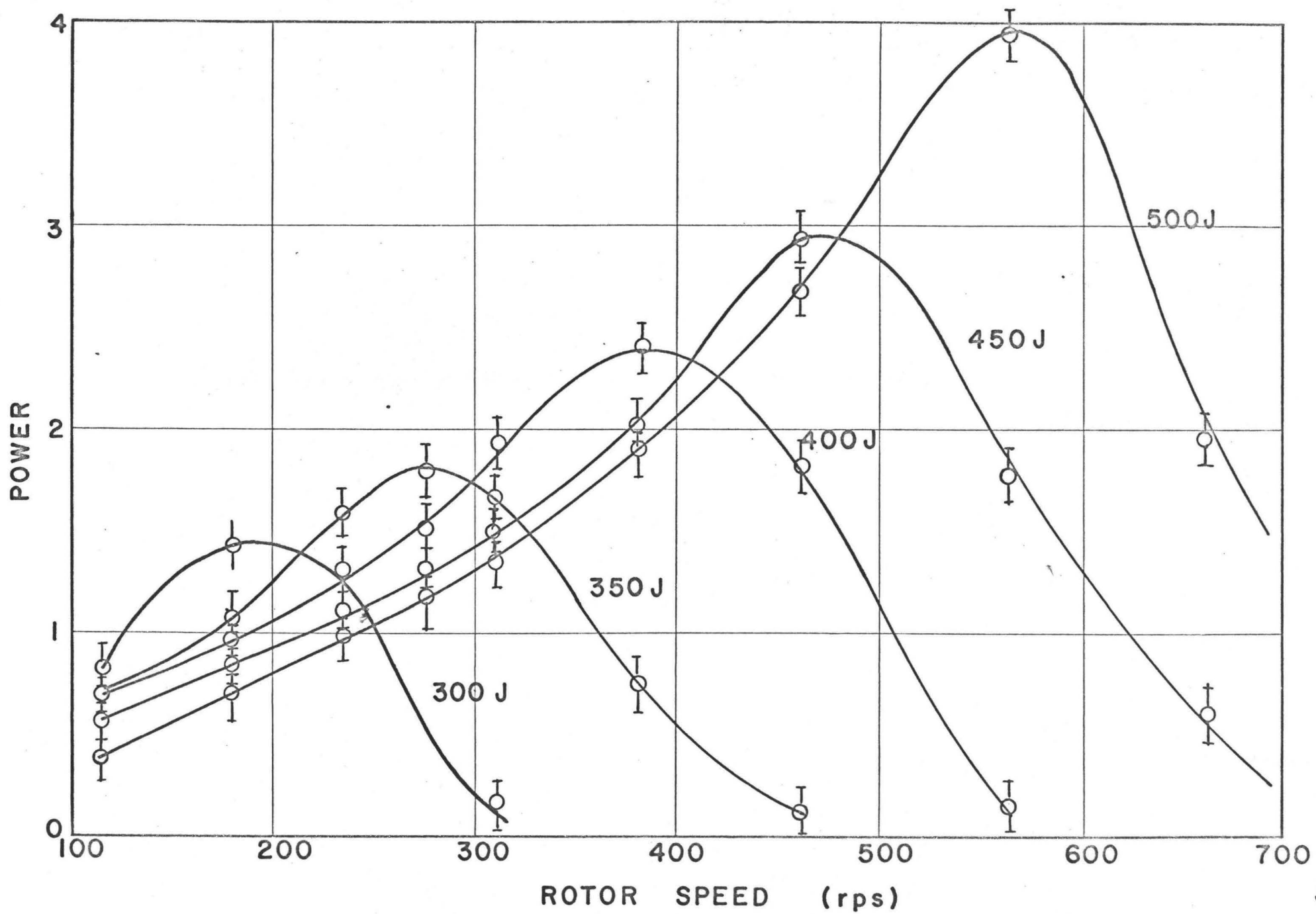
Figure (5-7) is a plot of the peak output power of the giant pulses that gave rise to the output energy characteristics of Figure (5-6). The plot represents the height of the leading pulse, when two or more output pulses are observed in a single pulsing of the laser. The power scale is arbitrary. The arbitrariness of the scale may be approximately removed by recalling that the giant pulses are, in our case, typically about 30 nsec. long. The appropriate output energy measurements may then be used to calculate giant pulse power content.

We see, upon referring to Figure (5-7), that the height of the lead pulse for a particular laser rod excitation has a single maximum and that output power decreases monotonically about that maximum for switching speeds on either side of the optimum. If we compare the switching speeds

Figure (5-7)

Experimental Output Power Characteristics of  
the Leading Pulse

These data were taken simultaneously with the data of Figure (5-6). It should be noted that the response time of the oscilloscope was not really fast enough to make accurate power measurements.



at which maximum power and maximum energy are obtained by simultaneously referring to the related characteristics of Figure (5-7) and (5-6), we see that peak power output occurs at higher switching speeds than does maximum output pulse energy content. This experimental observation appears to be somewhat baffling. It is, however, one of the more pleasant surprises of the laser rate equation solutions in that such behaviour is indeed attained.

It is not difficult to understand why a single giant pulse output from a given laser system will, in general, be narrower in time than a giant pulse allowed to evolve in the same system, but whose energy content is lower than that of the former pulse. The output energy characteristic for a laser rod excitation of 550 joules, as depicted in Figure (5-6), has a minimum at a switching speed of about 240 rps. At somewhat slower switching speeds the energy content of the laser output pulse is seen to increase. On the other hand, referring to the related power characteristic of Figure (5-7), we see that the peak power of the lead pulse is decreasing in this switching speed region. Hence, its width in time is increasing, but not nearly as fast as the corresponding decrease in pulse height. Thus, the sudden increase in energy content of the output is due to the evolution of a secondary pulse following the lead pulse and which contributes its energy content to that of the lead pulse. In the foregoing we have been discussing the onset of double pulse outputs. Multiple pulse outputs would be observed at still lower switching speeds. Observations of the time evolution of the giant pulse on an oscilloscope screen confirmed the point in question, namely; that the rather sudden increase in laser pulse output energy content as observed at sufficiently low

Figure (5-8)

Experimental Time Evolution of the Giant Pulse

The results shown in the Figure are for constant excitation (500 joules) and for a 46 cm cavity length.

1 - 663 rps

2 - 565 rps

3 - 461 rps

4 - 382 rps

5 - 313 rps

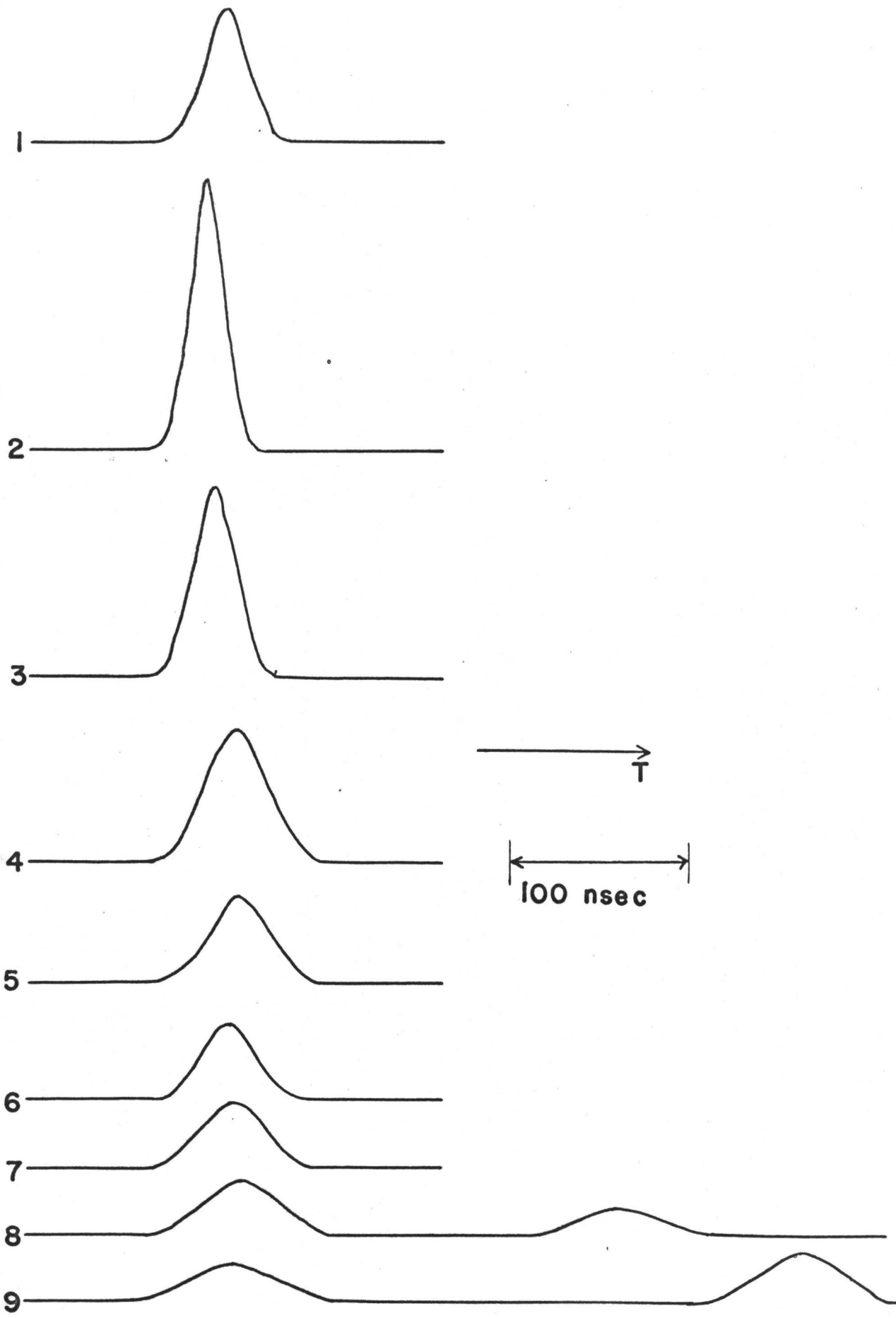
6 - 276 rps

7 - 236 rps

8 - 180 rps

9 - 115 rps

See Figure (5-6) for the corresponding output energy characteristic.



switching speeds, is due to the appearance of a secondary giant pulse.

Pulse narrowing is observed as a consequence of increased pulse energy content. Thus, it is not surprising that the peaks of the power characteristics increase more rapidly with excitation than do the optimum switching speed peaks of the corresponding energy characteristics.

In Figure (5-8) we show the various stages of pulse time evolution as a function of switching speed for constant excitation of the laser rod. The data necessary to depict such time developments was obtained from photographic records of pulse evolution as viewed on an oscilloscope screen. Figure (5-8) represents a faithful record insofar as giant pulse height and width are concerned, while in the case of double pulse outputs, pulse separation is also recorded.

## 5.6 Output Energy Characteristics - Lummer-Gehrcke

### Device Within the Cavity:

The introduction of an angular limiting device within the cavity of a rotating Porro prism Q-switched laser alters the operating characteristics of the laser. The alteration is particularly drastic in the case of the apparent switching speed of the Porro prism. The direct effects of the Lummer-Gehrcke plate can be summarized as follows:

1. Polarization of the beam due to the four Brewster angle windows which afford a lower reflection loss to a particular polarization.
2. A significant increase in cavity length for cavities whose output reflector Porro prism separation is of the order of 40 cms. This

increase in cavity length comes about, first of all, because of the introduction of the quartz medium (index of refraction  $n = 1.46$ ) within the previously air filled space. Secondly, the fact that the plates are oriented at a significant angle ( $27^\circ$ ) to the axis of the cavity contributes a further increase in cavity length. Thirdly, an increase in that path length also results from the fact that the propagating beam within the plates travels at a steep angle with respect to the axis of the given plate (critical angle =  $43^\circ$ ). We may amalgamate these effects by saying that an air filled space of 20 cm appears upon the introduction therein of the Lummer-Gehrcke device to have an optical path length of 40 cm. This effective increase in cavity length brought about by the aforementioned causes will increase the effective switching speed of the Porro prism.

3. An increase in effective switching speed accomplished by critical adjustment of the band-pass of the angular selective device.

4. Some extra insertion losses are added to the cavity arising from multiple internal reflections from imperfectly "clean" boundaries. A secondary apparent loss mechanism will be pointed out. If the laser prefers to lase in a given polarization and the introduction of the Lummer Gehrcke device changes that situation there will be an increase in the threshold for the given cavity configuration. We can, therefore, think in terms of an increase in the losses.

We have reviewed the direct effects of the presence of the Lummer Gehrcke plate on the cavity characteristics. Particular attention should be paid to the increase in cavity length. We can state quite generally that if other variables remain constant, then a doubling of the cavity

length will in fact result in a doubling of the effective switching speed of the prism. Now consider a particular cavity whose switching function  $\gamma(\theta)$  has been narrowed by a factor of 3.6 due to the presence of the angular limiting device. The cavity is also assumed to have been shortened from a separation of 45 cm to one of 40 cm between the output reflector and the Porro prism. The effective cavity lengths would then be 90 cm and 120 cm, respectively. The switching speed of the rotor would appear to be increased by a factor of  $\frac{120}{90} = 1.34$  due to the longer cavity length. The net apparent switching speed increase may then be obtained by multiplying the actual rotor speed by a factor of  $1.34 \times 3.6 = 4.8$ . We would thus expect the characteristics to peak at rotor switching speeds which are lower than those of the device-free cavity, as a result of the introduction of the angular limiting device into the cavity.

Referring to Figure (5-10), we see that the 450 joule characteristic peaks at a switching speed of 80 rps. Figure (5-10) represents the experimental output energy characteristics for a cavity length of 40 cm, and for a field setting of 270 on the Lummer Gehrcke device. The appropriate switching function is that of Figure (5-4) corresponding to a field setting of 270, where we also note that the output reflector reflectivity is 50%.

If we now refer to the results of Figure (5-5), we see that the 450 joule energy output characteristic peaks at 525 rps. Since the results depicted in Figure (5-5) were obtained by employing a 45 cm cavity length and in addition the width of the appropriate switching function (see Figure (5-3) ) at 450 joules excitation is 6 minutes of arc, it follows that we have results at our disposal that are equivalent to the

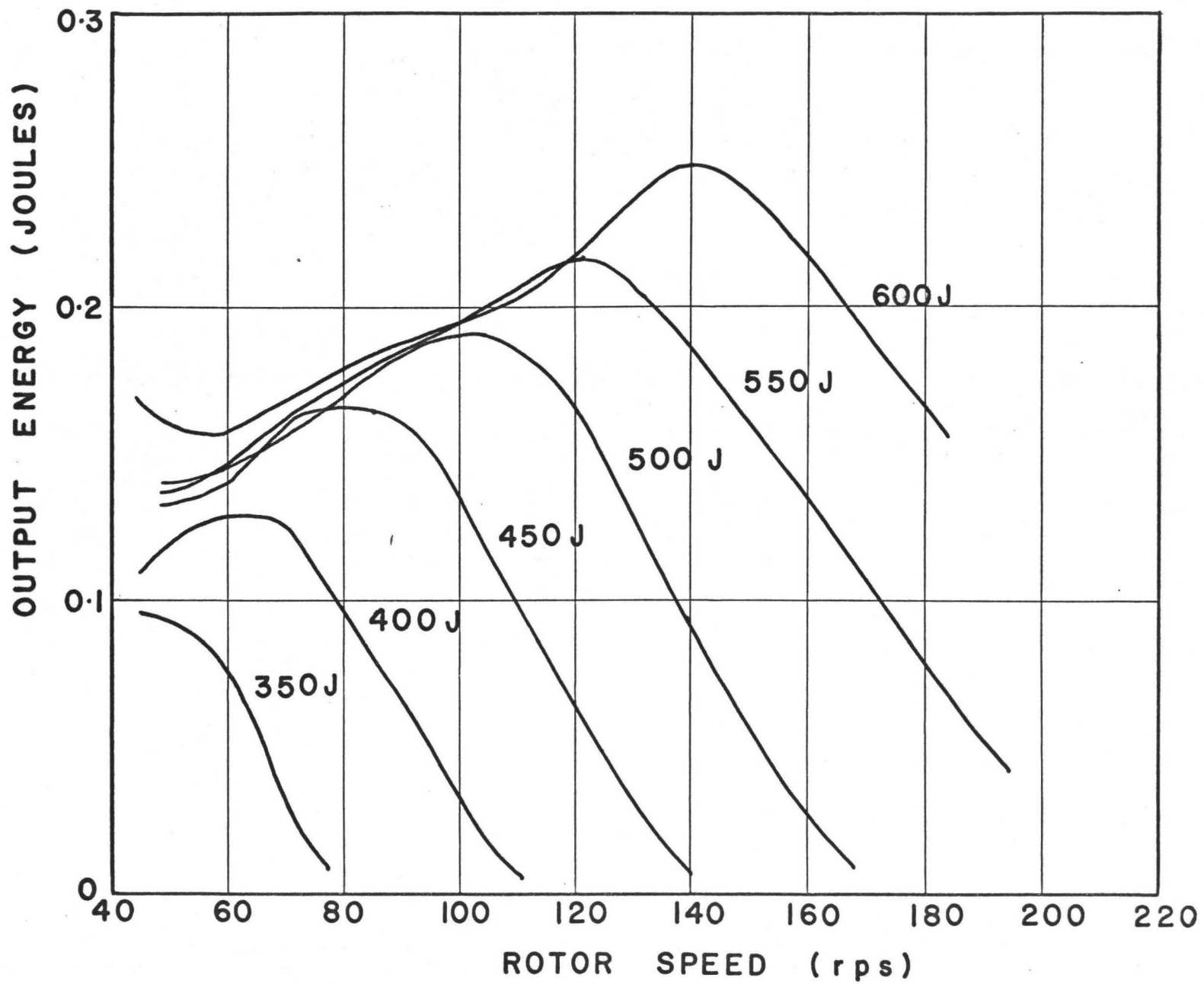
Figure (5-10)

Experimental Output Energy Characteristics with the  
Lummer Gehrcke Plate in the Cavity

Cavity length = 40 cms

Reflector Reflectivity = 50%

The field setting was 270. Refer to Figure (5-4)



situation postulated above. The only difference between the experimental conditions under which the data of Figures (5-5) and (5-10) were obtained and the postulated situation is that in the former case the output reflector reflectivities were not held constant. The effect of reflector reflectivities on the argument will be considered in Section 6.3.

We know that the 450 joule characteristic with the Lummer Gehrcke plate in the cavity should peak at  $\frac{525}{4.8} = 110$  cps. We recall (see Figure (5-10) ) that, in fact, it peaks at 80 cps. The difference in the two values is due to the two different reflector reflectivities used. Had a 75% output reflector reflectivity been used for the output energy measurements on the cavity with the angular limiting device, the 450 joule output energy characteristic could be expected to peak closer to 110 cps. However, since a 50% reflector reflectivity was used, the 450 joule characteristic naturally peaks at the lower value of 80 cps. The estimate is admittedly rough, especially since the shapes of the two switching functions we have been concerned with, are somewhat different. In the case of the simple cavity, the switching function of Figure (5-3) applies, whereas in the case of the angular limited cavity it is the switching function of Figure (5-4) corresponding to the field setting of 270 which applies. Also, we have noted that the relevant reflectivities are somewhat different. However, the general agreement between the two sets of characteristics is seen to be present. One cannot, without direct solution of the laser rate equations, verify precisely the degree of agreement between the two sets of characteristics. Nevertheless, in Section 6.3 we take into account the remnant reflectivity factor, employing an approximate calculation, the result of which is to improve upon the agreement already obtained for the

positions of the peaks of the two 450 joule characteristics.

The characteristics of Figure (5-10) show the general behaviour that we have come to expect on the basis of previous discussions. We will not discuss such behaviour further at this time.

### 5.7 Energy Utilization Factor Measurements:

An important consideration in giant pulse laser studies is the fraction of the available excitation energy in the laser rod which is converted into coherent photons upon the evolution of the pulse. This fraction is just the energy utilization factor. In this section we will concern ourselves with the measurement of that factor under strong pumping conditions. It is under such conditions that the energy utilization tends asymptotically towards its maximum value.

The strength of the  $1.06\mu$  fluorescence of  $\text{Nd}^{+3}$  just before the start of the evolution of the giant pulse provides us with a measure of the number of excited ions in the  ${}^4\text{F}_{3/2}$  state. The relatively short lifetime of the terminal  ${}^4\text{I}_{11/2}$  state assures us that it will be essentially empty under the conditions being considered.

Let us for a moment digress from our considerations and thereby pinpoint the conditions under which we assume the laser to be operating. The population inversion is several times above its threshold value at the instant the giant pulse evolves. The laser rod has gain as long as the pertinent population is inverted. We recall that the peak power in the laser pulse is reached when the population inversion is equal to its threshold value, having been driven to that point by the depleting effect of the positive feedback. We may say that the giant pulse goes through a

maximum when the system gain is equal to losses. The population inversion will, however, continue to drop because of the high flux density now present in the laser cavity. Its final value will depend upon the initial inversion, among other things, but if the initial inversion is large compared with the losses, the population inversion will be driven to a value close to zero. This final value will be essentially reached by the time the flux density has decreased to one tenth of its maximum value. The upper  ${}^4F_{3/2}$  level population has at this time almost reached its short term steady state value, which naturally depends on the population of the terminal  ${}^4I_{11/2}$  level at the same instant of time. If the latter level is not depopulated fast enough by transitions to the ground state, the final population of the  ${}^4F_{3/2}$  level will not be zero after the evolution of the giant pulse. It will take on a definite value just after the evolution of the pulse. It is now evident that, even under ideal circumstances, only a certain fraction of the initially excited ions will be allowed to contribute energy to the giant pulse.

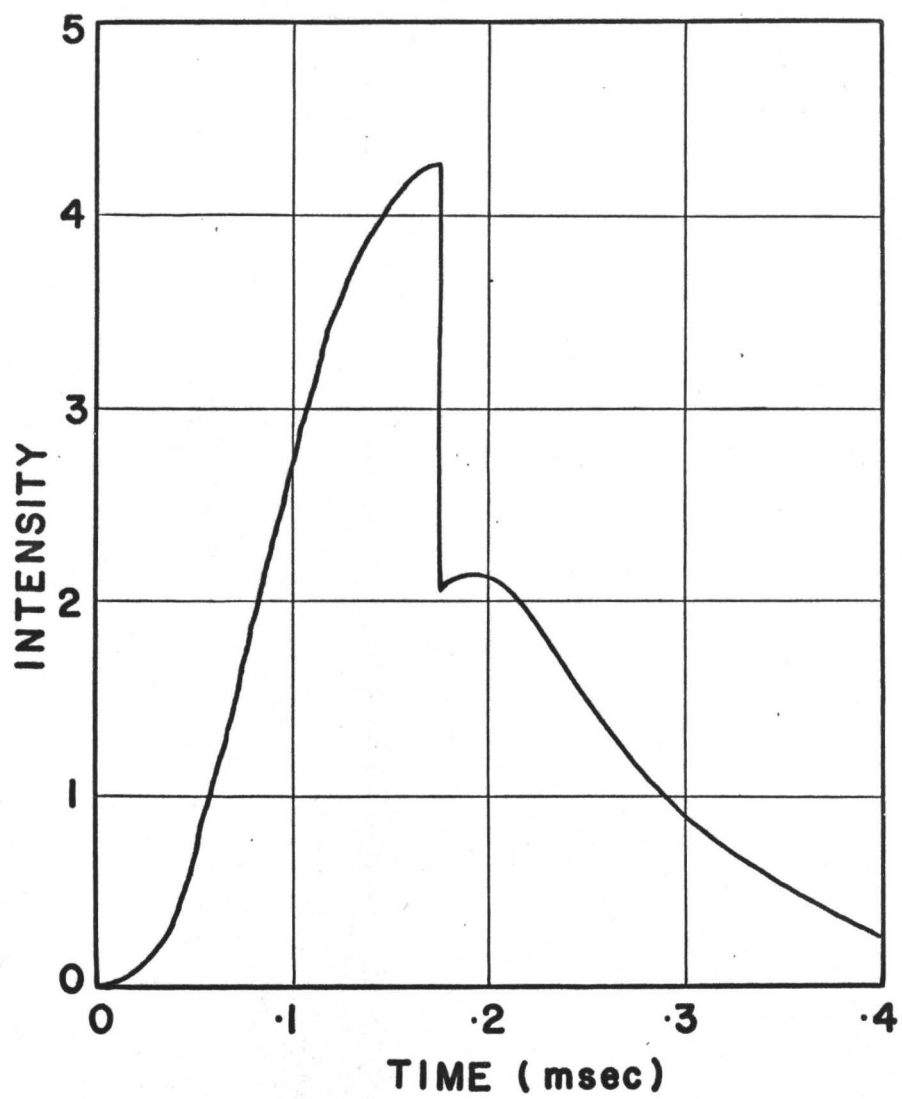
From the foregoing it is concluded that a measure of the fluorescent strength, just before and just after the evolution of the giant pulse, yields a value of the energy utilization factor. The quantity yielded by the measurement will be independent of laser rod excitation as long as the pumping is strong enough and operation takes place in the optimum energy output region of the switching speed characteristic corresponding to that excitation.

In order to measure the fluorescent strength of the  $1.06\mu$  transition, a grating spectrograph was utilized to provide the necessary dispersion. Fiber-optics were used to pick off fluorescent radiation from the

Figure (5-11)

Experimentally Observed Fluorescent Strength of the  
 ${}^4F_{3/2} \rightarrow {}^4I_{11/2}$  Transition of  $Nd^{+3}$  During the Pumping  
Interval

The step discontinuity is due to the evolution of the giant pulse.



laser rod. The entrance pupil of the fiber-optics bundle was located close to and facing one of the crystal end faces but just outside the spatial extent of the Q-spoiled beam. The exit pupil was positioned in such a manner as to illuminate the entrance slit of the grating spectrograph. An appropriately located photomultiplier detected the fluorescent strength of the  $1.06\mu$  transition as a function of time. The signal from the photomultiplier was displayed on an oscilloscope screen.

A result of a measurement of the fluorescent strength is shown in Figure (5-11). The measurement was made with the laser operated at 600 joules excitation with a cavity length of 45 cms and a 50% output reflector reflectivity. With reference to this figure it is to be noted that the flashlamp pump builds up the fluorescent intensity to a peak value, which is reached when excitation losses by spontaneous emission are equal to the rate of population of the upper level by the flashlamp pumping pulse. At this time the Q-spoiled pulse is allowed to evolve, and so force the fluorescent intensity to drop sharply to a value which is proportional to the  ${}^4F_{3/2}$  population just after the evolution of the giant pulse. Spontaneous emission now takes its toll on the upper level population and the fluorescent intensity falls exponentially to zero once the pumping pulse from the flashlamp has died out.

From the figure one would conclude that the energy utilization factor is approximately 50%. It must be remembered, however, that the signal has background "noise" from the flashlamp superimposed on it. When this background noise is taken into account the true energy utilization factor is found to be 61%. The energy utilization factor just quoted will be close to its saturation value because Q-spoiling was allowed to take place at optimum energy output and, furthermore, because 600 joules

excitation corresponded to three times threshold. Calculations show that, at three times threshold, 94% of the available energy will be released in the giant pulse.

This 61% energy utilization factor saturation value provides dramatic proof of the conversion efficiency of the Q-switched laser system used in obtaining the experimental results presented in this thesis. At this point we indicate that theory predicts a saturation value of approximately 68% for the energy utilization factor (see Section 5.3). Reasons for the discrepancy will be presented in Chapter 6.

## CHAPTER 6

### DISCUSSION OF RESULTS

#### 6.1 Determination of the Initial Flux in the Cavity and its Relation to the Positions of the Energy Maxima in the Switching Speed vs Energy Output Characteristics:

In the Appendix it is shown that the initial normalized flux  $\phi_{oi}$  is given approximately by the expression:

$$\phi_{oi} = - \frac{\Delta\Omega}{4\pi} \frac{\tau_c}{\tau_r} \ln R \quad \dots(6-1)$$

where  $\tau_c$  is the mean lifetime of a photon in the cavity and  $\tau_r$  is the spontaneous radiative lifetime of the laser transition under consideration.  $R$  is the output reflector reflectivity and  $\Delta\Omega$  is the solid angle containing  $\phi_{oi}$ . We recall that  $\phi_{oi}$  is the initial value of  $\phi_o$  appropriate to equations (2-19), (2-20) and (2-21) just at the time when the laser material gain overcomes the cavity losses and the cavity is perfectly aligned. It is in general not necessary to worry greatly about the accuracy of  $\phi_{oi}$ , as estimated from expression (6-1), since the dependence of the optimum switching speed on  $\phi_{oi}$ , for a particular output energy characteristic, can be seen after some thought to be logarithmic. Thus the position of the optimum switching speed for a given excitation of the laser rod is relatively insensitive to variations in  $\phi_{oi}$ .

For the  $\text{Nd}^{+3}$  doped glass laser rods used in the experiments forming the basis for this work, the value  $\tau_r = 360 \mu\text{sec}$  is appropriate.  $\tau_c$  is estimated to be of the order of magnitude of the time per pass of a photon in the cavity. Since we are dealing with cavities with an effective cavity length of approximately 90 cm, we can set this value as  $\tau_c \approx 3 \text{ nsec}$ . The appropriate reflectivity is 75%, therefore,  $\ln R = -0.29$ . Further, if we assume the diffraction limit for  $\Delta\Omega$ , we can set the magnitude of this quantity as  $\Delta\Omega \approx (1 \text{ minute})^2 = (3 \times 10^{-4} \text{ radians})^2 = 9 \times 10^{-8} \text{ steradians}$ . Upon inserting the quantities just estimated into equation (6-1) we arrive at  $\phi_{oi} \approx 0.2 \times 10^{-13}$ . This is the value of  $\phi_{oi}$  at threshold for the aligned cavity (125 joules for the case being considered).  $\phi_{oi}$  will increase in proportion to the input pump energy. Hence at 400 joules the appropriate value for  $\phi_{oi}$  is approximately  $10^{-13}$ . This value of  $\phi_{oi}$  represents an estimate which most likely is good to within an order of magnitude.

We have indicated earlier (see Section 2.5) that the initial lower level population  $N_{10i}$  is to be taken as zero due to the expected short lifetime of the terminal  $^4I_{11/2}$  laser level of  $\text{Nd}^{+3}$  in glass. The method of obtaining  $N_{oi}$  has also been outlined. This information together with the form of the switching function is sufficient to allow one to proceed with the solution of equations (2-19), (2-20) and (2-21) with  $\tau$  treated as a parameter. If it so happens that the estimate of  $\phi_{oi}$  is too large or too small, we expect the output energy characteristics, as calculated from the above mentioned coupled differential equations, to peak sooner or later respectively than in the case of the experimentally observed characteristics. The reason for this expectation is not difficult to

understand. The value of  $\phi_0$  up to which the field in the cavity must build in order to significantly disturb the inversion  $N_0$ , is independent of  $\phi_{oi}$ . It follows that if too large a value is assumed for  $\phi_{oi}$ , the switch,  $\gamma(T)$ , must sweep at a relatively fast rate in order that  $\phi_0$  build up to its perturbing value in the time vicinity where  $\gamma(T)$  takes on its minimum value. The calculated energy maximum of the characteristic will therefore lie at a faster switching speed value than that of the corresponding experimentally observed characteristic.

The value of  $\phi_{oi}$  as estimated from equation (6-1) yields a very satisfactory fit of the positions of the energy maxima of the calculated output energy characteristics to those corresponding positions which are observed experimentally. We conclude that equation (6-1) is valid for the case we have considered and provides the basis for a useful estimate of  $\phi_{oi}$ . Finally, it may be pointed out that the value of  $\phi_{oi}$  can be translated back into physically more meaningful dimensions by reversing the appropriate parts of the argument used in the derivation carried out in the Appendix.

We can employ a simple physical argument as a cross check on the estimate of  $\phi_{oi}$  obtained using equation (6-1). If we allow the crystal-- upon being pumped--to de-excite itself by the process of spontaneous emission, we can in fact assume for simplicity that a "pulse" (of  $360 \times 10^{-6}$  sec. duration for our pumping configuration) has been emitted isotropically into space by the laser rod. On the other hand, if we now imagine the laser to be Q-spoiled, we obtain a giant pulse whose half width is of the order of  $20 \times 10^{-9}$  sec. and is contained in a solid angle

$\Delta\Omega$ . It follows immediately that:

$$\frac{\phi_{op}}{\phi_{oi}} = \frac{360 \times 10^{-6}}{20 \times 10^{-9}} \times \frac{\Delta\pi}{\Delta\Omega}$$

If we take the value  $\Delta\Omega = 9 \times 10^{-8}$  steradians we obtain

$$\frac{\phi_{op}}{\phi_{oi}} = 0.2 \times 10^{13}$$

Calculations show that  $\phi_{op}$  is of the order of 0.2 in the case of interest. Hence a value of  $\phi_{oi} = 10^{-13}$  is in good agreement with our previous estimate.

It is important to note that there are certain limitations in the arguments used to arrive at the results outlined above. For instance, no mention has been made of the fact that the  ${}^4F_{3/2}$  level of  $Nd^{+3}$  can undergo three known approximately equal strength spontaneous radiative transitions in its quest to reach the ground state<sup>(44)</sup>. Under Q-spoiled laser action, on the other hand, the  ${}^4F_{3/2}$  level will mainly be depopulated through stimulated emission to the  ${}^4I_{11/2}$  level. It is not difficult to see that these considerations will influence somewhat the ratio  $\frac{\phi_{op}}{\phi_{oi}}$  as written above.

## 6.2 Estimation of the Output Energy of the $Nd^{+3}$

### Doped Glass Q-Switched Laser:

An expression which is useful in estimating the output energy of a Q-spoiled  $Nd^{+3}$  doped glass laser is already available to us. This expression is explicitly;

$$\left(\frac{N_K}{\Delta\omega}\right)_{\text{Threshold}} = -\ln(R) \frac{4\tau_r \eta^2}{\lambda_0^2 \ell}$$

and follows directly from equation (2-29). We may write  $\Delta\omega = \frac{2\pi c \Delta\lambda}{\lambda_0^2}$  where  $\Delta\lambda$  is the spectral half-width of the  $1.06\mu$  transition of  $\text{Nd}^{+3}$ , and  $\Delta\omega$  is the corresponding angular frequency half-width. If  $V_R$  is the volume of the laser rod, the number of excited  $\text{Nd}^{+3}$  ions at threshold is then  $V_R N_K$ , which is, in the case of interest, just the number of ions in the  ${}^4F_{3/2}$  state. Thus:

$$V_R N_K = -\ln(R) \left[ \frac{4\tau_r \eta^2}{\lambda_0^2 \ell} \right] \frac{2\pi c \Delta\lambda}{\lambda_0^2}$$

Each transition contributes energy  $h\omega = \frac{hc}{\lambda_0}$  to the output beam. Hence, the net available energy in the laser rod at threshold,  $E_{AT}$ , for de-excitation by Q-spoiled laser action to the  ${}^4I_{11/2}$  level is

$$E_{AT} = V_R N_K \frac{hc}{\lambda_0} = -\ln(R) \left[ \frac{8\pi\tau_r c^2 \eta^2 \Delta\lambda h}{\lambda_0^5 \ell} \right] V_R \quad \dots(6-2)$$

In order to find the available energy at 450 joules excitation knowing that threshold is 125 joules (this is just the case which applies to the experimental results depicted graphically in Figure (5-5), we need to multiply  $E_{AT}$  by the ratio  $\frac{450}{125}$ .

TABLE 6-1

$\ln(R)$	=	- 0.29	$R = 75\%$
$\tau_r$	=	$360 \times 10^{-6}$	sec.
$\eta^2$	=	$1.58^2 = 2.34$	
$\lambda_0^5$	=	$(1.06 \times 10^{-4})^5 = 1.34 \times 10^{-20}$	$\text{cm}^5$
$c^2$	=	$9 \times 10^{20}$	$\text{cm}^2 / \text{sec}^2$
$l$	=	15.2	cm
$V_R$	=	2.4	$\text{cm}^3$
$8\pi$	=	25.1	
$\Delta\lambda$	=	$0.03 \times 10^{-4}$	cm
$h$	=	$6.63 \times 10^{-34}$	joule - sec.

Table 6-1 summarizes the values of the quantities used in the energy estimate and are applicable under the experimental conditions used to arrive at the results of Figure (5-5). Using the values of the Table in equation (6-2) we arrive at  $E_{AT} = 0.13$  joules. At 450 joules excitation the available energy is then equal to 0.46 joules.

Using the experimental value of 65% energy utilization, the optimum energy output to be expected in the giant pulse at 450 joules excitation is  $0.65 \times 0.46 = 0.3$  joules, a value which is in good agreement with the experimental value of 0.33 joules obtained from Figure (5-5).

This agreement is presented as an indication that the Q-spoiled laser rate equation model is capable of predicting in a satisfactory manner the absolute energy content to be expected in the Q-spoiled output beam from a  $\text{Nd}^{+3}$  glass laser.

Having established the direct relation between the observed peak output energy and the predicted value of the same quantity, we can now simply concentrate on the relative behaviour of the predicted and the observed energy output characteristics. We may scale the calculated quantity  $\int \phi_0 dT$  appropriately to fit the 450 joule characteristic for the particular case involving the results depicted in Figure (5-5). Once the scaling factor has been determined for that characteristic, it is not varied when it is to be applied to the results of calculations relevant to lower excitation characteristics. The method can be similarly employed to deal with other situations which may arise.

### 6.3 Theoretical Switching Speed vs Output

#### Energy Characteristics:

In the previous two Sections we concentrated on two important aspects of the solutions of the rate equations. In the first of those Sections we indicated that  $\phi_{oi} \approx 10^{-13}$ , and later we estimated the available energy in the laser rod to be 0.46 joules at 450 joules excitation. The available energy estimate gave a fairly close fit of the expected and measured peak output energy from the laser rod operating under 450 joules of excitation.

In this Section we shall direct our attention to the relative behaviour of the calculated output energy characteristics and then proceed to make a comparison of this relative behaviour with that of the observed characteristics. We will, in specific terms, be concerned with the experimental characteristics depicted in Figure (5-5). We will allow ourselves the freedom to arbitrarily fit the calculated quantity  $\int \phi_0 dT$  to

a particular point on one experimental characteristic, having already established that the rate equations yield the correct output energy to within a reasonable degree of accuracy.

Figure (6-1) shows the calculated output energy characteristics obtained by solving the set of laser rate equations (2-19), (2-20) and (2-21). The solutions were carried out on the basis of the appropriate experimental switching function shown in Figure (5-3). The switching function was approximated in the calculation by two ramps having slopes of equal magnitude and opposite sign. Table 6-2 summarizes the initial values of  $\phi_0$ ,  $N_0$  and  $N_{10}$  together with the numerical values of other relevant quantities used in the solution of the laser rate equations (2-19), (2-20) and (2-21) for a laser rod excitation corresponding to 450 joules.

TABLE 6.2

QUANTITY	(INITIAL) VALUE
$\phi_{oi}$	$10^{-13}$
$N_{oi}$	1.036
$N_{10,i}$	0.0
$\int \phi_0 dT$	0.0
$\tau$	400 n sec
$\frac{2K_1}{K_1 + K_2}$	0:59
$T_1$	3.29 nsec

Figure (6-1)

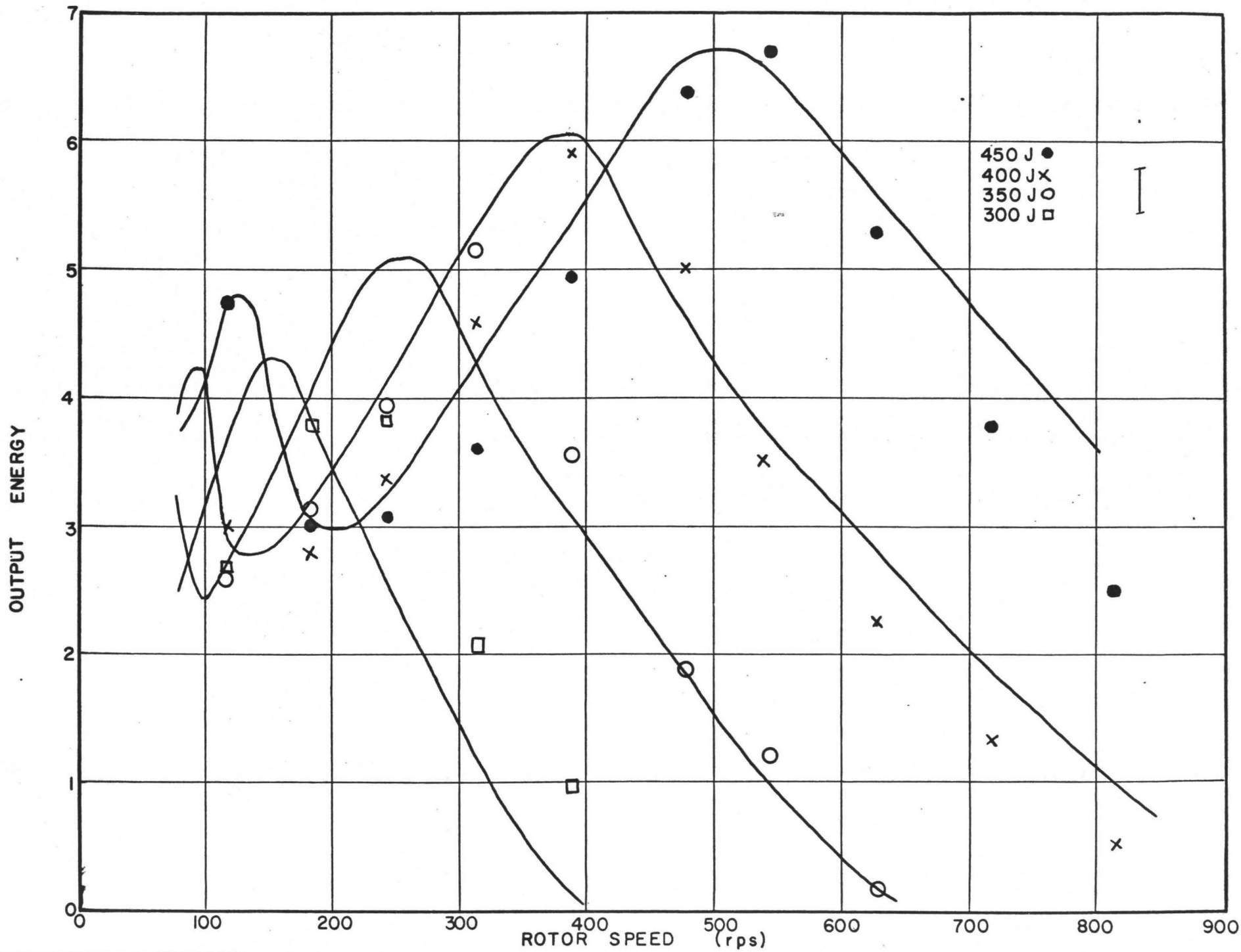
The Calculated Output Energy Characteristics Together  
with the Observed Experimental Data

Cavity length = 46 cms

Output reflector reflectivity = 75%

Terminal level lifetime = 400 nsec.

The calculated characteristics are for excitations of  
450, 400, 350 and 300 joules.



For the other laser rod excitations of interest, the only quantity which is varied appropriately is  $N_{oi}$ . The degeneracy factor  $\frac{2K_1}{K_1 + K_2}$  was determined elsewhere in this Thesis (see Section 2.2-5). The value of  $\tau$  is an estimate arrived at by comparing the behaviour of the theoretical characteristics with the experimental ones as  $\tau$  is varied incrementally.

Before entering into a discussion of the complete set of output energy characteristics and their relation to the observed experimental behaviour, it is worth while showing in detail just how  $\tau$  is chosen. Figure (6-2) shows four calculated characteristics corresponding to 450 joules excitation. They differ from one another only in the choice of  $\tau$  used to calculate them, and which has been varied incrementally from 100 nsec. to 800 nsec. The appropriate experimental points are shown in the same Figure for comparison. The experimentally observed turn-up point observed at about 200 rps is seen to be best described by the calculated characteristic based on  $\tau = 400$  nsec. One cannot immediately draw the conclusion that  $\tau$  is of the order of 400 nsec. because of the particular behaviour exhibited by the characteristics as  $\tau$  is varied. To make the point clear, as  $\tau$  is decreased still further from 100 nsec., the turn-over point, instead of climbing the characteristic with decreasing  $\tau$  (as it has shown a tendency to do in Figure (6-2) ), in fact starts to appear at lower switching speeds once again. This behaviour is shown in Figure (6-3). Thus, for  $\tau = 25$  nsec., the turn-over point appears once more at about 200 rps. This means that one must distinguish between  $\tau = 25$  nsec. and  $\tau = 400$  nsec by arguing from a point of view not based on the position of the turn-over point. It is seen that the secondary maximum in the output energy characteristics for the short lifetime region is not as

Figure (6-2)

The 450 Joule Excitation Characteristic for Long  
Terminal Level Lifetimes

The points and circles represent two sets of independent experimental data.

The solid lines represent the calculated characteristics for terminal level lifetimes of:

- 1 - 100 n sec.
- 2 - 200 " "
- 3 - 400 " "
- 4 - 800 " "

Terminal level lifetimes

The degeneracy factor used in the calculations was 0.59 in all cases.

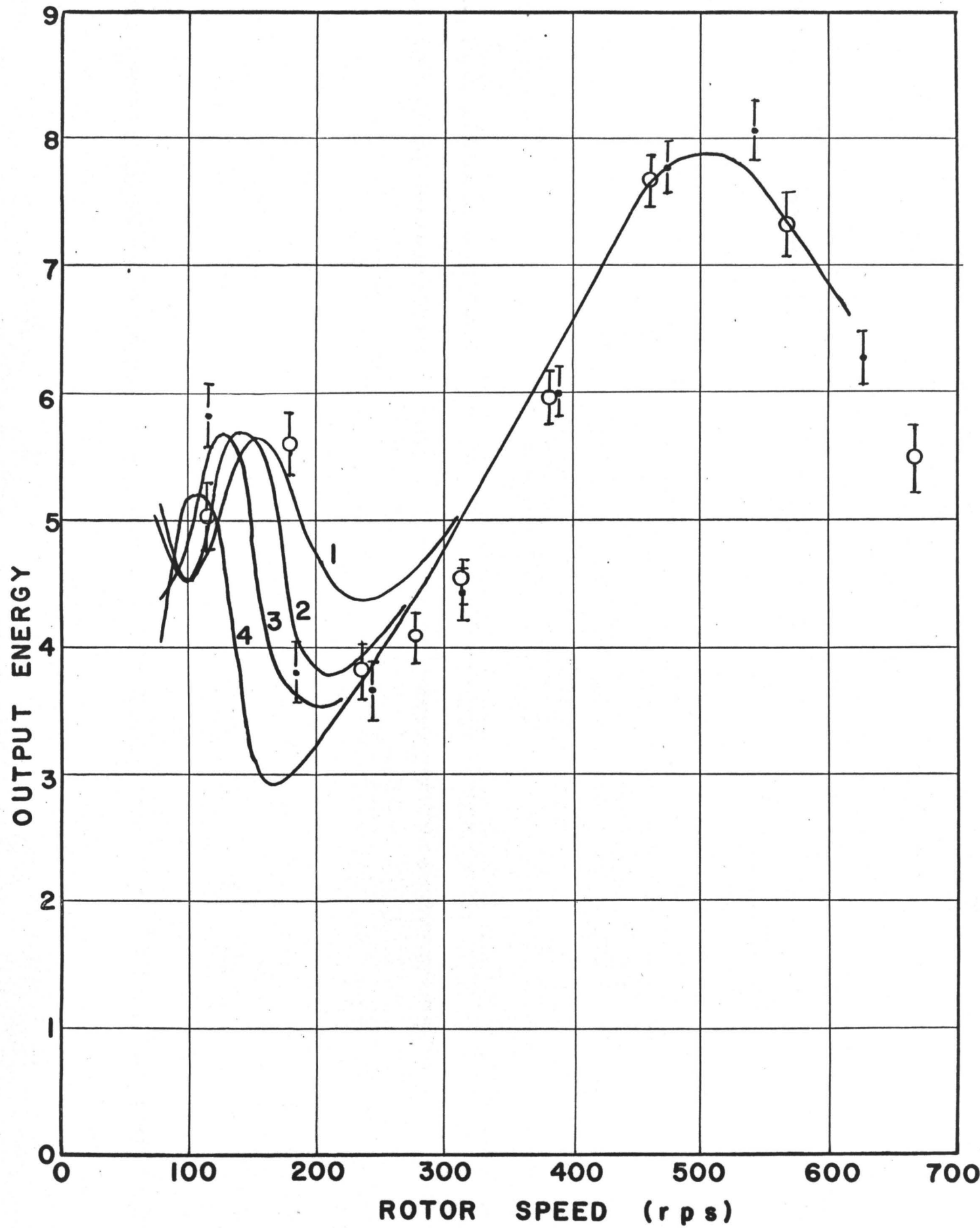


Figure (6-3)

The 450 Joule Excitation Characteristic for Short  
Terminal Level Lifetimes

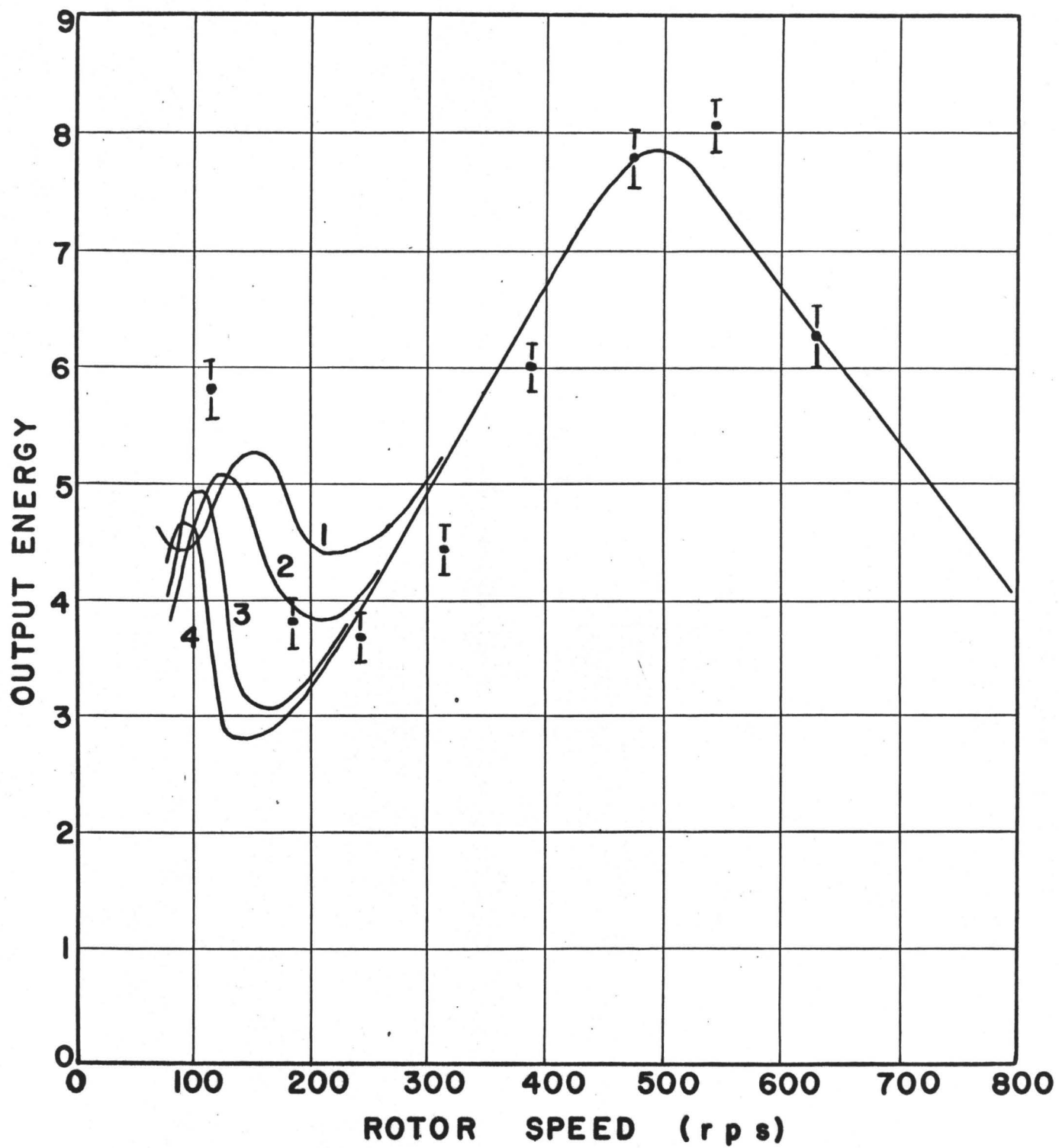
The points represent one of the sets of data from Figure (6-2)

The solid lines represent the calculated  
characteristics for terminal level lifetimes of:

- 1 - 50 nsec.
- 2 - 25 " "
- 3 - 1.25 " "
- 4 - 6 " "

Terminal Level Lifetimes

The degeneracy factor used in the calculations was  
0.59 in all cases.



marked as it is in the long lifetime region. However, the recovery in the experimental characteristics is quite strong, favouring the long lifetime  $\tau$  (= 400 nsec.) over the short lifetime  $\tau$  (= 25 nsec.). The calculated energy utilization factor for the case  $\tau = 400$  nsec. is 68% at optimum energy output whereas for the case  $\tau = 25$  nsec. it is 82%. It is evident upon comparing these two values with the appropriate experimentally observed energy utilization factor of 61% that once again  $\tau = 400$  nsec. is a favoured choice over  $\tau = 25$  nsec.

Theoretical estimates of the multiphonon spontaneous emission lifetime of the  ${}^4I_{11/2}$  level indicate that the long lifetime case is probably the one being observed. Those estimates will form the basis for a discussion in Section 6.4.

The arguments just outlined suggest the choice of  $\tau = 400$  nsec. in the calculations utilizing the rate equations. This choice will be assumed to hold true from this point on.

Referring once more to Figure (6-1) we clearly see the degree of agreement that is present between the experimental points and the theoretical characteristics. The theoretical characteristics cut off somewhat slower than is indicated by the experimental points. Also the fit of the observed and calculated output energy peaks corresponding to low excitations leaves something to be desired. On the other hand, the experimental and theoretical behaviour of the magnitude of the energy maxima as the laser rod excitation is varied is consistent. The overall behaviour predicted on the basis of the rate equations is also in good agreement to that observed experimentally.

In looking for reasons for the lack of detailed agreement between

theory and experiment, one must look more closely at the physical system comprising the active amplifying medium as well as the resonator structure and properties thereof. The use of a rectangular line profile in the model for the  ${}^4F_{3/2} \rightarrow {}^4I_{11/2}$  transition of  $\text{Nd}^{+3}$  is certainly not a very accurate approximation, but it is one that must be made to keep the problem simple enough to be handled analytically. The rectangular approximation will break down for large changes in the excitation to threshold ratio. The breakdown will not be manifested too strongly in the build-up time of the pulse, nor on the positions of the energy maxima of the characteristics. However, it will manifest itself in the behaviour of the energy utilization factor. In particular, the rectangular line approximation would appear to be valuable as long as the envelope of the laser emission spectrum remains fairly constant. This case will result if the excitation-over-threshold ratio is not varied significantly during an experiment. The case close to cut off represents large variations in the ratio. The effect of the spectral shape of the  ${}^4F_{3/2} \rightarrow {}^4I_{11/2}$  transition on the laser emission will manifest itself in a variation of the latter's spectral envelope half-width. This will be particularly true if the energy utilization factor is far from its ideal optimum value. At low excitation-threshold ratios the spectral envelope of the laser emission will be relatively narrow, widening towards a saturation value at high excitation to threshold ratios. The saturation value would be the line width of the lasing line only in the case where there is no energy transfer within the lasing line for frequencies separated by the separation of the longitudinal modes of the cavity. The narrowing of the spectrum envelope of the laser emission at low excitation to threshold ratios will result in a lower

overall energy utilization factor than that obtained on the basis of an assumed rectangular line shape. This point of view leads us to conclude that the experimental characteristics should cut-off faster than the theoretical, as is observed. The actual calculation of the size of the effect would be difficult to carry out.

It is important to note then that spectral line dynamics and the mode structure of giant pulse lasers are likely not unimportant considerations in determining the performance of a device. Another point to keep in mind is that the output beam divergence represents a considerable fraction of the switching function,  $\gamma(\theta)$ , angular extent. This is particularly true in the case of switching functions which have been narrowed by the introduction into the cavity of an angular limiting device. It has been observed experimentally by us, that the narrower the switching function with respect to the natural divergence of the beam, the poorer will be the determination of the true switching function by threshold-misalignment measurements. The conclusion may be reached by considering the output beam as being composed of its component plane waves. The angular content of the beam is pictured as being spread over a relatively large portion of the switching function  $\gamma(\theta)$ . With each plane wave component an appropriate average loss can thus be associated. The normal cut-off condition would occur when the centre of the angular content of the "evolved" beam occurs just at the point when losses are equal to gain. However, cut-off will in fact occur sooner because the assumed angular field configuration is not, as it were, "allowed". An estimate of the size of the effect of diffraction would be difficult since one is dealing with a misaligned cavity. Essentially, then we conclude that the switch,

as determined by threshold-misalignment methods, is a first approximation to the real situation and it will be a good approximation as long as the switch is wide compared to the angular divergence of the output beam.

It was mentioned earlier that the peaking of each individual characteristic, as the excitation is varied, shows a degree of disagreement when experimental and theoretical results are compared. The position of the energy maxima for different excitation may be shown theoretically to be dependent on the shape of the switching function. The disagreement probably results from extrapolating the shape of the switch determined by threshold - misalignment measurements to above-threshold giant pulse output conditions.

We refer now to the characteristics of Figure (5-10), for a cavity configuration which includes the presence of the Lummer Gehrcke angular selective device. The solutions to the rate equations, for the given situation, may well be expected to yield characteristics whose positions along the switching speed axis will be in essential agreement with those observed experimentally. To prove this statement we need only consider reflector reflectivities since we have already accounted for the other factors which affect switching speed in Section 5.6. To see just how one includes the effect of reflector reflectivity on the characteristics let us look at the equation for the build-up of  $\phi_0$ , namely;

$$\frac{d\phi_0}{dT} = \phi_0 (N_0 - \gamma(T)) \quad \dots(6-3)$$

We note that  $N_0$  is a constant during the build up of the giant pulse. Hence, we can formally integrate equation (6-3) to arrive at the result:

$$\phi_o = \phi_{oi} e^{\int_{T_1}^{T_2} (N_o - \gamma(T)) dT}$$

When  $\phi_o$  reaches a certain value  $\phi_o'$  the approximation,  $N_o = \text{constant}$ , will no longer hold. This point is reached at the time just prior to the evolution of the giant pulse proper. The value of  $\phi_o'$  is fairly insensitive to the assumed operating conditions of the device, as is  $\phi_{oi}$ . Hence, a similar insensitivity will hold for the quantity

$$\int_{T_1}^{T_2} (N_o - \gamma(T)) dT$$

if the integral is evaluated over the total region where  $N_o = \text{constant}$ . The integral represents the area bounded by  $N_o$ ,  $\gamma(T)$ ,  $T_1$ , and  $T_2$ . If  $T_1$  is defined by  $N_o = \gamma(T_1)$  and  $T_2$  by  $\gamma_{\min} = -\ln R = \gamma(T_2)$ , we have the approximate condition for optimum energy utilization. The integral then becomes equal to the one half of the area bounded by  $\gamma(T)$  and  $N_o$ . We know that if we change the output reflector reflectivity from  $R_1$  to a higher value,  $R_2$ , the threshold for the aligned cavity will have decreased by a factor of  $\frac{\ln R_1}{\ln R_2}$ . The aligned threshold for the cavity used to measure the characteristics of Figure (5-10) was 200 joules with a 50% reflector. This threshold would have been expected to be about 85 joules had a 75% reflector been used. Note that the area bounded by the switching function and  $N_o$  is roughly proportional to excitation minus threshold. Thus, for the 450 joule characteristic we considered in Section 5.6, the switching speed at which maximum energy output would have been expected, (if a 75% reflector reflectivity had been employed),

would be:

$$\frac{450 - 85}{450 - 200} \times 80 \text{ RPS} = 117 \text{ rps}$$

This value compares favourably with the value of 110 rps estimated in Section 5.6. We conclude that the rate equation solutions remain valid over a reasonably wide range 80 - 500 rps.

#### 6.4 De-excitation of the ${}^4I_{11/2}$ Level of $\text{Nd}^{+3}$ by

##### Multiphonon Emission:

In this Section we apply the multiphonon spontaneous emission theory of Kiel<sup>(45)</sup> to the  ${}^4I_{11/2}$  level of  $\text{Nd}^{+3}$  to obtain an estimate of the lifetime of that level.

In contrast to multiphoton emission, multiphonon emission occurs with relatively high probability. The reason for this can be found in the densities of modes which differ by a factor of  $\frac{C^2}{v^2} = 10^{11}$ .

To give an example from the field of lasers, Kiel has calculated the 5 phonon emission rate for non-radiative transitions from the green  ${}^4T_2$  absorption band of ruby to the narrow  ${}^2E$  state. The  $2700 \text{ cm}^{-1}$  separation of these two states is far above the energy of either the acoustical or optical modes of ruby so that direct single phonon lattice transitions are not possible. Yet Maiman has shown that the efficiency of the transfer of the excitation from the  ${}^4T_2$  to the  ${}^2E$  state is nearly perfect<sup>(45)</sup>. Multiphonon processes must evidently be invoked here. Kiel has done this for the  ${}^4T_2 \rightarrow {}^2E$  transition of ruby and concludes that the 5 phonon transition rate is:  $W_5 \approx 10^6 \text{ sec.}^{-1}$

$W_5$  is the inverse of the lifetime of the  ${}^4T_2$  state and the subscript refers to the number of phonons which are assumed to be emitted in the calculation. This result obtains because the  ${}^4T_2 \rightarrow {}^2E$  transfer is nearly perfectly efficient. Kiel also points out that since there are optical modes for even 3 or 4 phonon processes available,  $W$  could easily be  $10^8 \text{ sec}^{-1}$ .

The above example indicates that the emission probability does not drop off very rapidly as higher and higher order processes are invoked, in contrast to the case of multiphoton emission. Since optical phonons are generally more energetic than acoustic phonons it is a good approximation to consider that they alone are effective in coupling energy levels which are greatly separated<sup>(45)</sup>.

As an indication of the concepts involved in multiphonon spontaneous emission, it is worth while considering the case of emission of a single optical phonon by an excited ion in a matrix host. We start by recalling the golden rule:

$$W_1 = \frac{2\pi}{\hbar} \rho(K) |H'_{KM}|^2$$

where  $W_1$  is the rate of occurrence of transitions,  $\rho(K)$  is the density of final states and  $M$  is the initial state.  $H'_{KM}$  is the matrix element of the perturbation Hamiltonian which is given by<sup>(28)</sup>

$$H' = \sum_s v_s Q_s = \sum_s v_s \sum_i a_{si} q_i$$

The  $Q_s$  terms are normal co-ordinates of the modes causing the transition while the  $v_s$  terms are the associated energy gradients. The  $Q_s$  terms

arise from thermal motions of the lattice and so are considered to be linear functions of the normal co-ordinates  $q_i$  associated with lattice heat waves.

In order to evaluate the density of final states  $\rho(K)$  we consider that the density of states of a particular optical branch is uniform over the frequency range  $\Delta\nu$  and zero outside this range. The number of modes per branch is equal to the number of primitive cells contained in the material being studied. Hence we may write:

$$\rho(K) = \frac{V}{R_0^3 h \Delta\nu} \quad \dots(6-4)$$

where  $V$  is the volume of the host material, and  $R_0^3$  the volume of the primitive cell. Equation (6-4) is evidently an approximation to the real situation. We obtain:

$$W_1 = \frac{4\pi^2 V}{h^2 R_0^3 \Delta\nu} \left| \langle K \mid \sum_s v_s \sum_i a_{si} q_i \mid M \rangle \right|^2$$

$$= \frac{4\pi^2 V}{h^2 R_0^3 \Delta\nu} \left| \sum_{s_i} a_{s_i} \langle K_e \mid v_s \mid M_e \rangle \langle K_p \mid q_i \mid M_p \rangle \right|^2$$

where the summation extends over the localized modes and the lattice modes. The summation over the lattice modes will only contain one non-zero term which we assume to be the  $i^{\text{th}}$ . After evaluating the appropriate matrix element we can therefore write for the  $i^{\text{th}}$  phonon:

$$W_{li} = \frac{4\pi^2 V}{h^2 R_0^3 \Delta\nu} \left| \sum_s a_{s_i} \langle K_e \mid v_s \mid M_e \rangle \right|^2 \frac{\hbar n_i}{2\pi M_i \omega_i}$$

where  $M$  is the mass of the host material and  $\omega_i$  is the angular frequency of the emitted phonon which conserves energy approximately. The quantity  $n_i$  is the number of phonons in the  $i^{\text{th}}$  mode; we can set  $n_i \approx \frac{1}{2}$  for room temperature operation. The quantity  $a_{si}$  of course depends on the details of the crystal structure surrounding the ion being studied. The result is complete if we sum over all the optical branches. If we consider that the relaxations due to the different normal modes of vibration of the complex take place independently then,

$$W_{li} = \frac{1}{2hPA\omega_i \Delta\nu} \sum_s \langle a_{si}^2 \rangle \left| \langle K_e | v_s | M_e \rangle \right|^2 \dots (6-5)$$

where  $P$  is the number of ions in the primitive cell and  $A$  their average mass. Our final result as represented by equation (6-5) is in essential agreement with the appropriate result of Kiel for the single phonon spontaneous emission transition rate.

The method of calculation just outlined can be generalized to account for an  $n^{\text{th}}$  order process. The golden rule can once again be applied if one substitutes the  $n^{\text{th}}$  order matrix element for the usual first order matrix element<sup>(26)</sup>. The calculation of the density of final states must, however, be treated with care. To be specific,  $n^{\text{th}}$  order convolution of the single phonon density of states must be applied.

We will simply write down our result for the rate of spontaneous emission of phonons in second order.  $W_{2ij}$  can be shown to be given by the expression:

$$W_{2ij} = \frac{8}{h^2(v(0)-v(K_{\max}))} \left( \frac{h}{32\pi^2 PA} \right)^2 \left| \sum_{\text{elect states}} \sum_{sd} a_{si} a_{dj} \langle K_e | v_s | n_e \rangle \langle n_e | v_a' | M_e \rangle \right|^2 \dots (6-6)$$

$(E_M - E_n) \sqrt{v_i v_j}$

Once again we must sum over all the optical branches.

Kiel has argued that the relation between the probability of an n-phonon process and an (n-1)-phonon process is approximately (for a 3-fold degenerate branch)

$$\frac{W_n}{W_{n-1}} = \frac{C h |\langle K_e | v_s | n_e \rangle|^2}{10\pi P A v_s (E(n_e) + h\nu_1 - E(M_e))} \dots (6-7)$$

where C is the number of equivalent processes. Equation (6-7) together with the transition rate for a one phonon process provides us with an approximate means of calculating the n<sup>th</sup> order optical phonon transition rate between two given levels.

The application of the procedure to  $Nd^{+3}$  in glass cannot be approached without trepidation. However, it is instructive to do so in the sense that an idea of the order of magnitudes of the transition rates involved will be gained. Before entering into the detailed calculations it is worth while noting that the ratio  $W_2/W_1$  as obtained from equations (6-5) and (6-6) is given by:

$$\frac{W_{2ij}}{W_{1l}} = \frac{h}{8\pi P A} \frac{\sum_{(in. elect. states)sd} \sum \frac{\langle a_{si}^2 \rangle \langle a_{dj}^2 \rangle |\langle K_e | v_s | n_e \rangle|^2 |\langle n_e | v_d | M_e \rangle|^2}{(E_M - E_n)^2 v_i v_j}}{\sum_K \langle a_{Kl}^2 \rangle \frac{|\langle K_e | v_K | M_e \rangle|^2}{v_l}} \dots (6-8)$$

The above result is to be compared with Kiel's result given by equation (6-7) after setting  $n = 2$ . We see that the two expressions are in

essential agreement. The disagreement is minor - we obtain the figure 8 as opposed to Kiel's 10 in the denominator. Our analysis also results in the appearance of the mode expansion coefficients  $a_{si}$ .

With the above considerations in mind we are now in a position to apply the theory to the  ${}^4I_{11/2} \rightarrow {}^4I_{9/2}$  non-radiative transition of  $\text{Nd}^{+3}$  in glass. The Debye temperature  $\theta_D$  of glass is about  $1000^\circ\text{K}$ . Hence,

$$v_{\max} = \frac{k\theta_D}{h} = 2.1 \times 10^{13} \text{ cps} = 700 \text{ cm}^{-1}$$

Since the energy separation between the  ${}^4I_{11/2}$  and the  ${}^4I_{9/2}$  levels of  $\text{Nd}^{+3}$  is  $2000 \text{ cm}^{-1}$ , it is evident that 3-phonon processes will be the most likely to occur. Now for rare earths the matrix elements

$|\langle K_e | v_K R | M_e \rangle|^2 \approx 10^5 \text{ cm}^{-2}$ , where  $R$  is the radius of the complex being considered<sup>(45)</sup>. It can be shown that  $W_3$  is given approximately by:

$$W_3 = \frac{4\pi C}{\hbar^2 \Delta\nu} \left( \frac{h}{32^2 \text{PAR}^2} \right)^3 \frac{|\langle K_e | v_K R | M_e \rangle|^6}{(h\nu)^4 \nu^3}$$

where  $C$  is the number of equivalent processes.

The quantity  $C$  may be calculated quite readily. We assume that only the component states of the  ${}^4I_{11/2}$  and  ${}^4I_{9/2}$  multiplets of  $\text{Nd}^{+3}$  need be included in the calculation. We are thus dealing with 22 electronic states, which for a given set of optical modes give rise to  $(22)^2 = 484$  equivalent processes. Assuming that there are 3 normal modes of the neighbours which have the right frequencies, we obtain  $C = 484 \times (3)^3 = 13,000$ . If we now assume  $\Delta\nu = 28 \text{ cm}^{-1}$  (i.e.,  $\frac{1}{25}$  of  $v_{\max}$ ) we may calculate  $W_3$  from

the above formula. We obtain  $\frac{1}{W_3} = 30$  nsec. In the calculation it was assumed that each of the 13,000 equivalent processes contributed strongly. Thus the magnitude of  $\frac{1}{W_3} = 30$  nsec. is an estimate of the shortest possible lifetime of the  ${}^4I_{11/2}$  state as determined by multiphonon spontaneous emission. The existence of selection rules which must be accounted for in the matrix element calculations could easily increase the lifetime of the  ${}^4I_{11/2}$  state of  $Nd^{+3}$  by an order of magnitude.

We conclude that it is unlikely that the lifetime of the  ${}^4I_{11/2}$  level of  $Nd^{+3}$  is shorter than 30 nsec. Our experimental results are consistent with two values of the lifetime of the  ${}^4I_{11/2}$  level of  $Nd^{+3}$  - one that is shorter than 30 nsec. and one that is longer - so that to account for the results of this Section we must choose the longer of the two. On this basis we may conclude that the lifetime  $\tau$  of the  ${}^4I_{11/2}$  level is given by:

$$\tau = 400 \text{ nsec.}$$

### 6.5 Temporal Development of the Giant Pulse:

This Section will concern itself with those aspects of a giant pulse laser involving the time base growth and decay of the output pulse. In particular, attention will be focused on the time half-widths of the experimentally observed giant pulses. They will be shown to be in good agreement with those which are calculated from the rate equations. We will deal with the separation between multipulses as calculated and observed. In this connection we will restrict ourselves to the double pulse region. The discussion of the giant-pulse widths will necessarily be semi-quantitative

since the response time of the oscilloscope used to make the time evolution observations was of the order of the giant pulse half-width.

Figure (6-4) shows the time development of the calculated giant pulse, under certain conditions which are included in the Figure for reference. We note that the pulse is occurring close to the point of highest energy output of the 450 joule characteristic of Figure (6-1) and so is characterized by close to the narrowest expected giant pulse width. The insert in Figure (6-4) is a faithful copy of a polaroid photograph of the oscilloscope screen showing the giant pulse obtained from the Q-switched laser under the same ideal conditions. The pulse widths of the observed and calculated output pulses are clearly in good agreement, both being of the order of 25 nsec. The somewhat steep rise and more gradual fall of the giant pulse intensity is clearly visible in both reproductions. Generally speaking, we may conclude that the magnitude of the observed and calculated pulse widths will be in good agreement since over the normal operational range of the laser we expect the pulse width to do no more than double. The calculated pulse width will also tend to increase under the less ideal circumstances being assumed, leaving little room for any significant discrepancy.

Figure (6-5) illustrates the calculated output pulse trains in the vicinity of the secondary maximum of the 450 joule characteristics of Figure (6-1) for various values of the terminal level lifetime. In that switching speed region (at approximately 125 rps) two output pulses characterize the beam.

The pulse appearing first in time, some 500 nsec after the laser gain just overcomes the cavity losses, is seen to be fairly insensitive

Figure (6-4)

Calculated Time Development of the Giant Pulse

Unit of time = 3.29 nsec

Excitation = 450 joules

$\tau$  = 400 nsec

Output reflector reflectivity = 75%

Gain overcame losses at  $T = -685$

Rotational rate = 616 rps

The pulse is occurring at a time of minimum losses

The small insert is the observed time evolution of  
the giant pulse - sweeprate is 20 nsec per division.

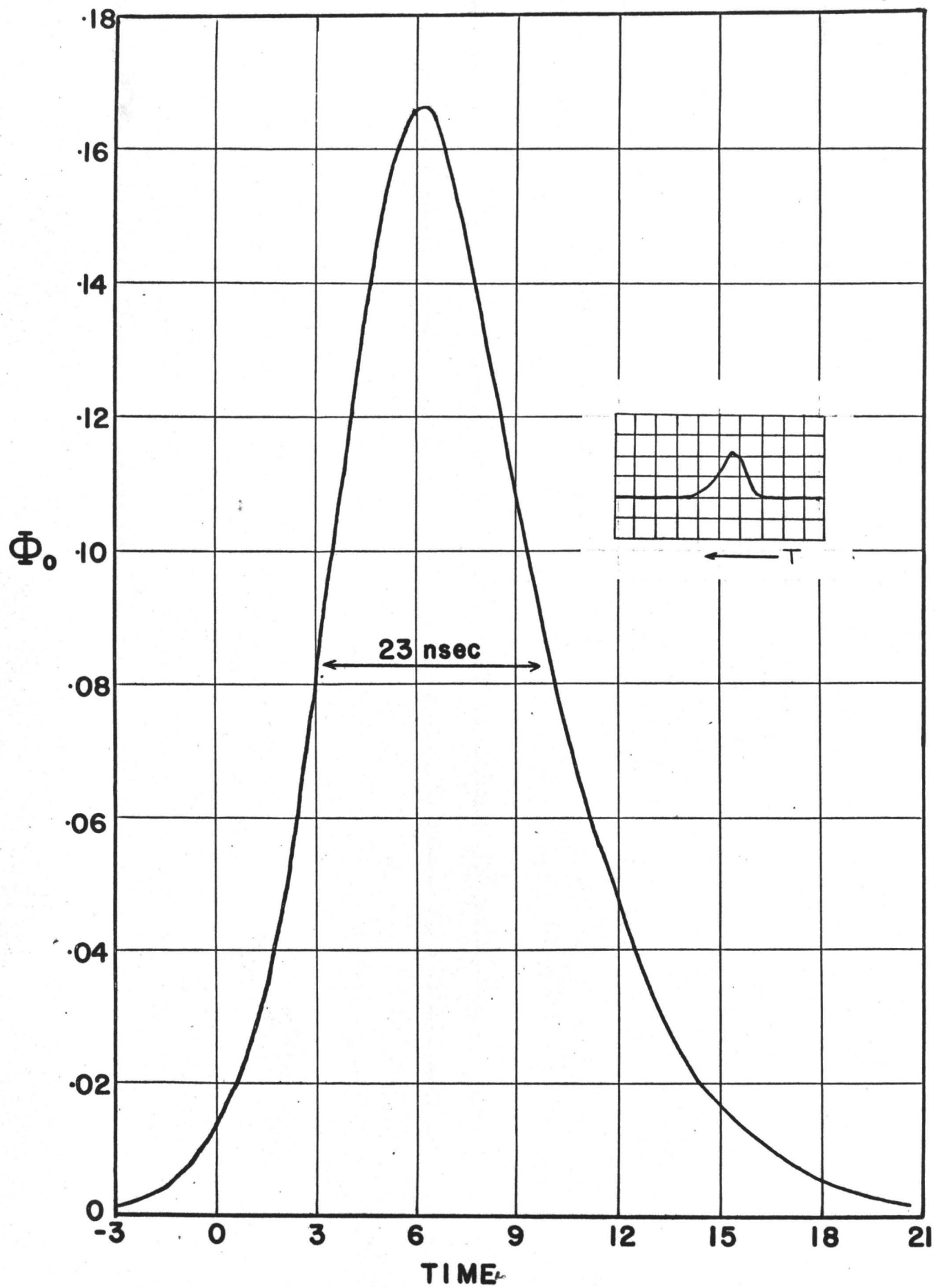


Figure (6-5)

Calculated Time Development of the Giant Pulse  
in the Double Pulse Region

The calculated pulse trains are for a terminal level lifetime of:

- 1 - 800 nsec
- 2 - 400 nsec
- 3 - 200 nsec
- 4 - 100 nsec

Unit of time = 3.29 nsec

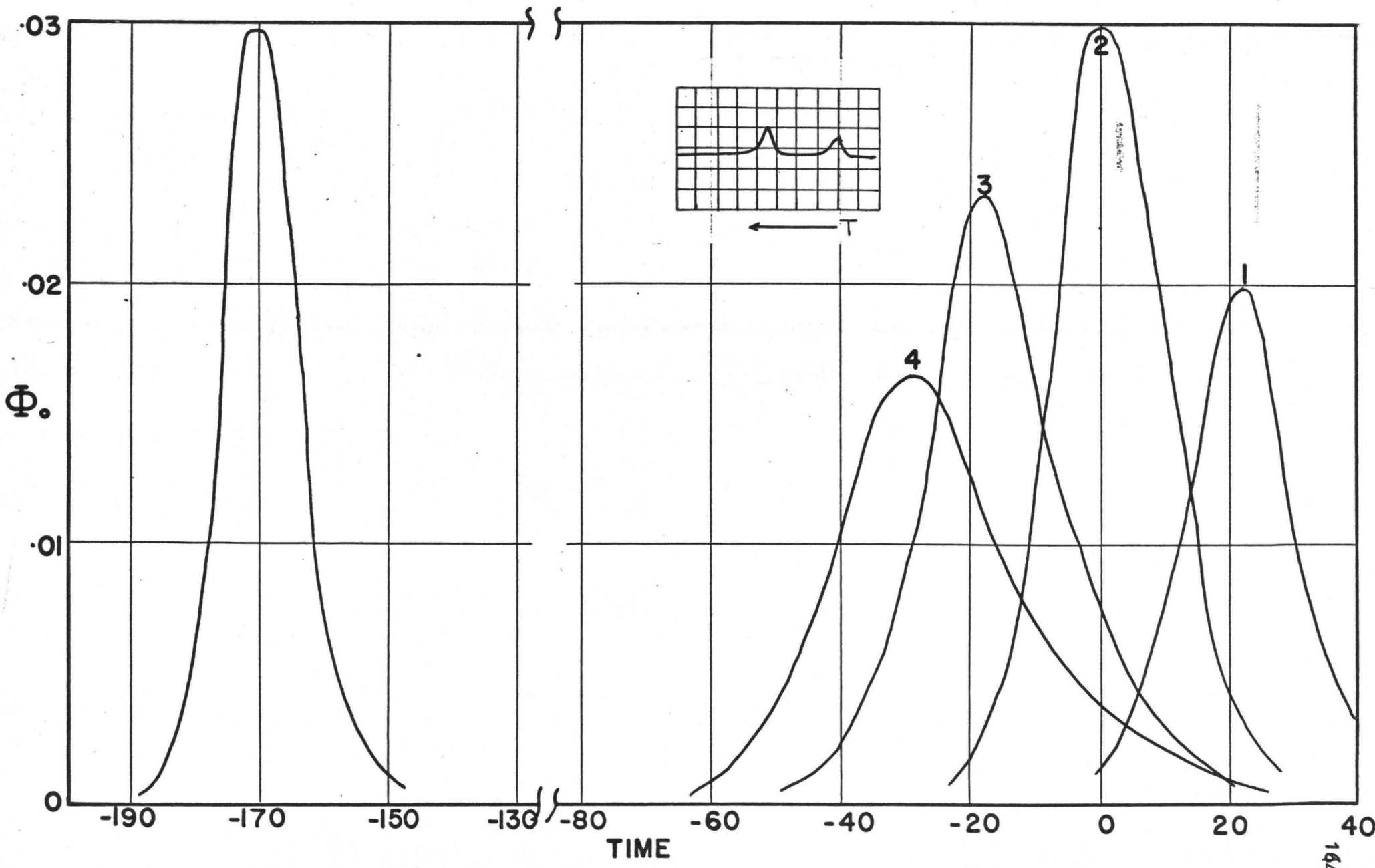
Excitation = 450 joules

Output reflector reflectivity = 75%

Gain overcame the losses at  $T = -328.8$

Rotational rate = 128.4 rps

The small insert is the observed time evolution of the giant pulse - sweep rate is 100 nsec per division.



to the lower level lifetime. The observation is not surprising since the pulse has a half width of 50 nsec which does not give the lower level enough time to reinvert the population significantly - even with an assumed lifetime of 100 nsec. The effects of the lower level lifetime are, however, felt strongly by the second pulse. For the range of lifetimes considered in Figure (6-5), we see that shorter lifetimes effect an earlier appearance of the second pulse. The largest secondary pulse in the Figure is seen to correspond to a terminal level lifetime of 400 nsec. The reason it is the largest is that it occurs closest to the zero of the time scale, which is precisely the time when the losses in the cavity are lowest. Comparing the two secondary pulses characterized by the lifetime  $\tau = 800$  nsec and 200 nsec, we note that they evolve at two different times which are, however, characterized by approximately equal losses. ( $\pm 20$  time units). However, in the first case the lifetime corresponds to  $\frac{800}{3.29} = 244$  time units. Roughly,  $\frac{190}{244} = 0.78$  is the number of lifetimes representing the separation between the two pulses in the first case, and  $\frac{150}{61} = 2.46$  is the corresponding number in the second case. We conclude that reinversion by lower level depopulation is almost complete by the time the second pulse evolves in the case of  $\tau = 200$  nsec, whereas this is hardly the case for  $\tau = 800$  nsec. Thus, the secondary pulse is more intense for  $\tau = 200$  nsec than it is for  $\tau = 800$  nsec - even if both secondary pulses are evolving when the losses are approximately equal.

The insert of Figure (6-5) illustrates the experimental time evolution of a double pulse output from the laser. The experimental situation under which the observation was made allows us to compare the pulse train of the insert with the pulse trains calculated from the rate

equations. We see first of all that the pulse widths are in good agreement. The pulse separation observed experimentally is about 350 nsec, which does not compare too favourably with the calculated separation of about 550 nsec. This is an indication that the threshold-misalignment loss function is not quite as accurate as one would hope it would be. However, the simplifications involved in arriving at the laser rate equation model are so drastic that better agreement between theory and experiment is unlikely to result. Another point of disagreement is in the relative heights of the two pulses of the train as observed and calculated. The lead pulse of the calculated pulse sequence has the largest amplitude while it is in fact observed experimentally that the secondary pulse is actually the one with the largest amplitude.

Finally, we sum up by saying that giant pulse widths as calculated on the basis of the rate equations are in good agreement with those widths as observed experimentally. The pulse separations in the double pulse region are in reasonable agreement. That agreement could conceivably be improved upon by varying somewhat the shape of the switch used in the rate equations.

## CHAPTER 7

### CONCLUSIONS

A theory of giant pulse regenerative action in a Q-spoiled laser, based on the modified laser rate equations of Wagner and Lengyel, has been presented. The theory of those authors was augmented to include the effects on giant pulse evolution of a terminal level lifetime and of laser level degeneracies, as well as of a time dependent loss function. We have shown that good agreement between theory and experiment results when the threshold-misalignment function is used as the time dependent loss function to solve the laser rate equations - as long as the angular width of the loss function is significantly wider than the diffraction limit of the cavity. An estimate of the relaxation lifetime of the  ${}^4I_{11/2}$  level of  $Nd^{+3}$  in glass was obtained by making comparison of the experimental and calculated output energy characteristics of the giant pulse laser. The value of  $\tau = 400$  nsec so arrived at was shown to be in essential agreement with the value for that quantity obtained from the multiphonon spontaneous emission theory of Kiel.

Experiments to determine the efficiency of utilization of the stored energy in the  $Nd^{+3}$  in glass laser rod were shown to indicate that the device was operating reasonably close to maximum efficiency. Calculations of the output energy of the laser, as based on the rate equations, were found to be in close agreement with the observed value of that quantity.

The effects of an angular limiting device on the switching speed output energy characteristics of the laser were considered. In particular it was found that it was possible to obtain an increase in apparent switching speed of a factor of six by incorporating the device into the cavity, without significant losses of output beam strength.

Comparison of the observed and calculated giant pulse widths indicated essential agreement. Multipulse separations in the double pulse region as observed and calculated showed some disagreement.

In future work on giant pulse  $\text{Nd}^{+3}$  in glass lasers it would perhaps be fruitful to study the dynamics of the  ${}^4\text{F}_{3/2} \rightarrow {}^4\text{I}_{11/2}$  laser transition during and after evolution of the giant pulse. With such a study it would be possible to arrive at information on cross-relaxation processes within the spectral line, and an attempt could then be made to include such effects into an analytical description of the laser device. Some work has already been done along this line by Michon<sup>(27)</sup> and others<sup>(14)</sup> but further effort in that direction would not be wasted.

One cannot help feeling that a more adequate switching function can be arrived at by means other than those described here. The problem of the switching function can of course be completely avoided by using fast switches as exemplified, in particular, by Kerr cells. Use of such switches, capable of lowering the cavity losses in a time less than the build-up time of the giant pulse, would allow a more detailed concentration on the actual physical processes taking place in the laser itself than is possible when mechanical means are used to switch the Q of the cavity.

Finally, we considered the introduction of an angular limiting device in a plane parallel Fabry Perot laser interferometer and illustrated the transverse mode selecting properties of such a device.

## APPENDIX

In the Appendix we wish to first calculate the quantity  $\phi_{oi}$  and later consider those transitions between the close lying electronic energy levels of an ion located in a crystal matrix which are accompanied by the spontaneous emission or absorption of a single acoustical phonon.

1. Let  $\phi$  be the number of photons per unit volume per unit angular frequency range in the cavity. Further, let those photons be contained within solid angle  $\Delta\Omega$ .

We recall the relationship:

$$\left(\frac{N_K}{\Delta\omega}\right)_{\text{Thresh.}} = -2 \ln R \left[ \frac{\tau_r \omega_{Kl}^2 \eta^2}{c^2 \pi^2 \ell} \right]$$

which yields the number of ions in energy level K per unit angular frequency range per unit volume.

If we neglect induced emission we may write the rate equation;

$$\frac{dN_K}{dt} = - \frac{N_K}{\tau_r}$$

where  $\tau_r$  is the radiative lifetime of the  $K^{\text{th}}$  level.

The number of photons per unit volume emitted spontaneously per second per unit angular frequency range at laser threshold into solid angle  $\Delta\Omega$  is then;

$$\frac{d\phi}{dt} = - 2 \ln R \left[ \frac{\omega_{K\ell}^2 \eta^2}{c^2 \pi^2 \ell} \right] \frac{\Delta\Omega}{4\pi} \frac{V_x}{V_c}$$

where  $V_x$  is the laser crystal volume, and  $V_c$  the cavity volume. Now, photons are lost at a rate given by:

$$\frac{d\phi}{dt} = - \frac{\phi}{\tau_c}$$

where  $\tau_c$  is the cavity lifetime. Assuming equilibrium to exist between the two rates we may write:

$$\phi = - 2 \frac{\Delta\Omega}{4\pi} \ln R \left[ \frac{\omega_{K\ell}^2 \eta^2}{c^2 \pi^2 \ell} \right] \frac{V_x}{V_c} \tau_c$$

Making the usual linear transformations we obtain for the quantity  $\phi_{oi}$  at threshold

$$[\phi_{oi}]_{\text{Thresh}} \approx - \frac{\Delta\Omega \tau_c}{4\pi \tau_r} \ln R$$

For excitations  $X$  times above threshold we have:

$$[\phi_{oi}]_X = X [\phi_{oi}]_{\text{Thresh}}$$

2. Under the action of a perturbation  $H'$ , the state  $m$  is assumed to make transitions to a band of states  $K$  characterized by a density of states  $\rho(E_K)$ . The transition rate  $W$  is given by the golden rule:

$$W = \frac{2\pi}{\hbar} \rho(E_K) | \langle K | H' | m \rangle |^2$$

The transition probability per unit time that an atom in state  $g$  absorb a lattice phonon  $i$  of energy  $\Delta E$  and make a transition to state  $e$  is then given by: (28)

$$W_{g \rightarrow e, i} = \frac{4\pi^2}{h} \rho(E_e) |\langle \psi_e, n_i - 1 | H' | \psi_g, n_i \rangle|^2$$

The above expression needs to be averaged over  $i$ ;

$$[W_{g \rightarrow e, i}]_{av} = W_{g \rightarrow e}$$

Now we may assume for  $H'$  the form;

$$H' = \sum_K v_K' \sum_i a_{Ki} q_i$$

and recalling that  $\langle n_i - 1 | q_i | n_i \rangle = \left[ \frac{hn_i}{4\pi^2 M \omega_i} \right]^{1/2}$

we obtain:

$$W_{g \rightarrow e} = \frac{1}{M} \left[ \rho(E_e) \left| \sum_K a_{Ki} \langle \psi_e | v_K' | \psi_g \rangle \right|^2 \frac{n_i}{\omega_i} \right]_{av}$$

The values of the density of states in terms of  $\omega$ , for longitudinal and transverse waves are given by:

$$\rho_l(\omega_i) = \frac{8\pi^2 \omega_i^2 V}{h v_e^3} \quad \rho_t(\omega_i) = \frac{16\pi^2 \omega_i^2 V}{h v_t^3}$$

where  $v_l$  and  $v_t$  are, respectively, the velocities of the longitudinal and transverse waves and  $V$  is the volume of the crystal. Assuming  $v_t = v_l = v$  we obtain:

$$\rho(\omega_i) = \frac{24\pi^2 \omega_i^2 V}{h\nu^3}$$

Assuming that the relaxations due to different normal modes take place independently and further allowing  $\hbar\omega = \Delta E$  to be the average value of  $\hbar\omega_i$  and  $\langle n_i \rangle$  the average value of  $n_i$  we obtain:

$$W_{g \rightarrow e} = \frac{24\pi^2 \omega}{h\nu^3 \rho} \langle n_i \rangle \sum_K \langle a_{Ki}^2 \rangle |\langle \psi_e | v_{K'} | \psi_g \rangle|^2$$

$$\text{where } \langle n_i \rangle = \frac{1}{e^{\Delta E/KT} - 1}$$

$$\text{Now } \langle a_{li}^2 \rangle_{av} = \dots = \langle a_{6i}^2 \rangle_{av} = \frac{\pi^2 R^2 \omega^2}{15\nu^2} \frac{20}{3}$$

if we assume  $\nu = \nu_l = \nu_t$  and further restrict ourselves to an  $XY_6$  complex.  $R$  is the equilibrium distance  $X \leftrightarrow Y$ .

$$W_{g \rightarrow e} = \frac{256 \pi^7 R^2 (\Delta E)^3}{3 \nu^5 \rho h^3} \frac{1}{e^{\Delta E/KT} - 1} \sum_K |\langle \psi_e | v_{K'} | \psi_g \rangle|^2$$

Similarly;

$$W_{e \rightarrow g} = \frac{256 \pi^7 R^2 (\Delta E)^3}{3 \nu^5 \rho h^3} \frac{e^{\Delta E/KT}}{e^{\Delta E/KT} - 1} \sum_K |\langle \psi_e | v_{K'} | \psi_g \rangle|^2$$

where  $\rho$  is the host matrix density.

TABLE A-1

$\rho$	$3.09 \text{ gms/cm}^3$
R	$10^{-8} \text{ cms}$
v	$5.5 \times 10^5 \text{ cms/sec}$
h	$6.63 \times 10^{-27} \text{ erg-sec.}$
K	$1.38 \times 10^{-16} \text{ erg/}^\circ\text{K}$
T	$300^\circ\text{K}$
$\Delta E$	$3.98 \times 10^{-14} \text{ ergs}$
$ \langle \psi_e   v_K   \psi_g \rangle ^2$	$4 \times 10^{-12} \text{ erg}^2/\text{cm}^2$
$\pi^7$	3020

Using the values in the Table we can calculate  $W_{g \rightarrow e}$  for  $\text{Nd}^{+3}$  in a glass matrix, and so obtain,

$$W_{g \rightarrow e} \approx 8.74 \times 10^{11} \text{ sec}^{-1}$$

This corresponds to a phonon broadened homogeneous linewidth of about  $5 \text{ cm}^{-1}$  for the  $\text{Nd}^{+3}$  ion in a glass matrix. The calculation shows that  $\text{Nd}^{+3}$  Stark split energy levels which are separated by about  $200 \text{ cm}^{-1}$  ( $3.98 \times 10^{-14}$  ergs) and are connected by the phonon matrix element

$\langle \psi_e | v_K' | \psi_g \rangle$  have a lifetime of the order of  $10^{-12}$  seconds at room temperature. Hence those levels tend to thermalize very rapidly.

Work done by Michon<sup>(46)</sup> indicates that the homogeneous line width of the  ${}^4F_{3/2} \rightarrow {}^4I_{11/2}$  transition of  $\text{Nd}^{+3}$  in glass is of the order of  $15\text{\AA}$

or  $15 \text{ cm}^{-1}$  at room temperature. Most of the broadening of the transition is inhomogeneous and due to the different environments in which the  $\text{Nd}^{+3}$  ions find themselves in the glass matrix.

## REFERENCES

1. McClung, R. J., and R. W. Hellwarth, "Giant Optical Pulsations from Ruby", J. Appl. Phys., 33, 828-9, (1962).
2. Collins, R. J. and P. Kisliuk, "Control of Population Inversion in Pulsed Optical Masers by Feedback Modulation", J. Appl. Phys, 33, 2009-11, (1962).
3. Hellwarth, R. W., "Control of Fluorescent Pulsations", in Advances in Quantum Electronics (Columbia University Press, New York, 1961), p. 334.
4. DeMaria, A. J., R. Gagosz, and G. Barnard, "Ultrasonic-refraction Shutter for Optical Maser Oscillators", J. Appl. Phys., 34, 453-6, (1963).
5. Helfrich, J. L., "Faraday Effect as a Q-Switch for Ruby Laser", J. Appl. Phys., 34, 1000-1, (1963).
6. McClung, F. J. and R. W. Hellwarth, "Characteristics of Giant Optical Pulsations from Ruby", Proc. IEEE, 51, 46-53, (1963).
7. Sorokin, P. P., J. J. Luzzi, J. R. Lankard, and G. D. Pettit, "Ruby Laser Q-switching Elements Using Phthalocyanine Molecules in Solution" IBM J. Res. Develop., 8, 182-4, (1964).
8. Soffer, B. H., and R. H. Hoskins, "Generation of Giant Pulses from a Neodymium Laser by a Reversible Bleachable Absorber", Nature, 204, 276, (1964).
9. Masters, J. I., J. Ward, and E. Hartouni, "Laser Q-Spoiling Using an Exploding Film," Rev. Sci. Instr., 34, 365-7, (1963).
10. Shiner, W., E. Snitzer, and R. Woodcock, "Self-Q-Switched Nd<sup>+3</sup> Glass Laser", Phys. Letters, 21, 412-413, June 1, 1966.

10. a Gandy, H. W., R. J. Ginther, and J. F. Weller, "Internal Q-Switching of  $H_0^{3+}$ -Stimulated Emission in Iron-Containing Glasses", Appl. Phys. Letters, 9, 277-279, October 15, 1966.
11. Basov, N. G., V. S. Zuev, and Yu. V. Senat-skii, "A Q-Switched Neodymium Glass Laser", Soviet Physics JETP, 21, 1047-1048, (1965).
12. Benson, R. C. and M. R. Mirachi, IEEE Trans. Mil. Electron, 8, 13, (1964).
13. Crowell, M. H., "Characteristics of Mode Coupled Lasers", IEEE J. Quantum Electronics, QE-1, 12-20, April 1965.
14. Cabezas, A. Y. and R. P. Treat, "Effect of Spectral Hole-Burning and Cross Relaxation on the Gain Saturation of Laser Amplifiers", J. Appl. Phys., 37, 3556-3563, (1963).
15. Borrelli, N. F. and M. L. Charter, "Energy Distribution in a Glass:  $Nd^{3+}$  Laser Rod", J. Appl. Phys., 36, 2172-2174 (1965).
16. Wenzel, J. H., "Giant-Pulse Laser Activity in Neodymium-Doped Silicate Glass: The Energy Conversion Process", J. Appl. Phys., 37, 3100-3110, (1966).
17. Wagner, W. G., and B. A. Lengyel, "Evolution of the Giant Pulse in a Laser", J. Appl. Phys., 34, 2040-6, (1963).
18. Vuylsteke, A. A., "Theory of Laser Regeneration Switching", J. Appl. Phys., 34, 1615-22, (1963).
19. Midwinter, J. E., "The Theory of Q-switching Applied to Slow Switching and Pulse Shaping for Solid State Lasers", British J. Appl. Phys., 16, 1125-1133, (1965).
20. Daly, R., and S. D. Sims, "An Improved Method of Mechanical Q-Switching using Total Internal Reflection", Appl. Opt., 3, 1063-6 (1964).

21. Gates, J. W., and R. G. N. Hall, "Optical Amplification of the Apparent Rate of Rotation of a Reflector in Q-switching a Laser Resonator", Nature, 206, 1141, (1965).
22. Dieke, G. H., "Spectroscopic Observations on Maser Materials", in Advances in Quantum Electronics, edited by J. R. Singer, Columbia University Press, New York, 1961.
23. Lengyel, B. A., Introduction to Laser Physics, (John Wiley and Sons, Inc., New York, 1966)
24. Wybourne, B. G., Spectroscopic Properties of Rare Earths, (Interscience Publishers, New York, 1965).
25. Judd, B. R., Operator Techniques in Atomic Spectroscopy, (McGraw-Hill Book Company, Inc., New York, 1963).
26. Schiff, L. I., Quantum Mechanics, Second Edition (McGraw-Hill Book Company, Inc., New York, 1955).
27. Michon, M., "The Influence of  $\text{Nd}^{3+}$  Ion Properties in a Glass Matrix on the Dynamics of a Q-Spoiled Laser", IEEE J. Quantum Electronics, QE-2, 612-616, (1966).
28. Smith, W. S., and P. P. Sorokin, The Laser (McGraw-Hill Book Company Inc., New York, 1966).
29. Yariv, A. and J. P. Gordon, "The Laser", Proc. IEEE, 51, 4-20, (1963).
30. Johnson, D. C. Frequency Doubling in  $\text{NiSO}_4 \cdot 6\text{H}_2\text{O}$ , (Ph.D. Thesis, McMaster University, 1966).
31. Morse, P. M., and H. Feshbach, Methods of Theoretical Physics (McGraw-Hill Book Company, Inc., 1953).
32. Born, M., and E. Wolf, Principles of Optics (Macmillan, New York, 1964).

33. Fox, A. G., and T. Li, "Resonant Modes in a Maser Interferometer", *Bell System Tech. J.*, 40, 453 (1961).
34. Stoke, G. W., An Introduction to Coherent Optics and Holography, (Academic Press, New York, 1966)
35. Whittaker, E. T., and G. N. Watson, A Course of Modern Analysis, (The Cambridge University Press, 1963).
36. Abramowitz, M. and I. A. Stegun, Handbook of Mathematical Functions, (National Bureau of Standards, 1964).
37. Smirnov, V. I., A Course of Higher Mathematics, (Pergamon Press, Oxford, 1964).
38. Watson, G. N., A Treatise on the Theory of Bessel Functions, 2nd Ed., (Cambridge University Press, Cambridge, 1958).
39. Hildebrand, F. B., Methods of Applied Mathematics, (Prentice-Hall, Inc. Englewood Cliffs, New Jersey, 1961).
40. Schuldt, S. B., and R. L. Aagard, "An Analysis of Radiation Transfer by Means of Elliptical Cylinder Reflectors" *Appl. Optics*, 2, 509-513, (1963).
41. Photomultipliers for Scintillation Counting, published by the Philips Electron Tube Division.
42. Ross, M., Laser Receivers, (John Wiley and Sons, Inc., New York, 1966).
43. General Electric Flashtube Data Manual, published by General Electric Photo Lamp Department.
44. Snitzer, E., "Neodymium Glass Laser", a paper presented at the Third International Symposium on Quantum Electronics, Feb. 1963, Paris, France.

45. Kiel, A., "Multiphonon Spontaneous Emission in Paramagnetic Crystals" in Quantum Electronics III edited by P. Grivet and N. Bloembergen, (Columbia University Press, New York, 1961).
46. Michon, M., Private Communication